Model Calculations of the Atmospheric Effects of Supersonic Aviation Which Were Used in the IPCC Special Report on Aviation and the Global Atmosphere

Lead Author:
Debra Weisenstein, AER, Inc., U.S.A.

Technical Support:
Karen Sage, NASA Langley Research Center, U.S.A.
Donald Brown, NASA Langley Research Center, U.S.A.

Co-Authors:
Richard S. Eckman, NASA Langley Research Center, U.S.A.
Malcolm K.W. Ko, AER, Inc., U.S.A.

Contributors:
Steven L. Baughcum, Boeing Company, U.S.A.
Martyn Chipperfield, University of Cambridge, U.K.
Michael Gauss, University of Oslo, Norway
William L. Grose, NASA Langley Research Center, U.S.A.
Robert S. Harwood, University of Edinburgh, U.K.
Ivar Isaksen, University of Oslo, Norway
Charles H. Jackman, NASA Goddard Space Flight Center, U.S.A.
Douglas E. Kinnison, Lawrence Livermore National Laboratory, U.S.A.
Giovanni Pitari, University L'Aquila, Italy
Helen Rogers, University of Cambridge, U.K.
Courtney J. Scott, AER, Inc., U.S.A.
Peter F. Vohralik, CSIRO, Australia
Vicky West, University of Edinburgh, U.K.

May 1999

Rationale

This report is intended to expand upon the IPCC Special Report on Aviation and the Global Atmosphere. It provides additional detail regarding the supersonic emission scenario calculations presented in Chapter 4—Modeling the Future Atmosphere. Due to the space limitations in that document, detailed plots and discussion for a majority of the model calculations were omitted. This document is intended to fill that gap and has been compiled for two reasons: (1) to aid those called upon to review the IPCC Special Report, and (2) to archive and document the calculations performed by nine modeling groups for up to 50 scenarios each. This document does not attempt to provide a synthesis of the modeling results or draw conclusions regarding the impact of aircraft on the atmosphere. That function is provided by the IPCC report.

The model descriptions and model results presented in this document represent the state of those models in 1997 when the calculations were performed. Because models are continually evolving and undergoing further development, these results should be considered as a historical snapshot. Please do not cite results presented herein without first obtaining permission from the group which performed the calculations.

Contents

Chapter 5

HSCT Perturbations for 2050

A total of 14 scenarios for the 2050 atmosphere were used in the IPCC supersonic aircraft assessment. Only 2-D models performed these scenario calculations. The scenarios were chosen to explore the effects of parametric modifications in the HSCT aircraft fleet, such as EI(NO_x), fleet size, cruise altitude, EI(SO_2), and SO_2 gas-to-particle conversion fraction. Most scenarios assumed the same subsonic fleet as was used for 2015. However, two scenarios (S11a and S12a) explored the effect of modifying the subsonic fleet, since projecting the fleet to 2050 is highly uncertain. The HSCT fleets consisted of either 500 or 1000 aircraft and were identical to those for 2015, though the larger fleet size was used for a majority of 2050 scenarios. A summary of the scenarios considered, along with the scenario designations, is given in Table 5.1. The reference atmosphere for each scenario is also listed in the table. Perturbations are given relative to these reference scenarios, which include identical boundary conditions and the same model formulation but omit the HSCT fleet.

Table 5.1: Specifications for Supersonic Aircraft Emission Scenarios in 2050

Scenario	Cl_y (ppbv)	Fleet Size	$EI(NO_x)$	Cruise Alt.	SAD Desc.	Special	Ref. Atm.
S9a	2.0	500	5	Std	SA0		D9
S9b	2.0	500	10	Std	SA0		D9
S9c	2.0	500	5	Std	SA1		D9
S9d	2.0	1000	5	Std	SA0		D9
S9e	2.0	1000	5	Std	SA2		D9
S9f	2.0	1000	5	Std	SA4		D9
S9g	2.0	1000	10	Std	SA0		D9
S9h	2.0	1000	5	Std	SA6		D9
S10a	2.0	1000	5	-2 km	SA0		D9
S10b	2.0	1000	10	-2 km	SA0		D9
S10c	2.0	1000	5	-2 km	SA6-2km		D9
S10d	2.0	1000	5	-2 km	SA2-2km		D9
S11a	2.0	1000	5	Std	SA0	2050 Subsonic IS92a	F
S12a	2.0	1000	5	Std	SA0	2050 Subsonic IS92e High Demand	G

5.1 H_2O Perturbations

Calculated changes to H_2O vapor due to HSCT emissions in 2050 are shown in Figure 5.1 for Scenario S9a relative to Scenario D9. These results are very similar to those for S1c-D, which includes the same 500 HSCT fleet but in 2015. Only the UNIVAQ model shows noticeable differences between 2015 and 2050 for this comparison. Figure 5.2 show perturbations to H_2O for Scenario S9d relative to D9, which includes a 1000 HSCT fleet. Perturbations in this case are double those from S9a-D9. Scenario S10a represent a 1000 HSCT fleet in 2050 with the cruise altitude shifted downward by 2 km. H_2O perturbations for this case are shown in Figure 5.3. The peak H_2O perturbation in this case is reduced by 50% (for AER and CSIRO), by 30% (for GSFC and UNIVAQ) and by 20% (for LLNL) relative to emissions at the standard cruise altitude.

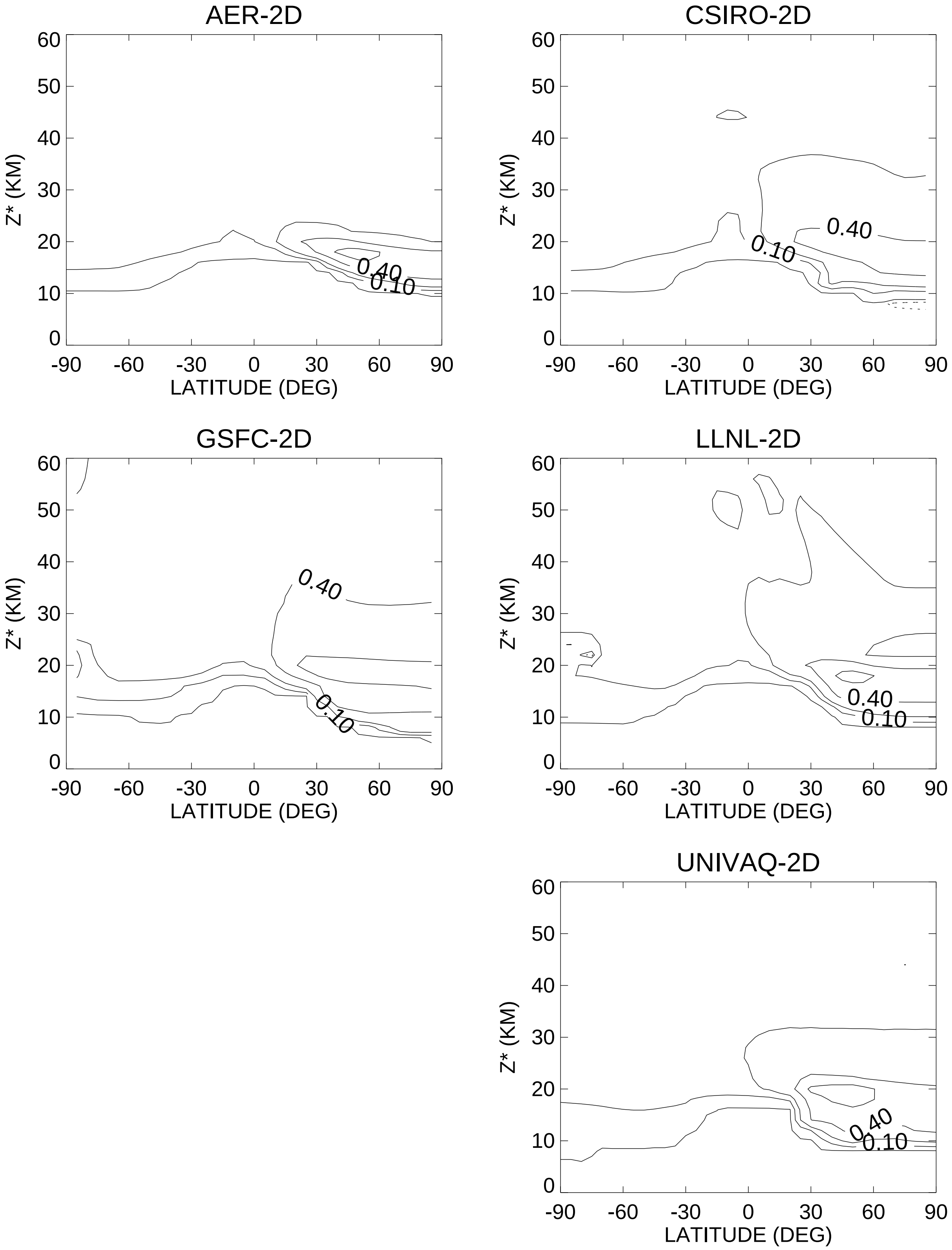

Figure 5.1: Calculated perturbation to H_2O (ppmv) as a function of latitude and altitude in June of 2050 due to H_2O emissions from a fleet of 500 HSCT aircraft under Scenario S9a relative to Scenario D9. Contours are 0, 0.1, 0.2, 0.4, 0.6 ppmv.

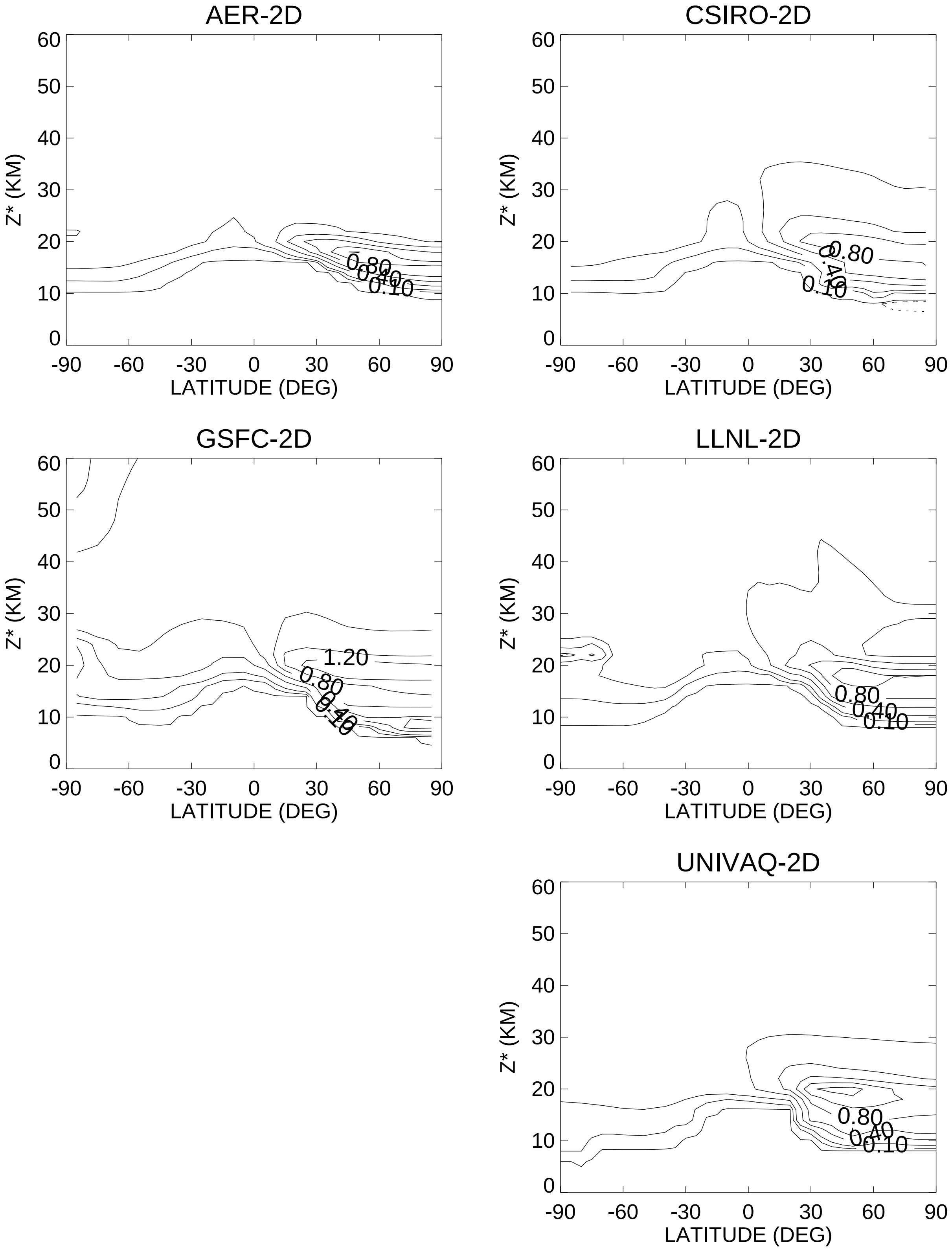

Figure 5.2: Calculated perturbation to H_2O (ppmv) as a function of latitude and altitude in June of 2050 due to H_2O emissions from a fleet of 1000 HSCT aircraft under Scenario S9d relative to Scenario D9. Contours are 0, 0.1 and 0.2 to 1.2 by 0.2 ppmv.

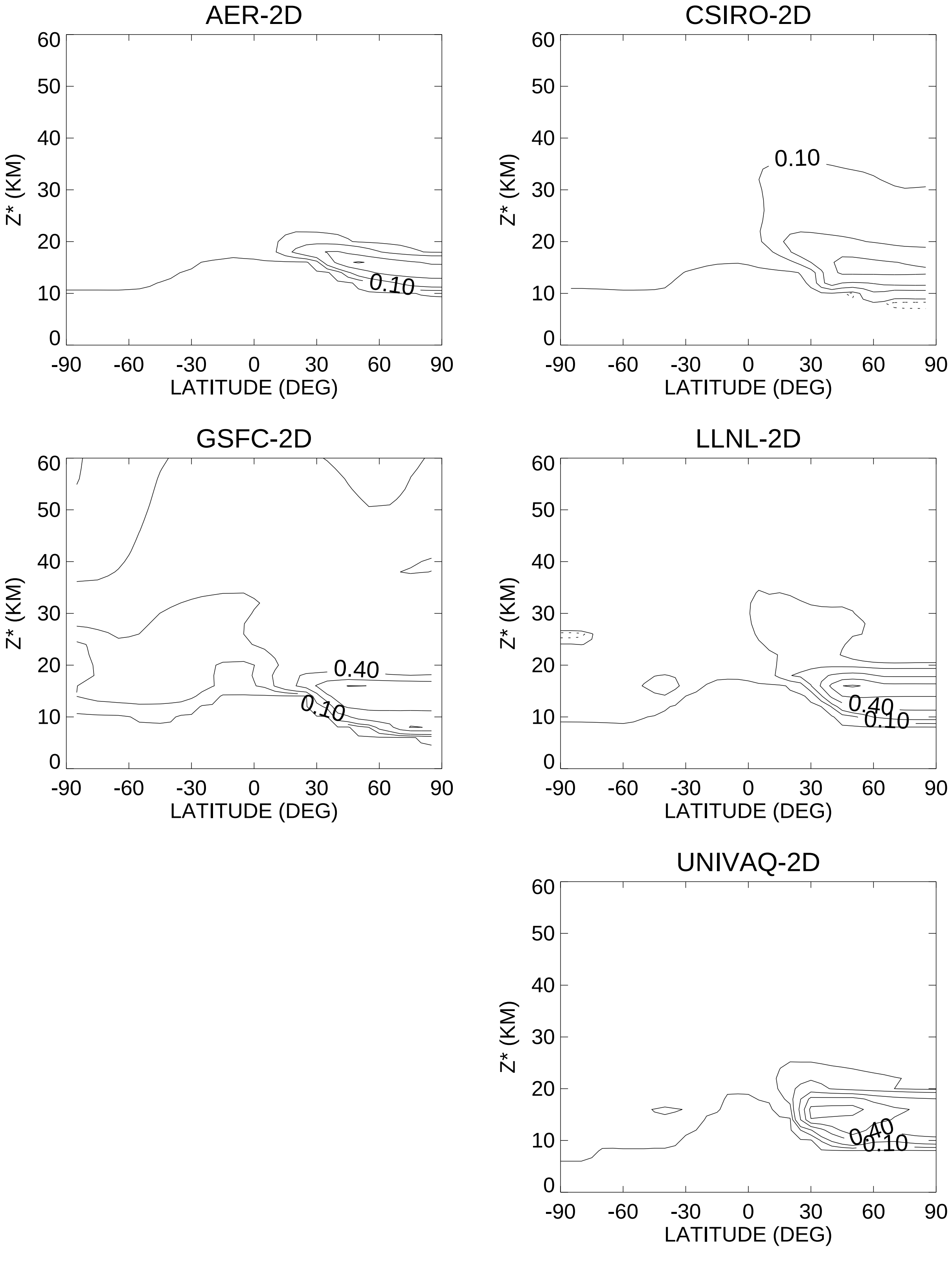

Figure 5.3: Calculated perturbation to H_2O (ppmv) as a function of latitude and altitude in June of 2050 due to H_2O emissions from a fleet of 1000 HSCT aircraft operating at 2 km below the nominal cruise altitude under Scenario S10a relative to Scenario D9. Contours are 0, 0.1 and 0.2 to 0.8 by 0.2 ppmv.

5.2 NO_y Perturbations

This section discusses calculated perturbation to NO_y for 2050. NO_x emission indices of 5 and 10 are used in the 2050 scenarios. Figure 5.4 shows the calculated perturbation to NO_y due to HSCT emissions from a fleet of 500 HSCTs with EI(NO_x)=5 in 2050 (Scenario S9a-D9). Differences from the similar 2015 perturbation (S1c-D) are small and mainly evident in the southern polar region where denitrification is calculated. For EI(NO_x)=10 with a 500 HSCT fleet (Scenario S9b-D9), NO_y perturbations are shown in Figure 5.5. These perturbations are roughly double those of S9a-D9 in the lower stratosphere.

Calculated NO_y perturbations for fleets of 1000 HSCTs in 2050 are shown in Figure 5.6 for an EI(NO_x) of 5 (S9d-D9) and in Figure 5.7 for an EI(NO_x) of 10 (S9g-D9). The NO_y perturbations are roughly twice those seen for the 500 HSCT fleet with the same EI(NO_x). In addition, the 1000 HSCT fleet with EI(NO_x)=5 has a similar NO_y perturbation to the 500 HSCT fleet with EI(NO_x)=10. Calculated maximum NO_y perturbations with EI(NO_x)=10 and 1000 aircraft range up to 2 or 3 ppbv in the models, which represents relative increases in NO_y of 20% or more at 45^oN and 20 km.

Scenario S10a and S10b represent 1000 HSCTs operating in 2050 at 2 km below the nominal cruise altitude with EI(NO_x)=5 and 10, respectively. Calculated NO_y perturbations for these scenarios are shown in Figures 5.8 and 5.9. NO_y perturbations are considerably reduced (by 50% in some cases) relative to similar scenarios at the standard cruise altitude.

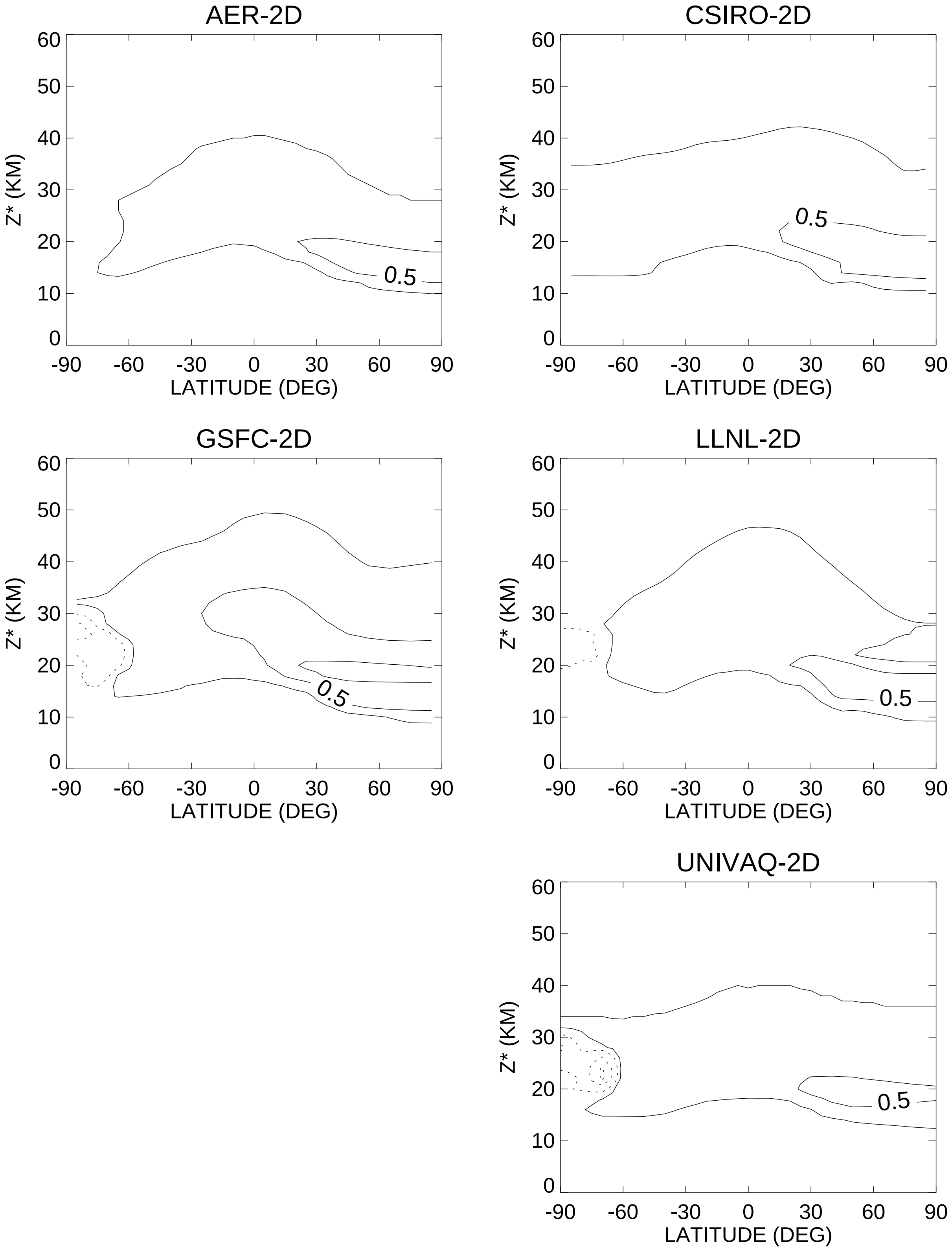

Figure 5.4: Calculated perturbations to NO_y (ppbv) as a function of latitude and altitude in June of 2050 due to NO_x emissions from a fleet of 500 HSCT aircraft with $EI(NO_x)=5$ under Scenario S9a relative to Scenario D9. Contours are -1, -0.5, 0, 0.5, 1.0 ppbv.

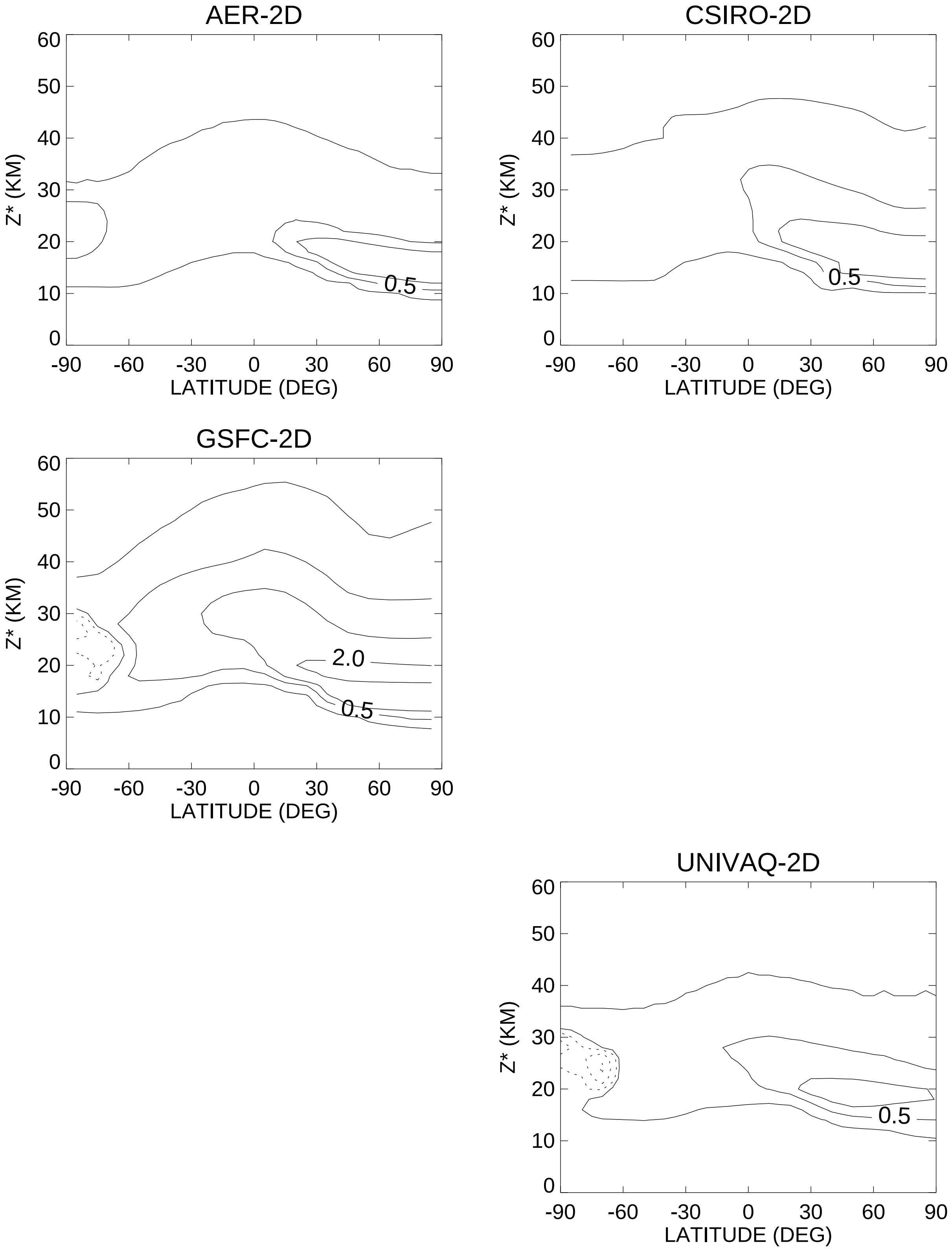

Figure 5.5: Calculated perturbations to NO_y (ppbv) as a function of latitude and altitude in June of 2050 due to NO_x emissions from a fleet of 500 HSCT aircraft with $EI(NO_x)=10$ under Scenario S9b relative to Scenario D9. Contours are -2, -1, -0.5, 0, 0.5, 1, 2 ppbv.

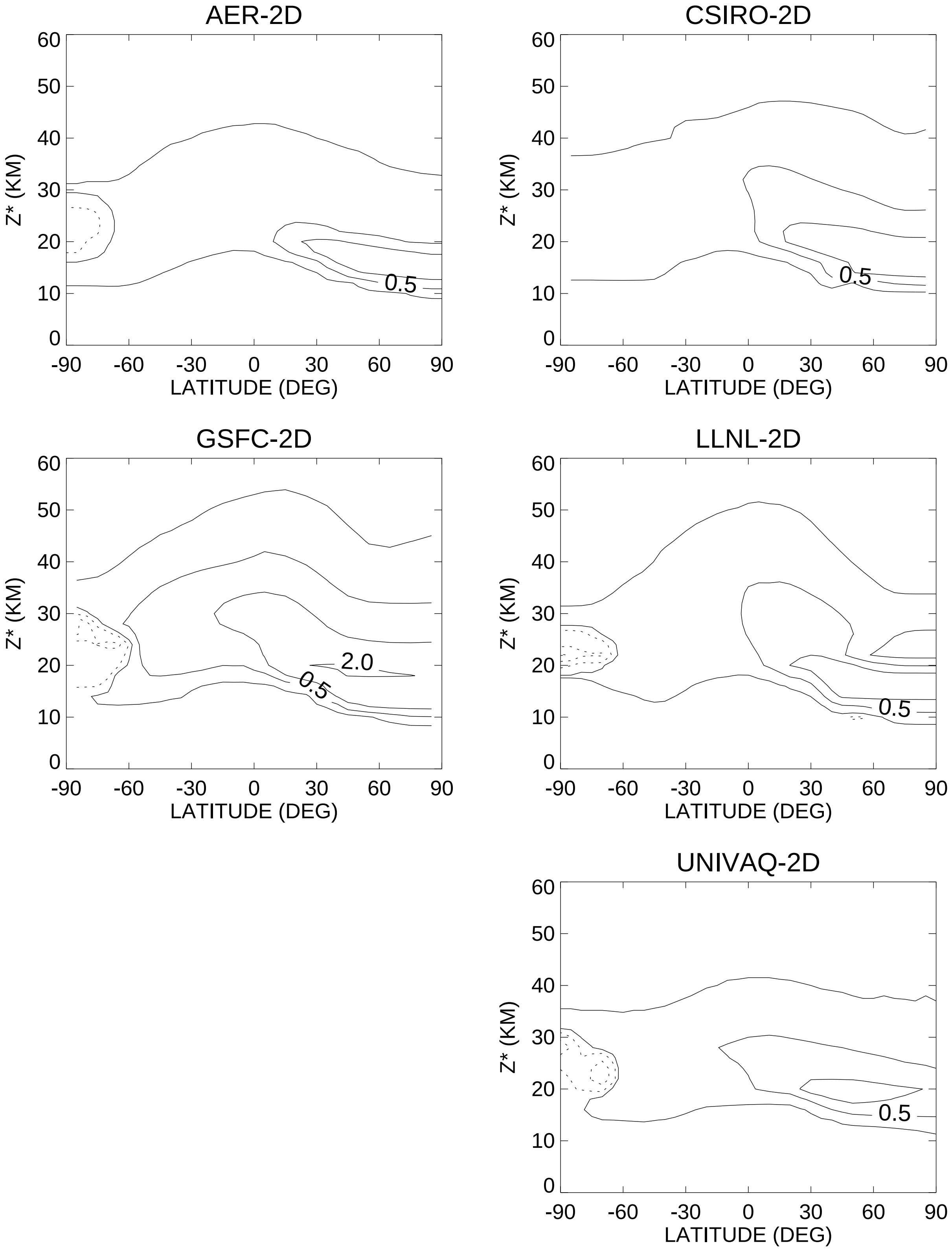

Figure 5.6: Calculated perturbations to NO_y (ppbv) as a function of latitude and altitude in June of 2050 due to NO_x emissions from a fleet of 1000 HSCT aircraft with $EI(NO_x)=5$ under Scenario S9d relative to Scenario D9. Contours are -1, -0.5, 0, 0.5, 1, 2 ppbv.

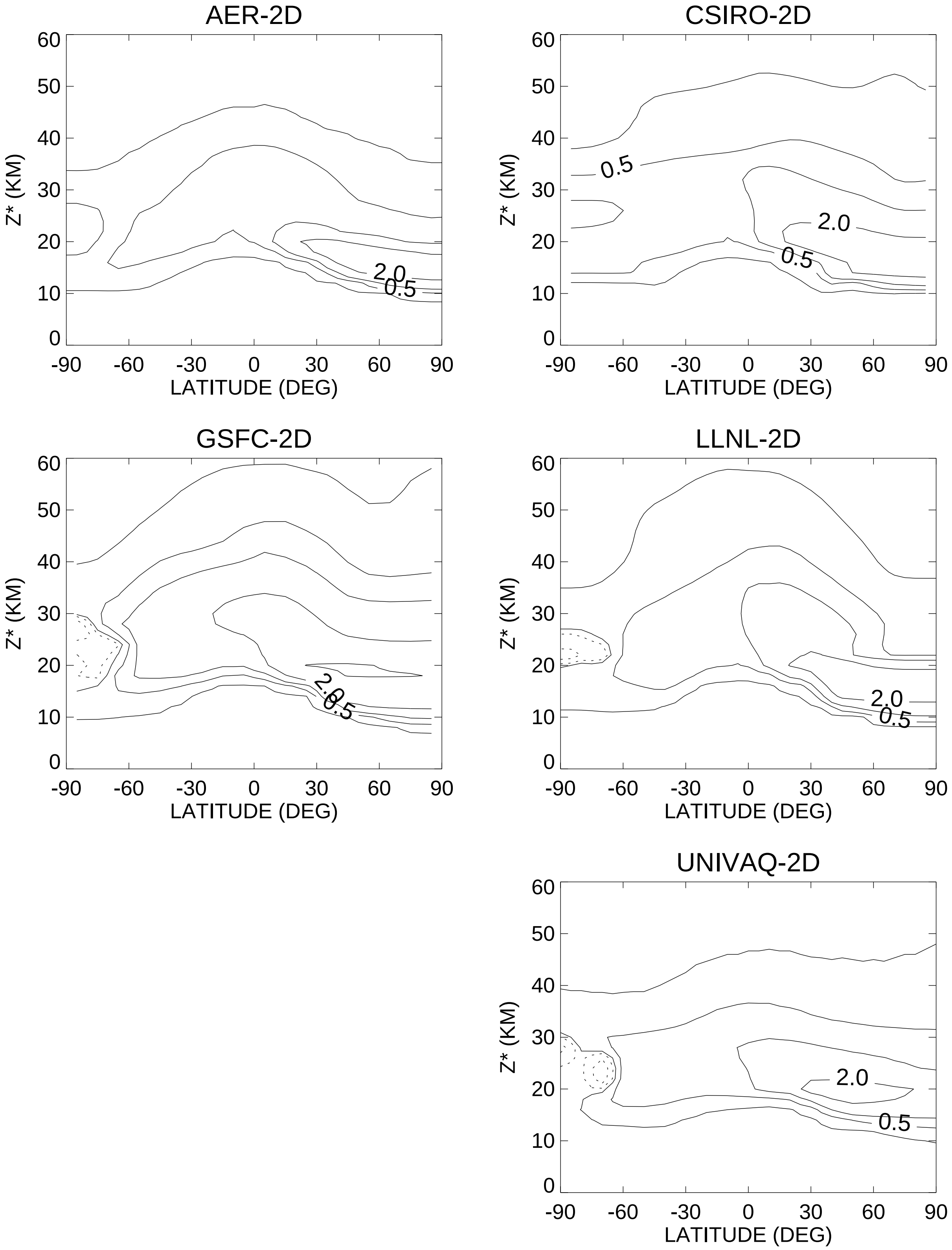

Figure 5.7: Calculated perturbations to NO_y (ppbv) as a function of latitude and altitude in June of 2050 due to NO_x emissions from a fleet of 1000 HSCT aircraft with $EI(NO_x)=10$ under Scenario S9g relative to Scenario D9. Contours are -1, -0.5, 0, 0.5, 1, 2, 3 ppbv.

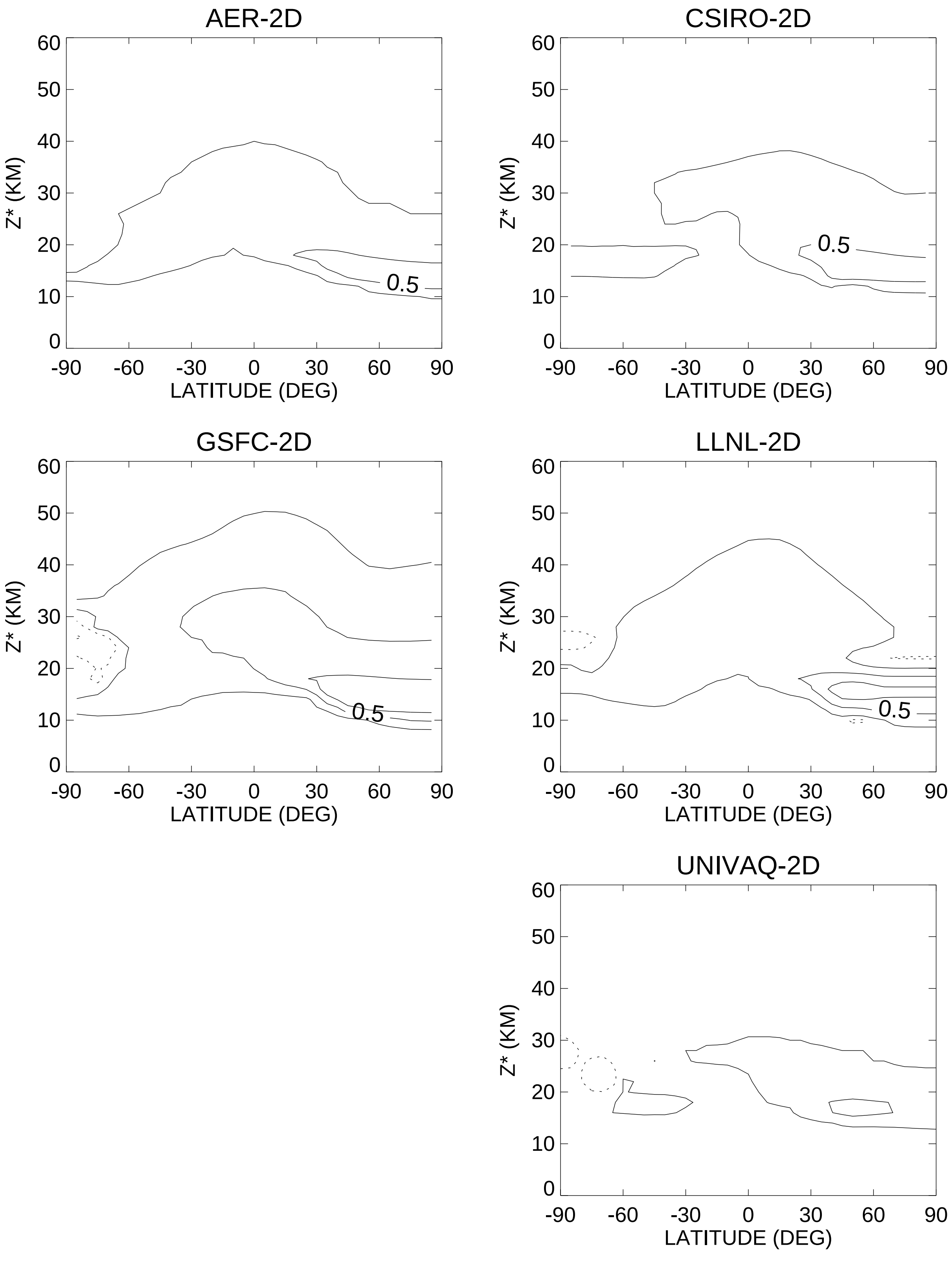

Figure 5.8: Calculated perturbations to NO_y (ppbv) as a function of latitude and altitude in June of 2050 due to NO_x emissions from a fleet of 1000 HSCT aircraft operating at 2 km below the nominal cruise altitude with $EI(NO_x)=5$ under Scenario S10a relative to Scenario D9. Contours are -0.5, 0, 0.5, 1 ppbv.

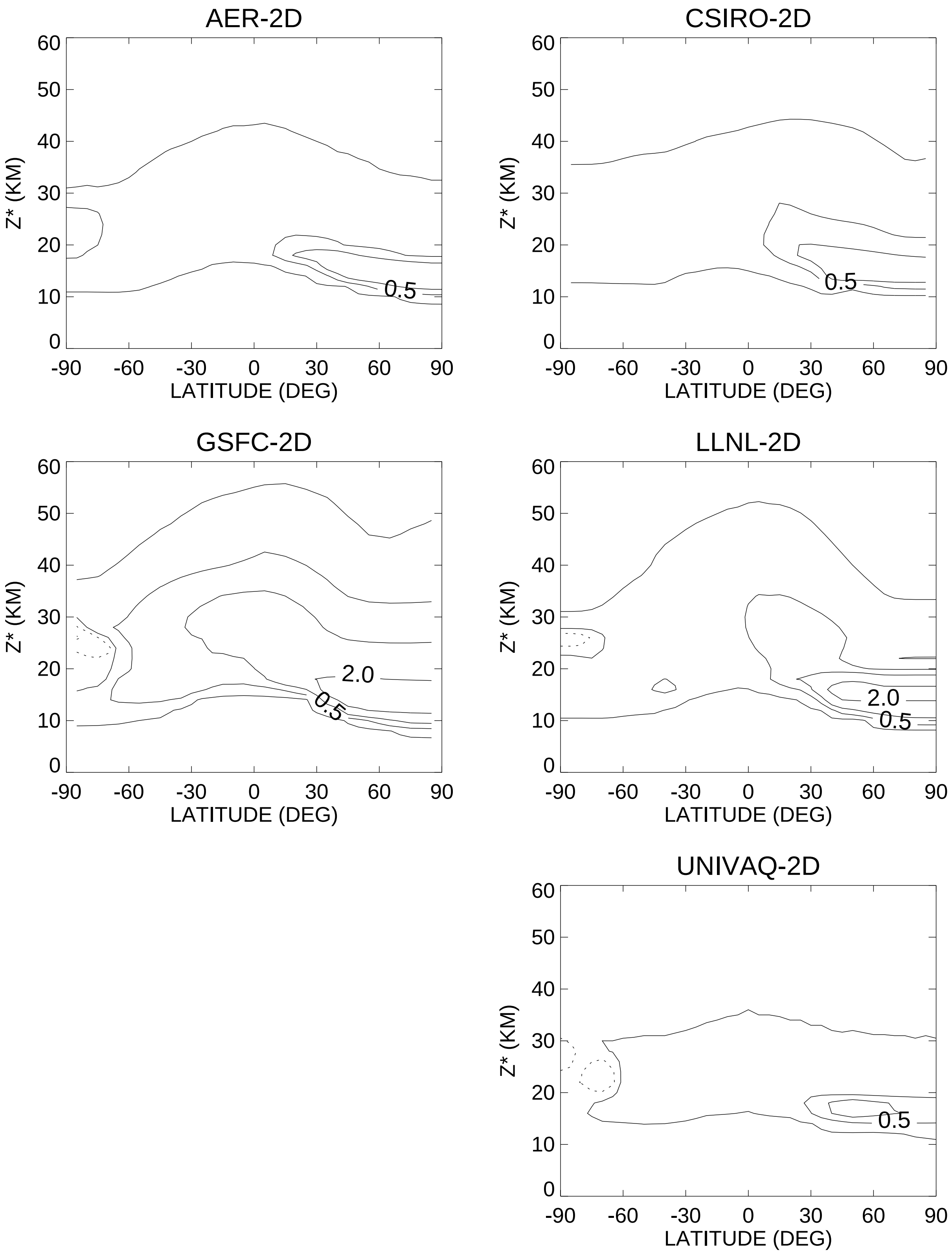

Figure 5.9: Calculated perturbations to NO_y (ppbv) as a function of latitude and altitude in June of 2050 due to NO_x emissions from a fleet of 1000 HSCT aircraft operating at 2 km below the nominal cruise altitude with $EI(NO_x)$=10 under Scenario S10b relative to Scenario D9. Contours are -0.5, 0, 0.5, 1, 2 ppbv.

Table 5.2: Annual Average Ozone Column Perturbations (in percent) for Each Model for the Northern Hemisphere (top number) and Southern Hemisphere (bottom number) in 2050

Scen -ario	Fleet Size	EI NO_x	SAD Desc.	Special	AER	GSFC	UNI-VAQ	LLNL	CSI -RO	THIN -AIR
S9a	500	5	SA0		-0.3	-0.5	0.03	-0.2	-0.3	-
					-0.1	-0.8	0.03	-0.1	-0.1	-
S9b	500	10	SA0		-0.4	-0.8	0.1	-	-0.4	-
					-0.09	-0.8	0.08	-	-0.2	-
S9c	500	5	SA1		-0.5	-0.8	-0.3	-	-0.4	-
					-0.2	-1	-0.08	-	-0.04	-
S9d	1000	5	SA0		-0.6	-1	-0.08	-0.5	-0.5	-
					-0.2	-1.4	-0.03	-0.3	-0.2	-
S9e	1000	5	SA2		-0.8	-1.3	-0.5	-0.8	-0.6	-
					-0.3	-1.7	-0.2	-0.6	-0.09	-
S9f	1000	5	SA4		-0.9	-1.4	-0.6	-0.9	-0.6	-
					-0.3	-1.8	-0.2	-0.6	-0.07	-
S9g	1000	10	SA0		-0.7	-1.6	0.02	-0.8	-0.9	-
					-0.2	-1.5	0.08	-0.2	-0.4	-
S9h	1000	5	SA6		-0.8	-1.1	-0.3	-0.6	-0.6	-
					-0.3	-1.5	-0.09	-0.4	-0.2	-
S10a	1000	5	SA0	Cruise -2 km	-0.2	-0.3	0.05	-0.1	-0.1	-
					-0.05	-0.5	0.05	-0.02	-0.05	-
S10b	1000	10	SA0	Cruise -2 km	-0.2	-0.6	0.2	-0.2	-0.09	-
					+0.01	-0.5	0.1	0.04	-0.05	-
S10c	1000	5	SA6-2km	Cruise -2 km	-0.4	-0.5	-0.1	-0.3	-0.2	-
					-0.1	-0.6	0.001	-0.2	-0.04	-
S10d	1000	5	SA2-2km	Cruise -2 km	-0.5	-0.6	-0.1	-0.4	-0.2	-
					-0.1	-0.6	-0.02	-0.2	-0.03	-
S11a	1000	5	SA0	Subsonic	-0.5	-0.9	-0.1	-	-0.5	-
				IS92a	-0.2	-1.4	-0.03	-	-0.2	-
S12a	1000	5	SA0	Subsonic	-0.5	-0.9	-0.1	-	-0.5	-
				High Demand	-0.2	-1.4	-0.03	-	-0.2	-

5.3 O_3 Perturbations

A synopsis of ozone column changes calculated for the 2050 scenarios is listed in Table 5.2 for the northern and southern hemisphere annual averages for each model. In the following sections, changes in ozone are plotted for each scenario. Changes in ozone as a function of altitude and latitude are shown for March, June, and October. These months were chosen to present both polar regions in their respective springtimes, since the northern and southern polar regions often respond differently to perturbations in H_2O and NO_x. Changes in total ozone as a function of latitude and season are also shown, since total column ozone is related to uv radiation which reaches the ground.

5.3.1 Base Scenarios (S9a,b,d,g)

These 2050 scenarios represent either 500 or 1000 aircraft HSCT fleets with $EI(NO_x)$ of 5 or 10, no aircraft sulfur emissions, and sulfate surface area densities of SA0. The background Cl_y for 2050 is 2.0 ppbv, and boundary conditions are as listed in Table 3.1.

Scenario S9a represents 500 HSCT aircraft with $EI(NO_x)=5$ and SA0 sulfate surface area density. Ozone changes for this scenario are shown in Figures 5.10, 5.11, and 5.12 for March, June, and October, respectively. Ozone changes are similar to or somewhat less than those for S1c-D, which represents the same aircraft fleet in 2015. The GSFC model, however, calculated more ozone depletion for this scenario in the southern hemisphere lower stratosphere in March and June. Changes in column ozone are shown in Figure 5.13. The UNIVAQ model shows positive ozone changes over most of the globe. The CSIRO and LLNL models show ozone depletions of less than 0.5% over most of the globe.

The NO_x emission index is increased to 10 in Scenario S9b, which represents 500 HSCT aircraft and SA0 sulfate surface area density. Figures 5.14, 5.15, and 5.16 show changes in ozone for this scenario relative to Scenario D9. Compared with S9a-D9, the ozone perturbations are smaller in the lower stratosphere and larger near 30 km. Column ozone changes, shown in Figure 5.17, are similar to S9a-D9, except for the CSIRO model, which shows increase depletion in the northern hemisphere.

Scenario S9d represents 1000 HSCT aircraft operating in 2050 with $EI(NO_x)=5$, no sulfur emissions, and sulfate surface area density of SA0. Calculated ozone changes for this scenario, which are shown in Figures 5.18-5.20, are approximately twice those found with 500 HSCT aircraft (Scenario S9a-D9). The GSFC model calculated ozone depletion in the southern hemisphere lower stratosphere of over 5%. Changes in column ozone for S9d-D9 are shown in Figure 5.21. Column ozone changes are also roughly double those of S9a-D9.

Scenario S9g also represents 1000 HSCT aircraft but with $EI(NO_x)=10$. Figures 5.22-5.24 show changes in ozone for this scenario relative to Scenario D9. Ozone depletions are significantly larger than for S9d-D9 in both the lower and middle stratosphere, though the GSFC and LLNL models show less ozone depletion in the southern hemisphere lower stratosphere. Changes in ozone column are shown in Figure 5.25. Annual average northern hemisphere ozone depletion is greater than 0.7% for 4 of the 5 models that performed this simulation.

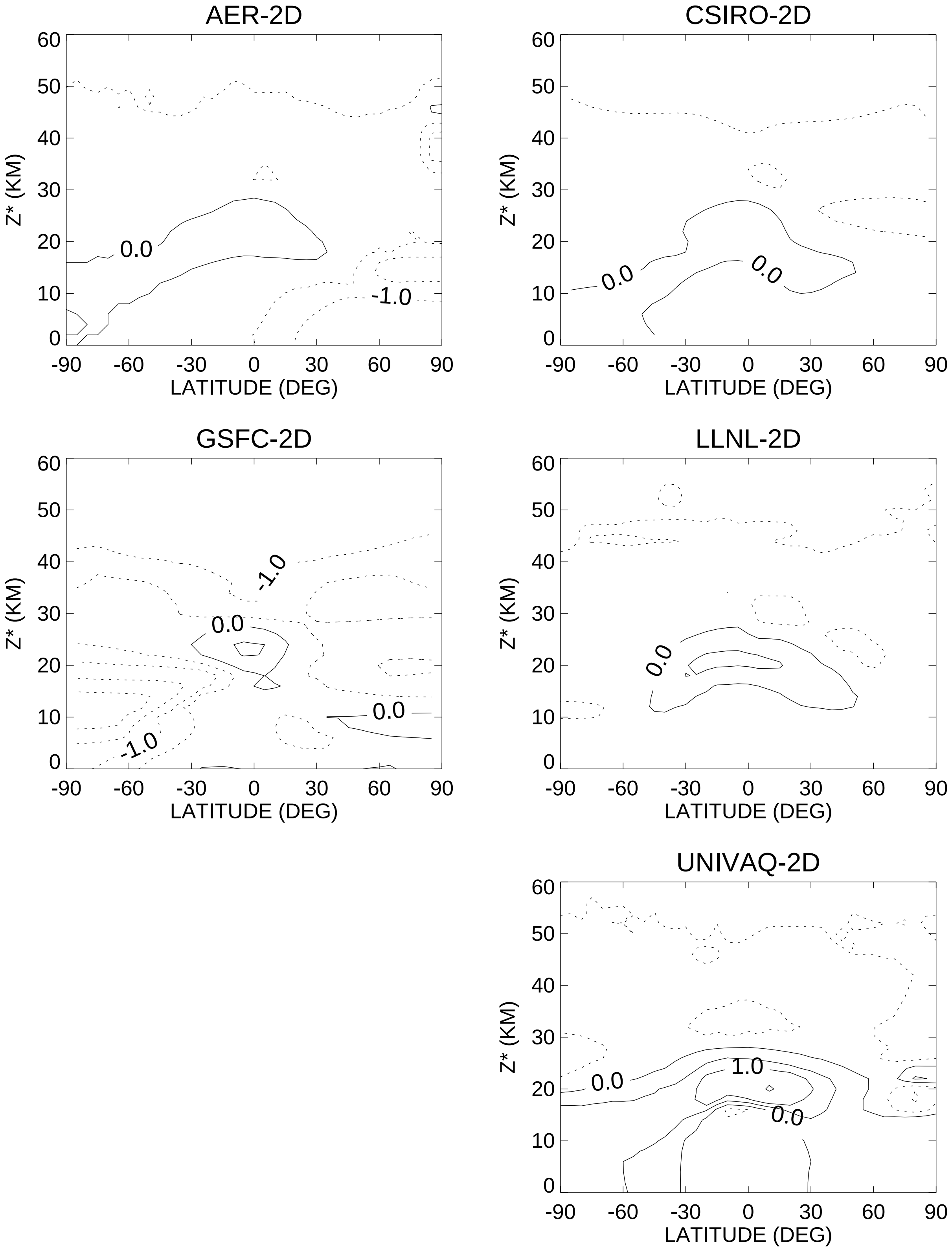

Figure 5.10: Calculated perturbations to O_3 (percent) as a function of latitude and altitude in March of 2050 due to emissions from a fleet of 500 HSCT aircraft with EI(NO_x)=5 under Scenario S9a relative to Scenario D9. Contours are -3, -2, -1, -0.5, 0, 0.5, 1, 2.

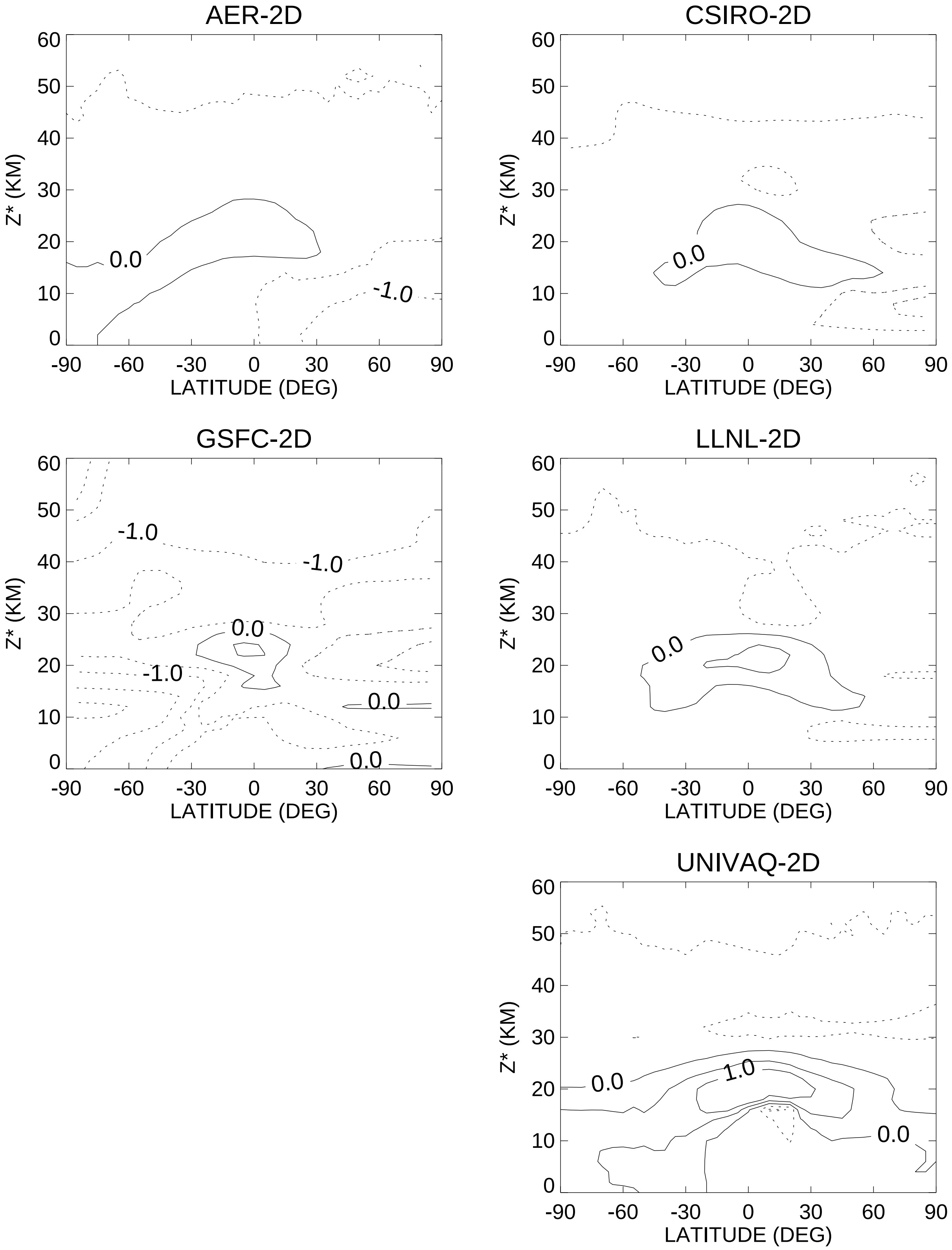

Figure 5.11: Calculated perturbations to O_3 (percent) as a function of latitude and altitude in June of 2050 due to emissions from a fleet of 500 HSCT aircraft with EI(NO_x)=5 under Scenario S9a relative to Scenario D9. Contours are -3, -2, -1, -0.5, 0, 0.5, 1.

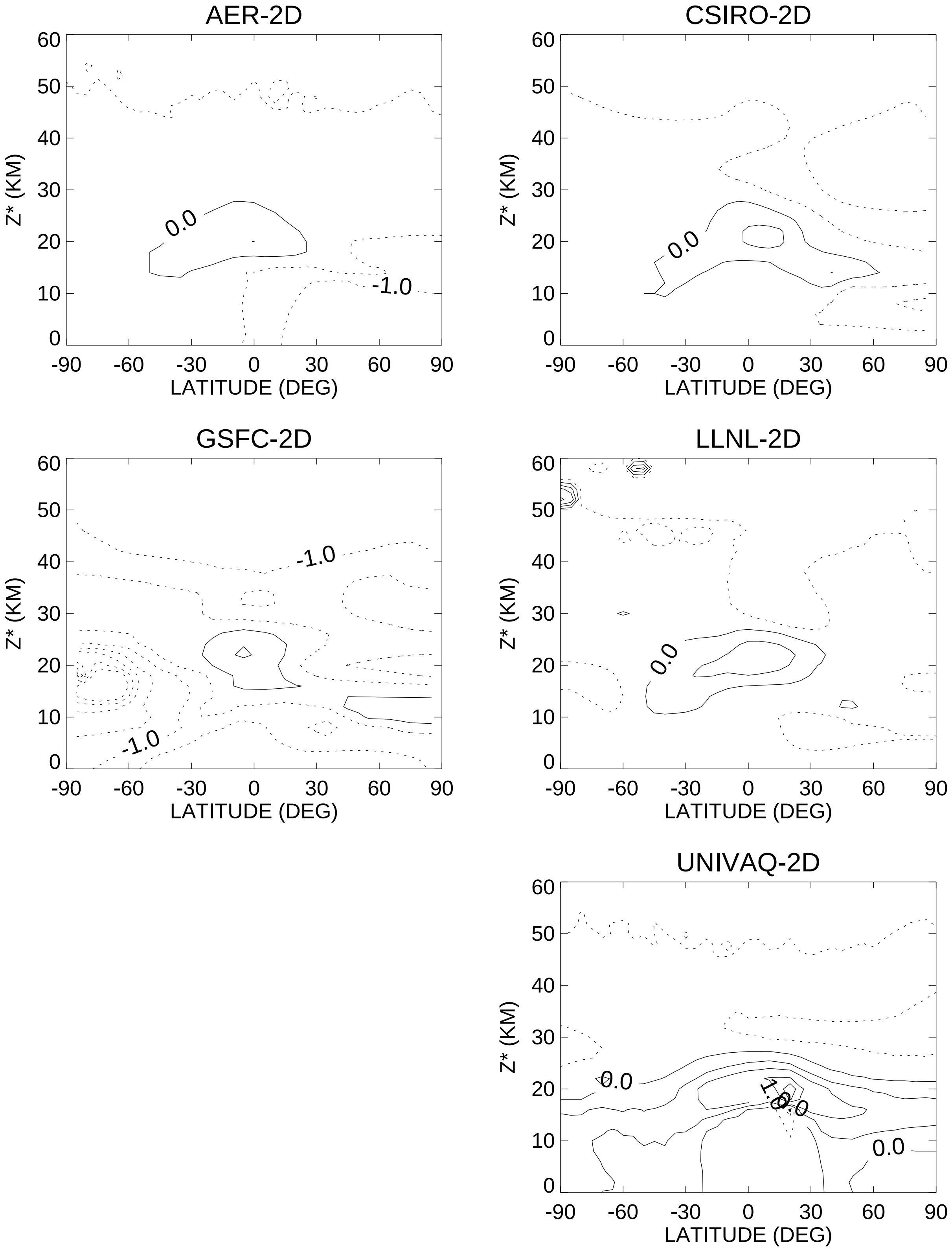

Figure 5.12: Calculated perturbations to O_3 (percent) as a function of latitude and altitude in October of 2050 due to emissions from a fleet of 500 HSCT aircraft with EI(NO_x)=5 under Scenario S9a relative to Scenario D9. Contours are -5, -4, -3, -2, -1, -0.5, 0, 0.5, 1, 2, 3.

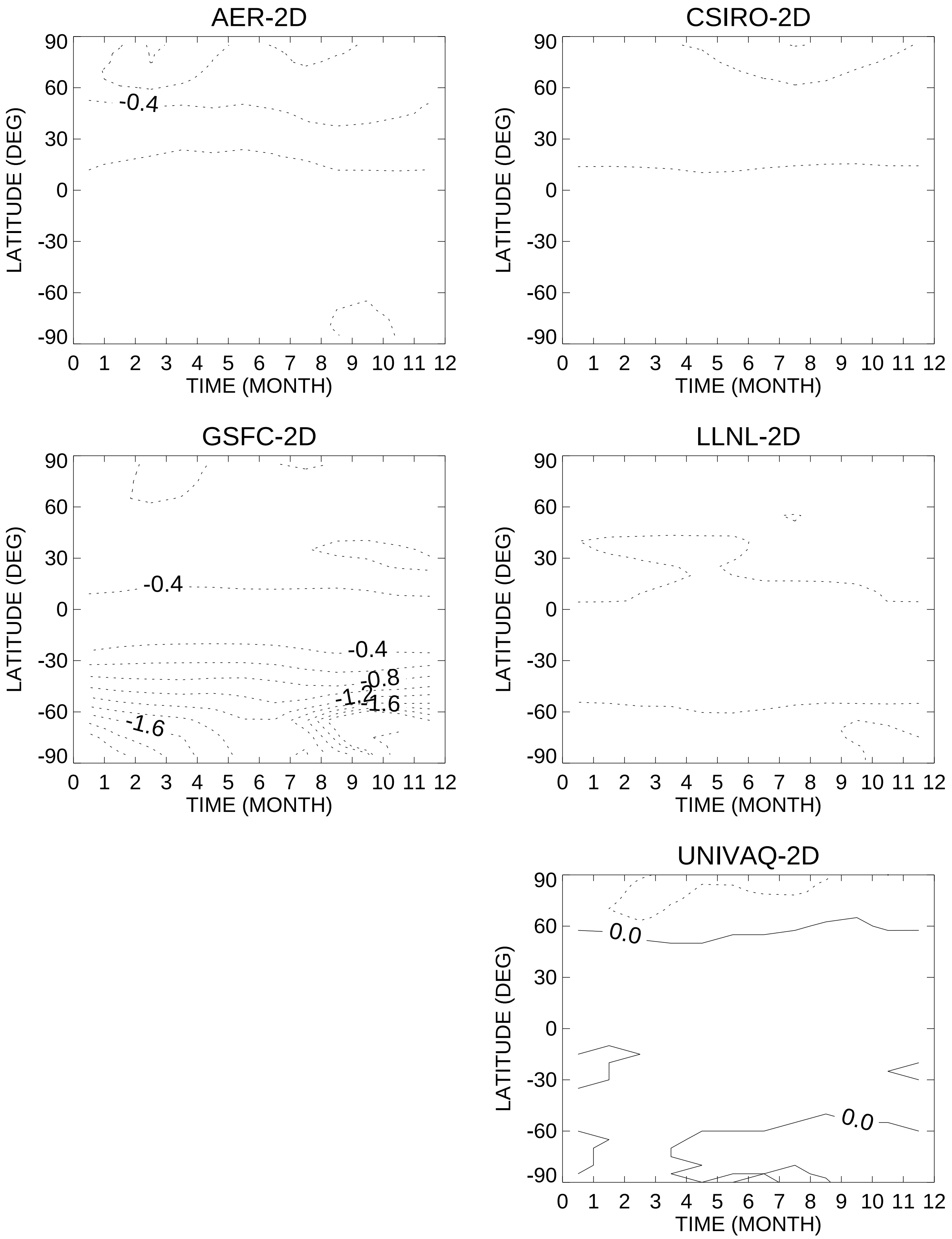

Figure 5.13: Calculated perturbations to column O_3 (percent) as a function of latitude and season in 2050 due to emissions from a fleet of 500 HSCT aircraft with EI(NO_x)=5 under Scenario S9a relative to Scenario D9. Contours are -3 and -2 to 0 by 0.2.

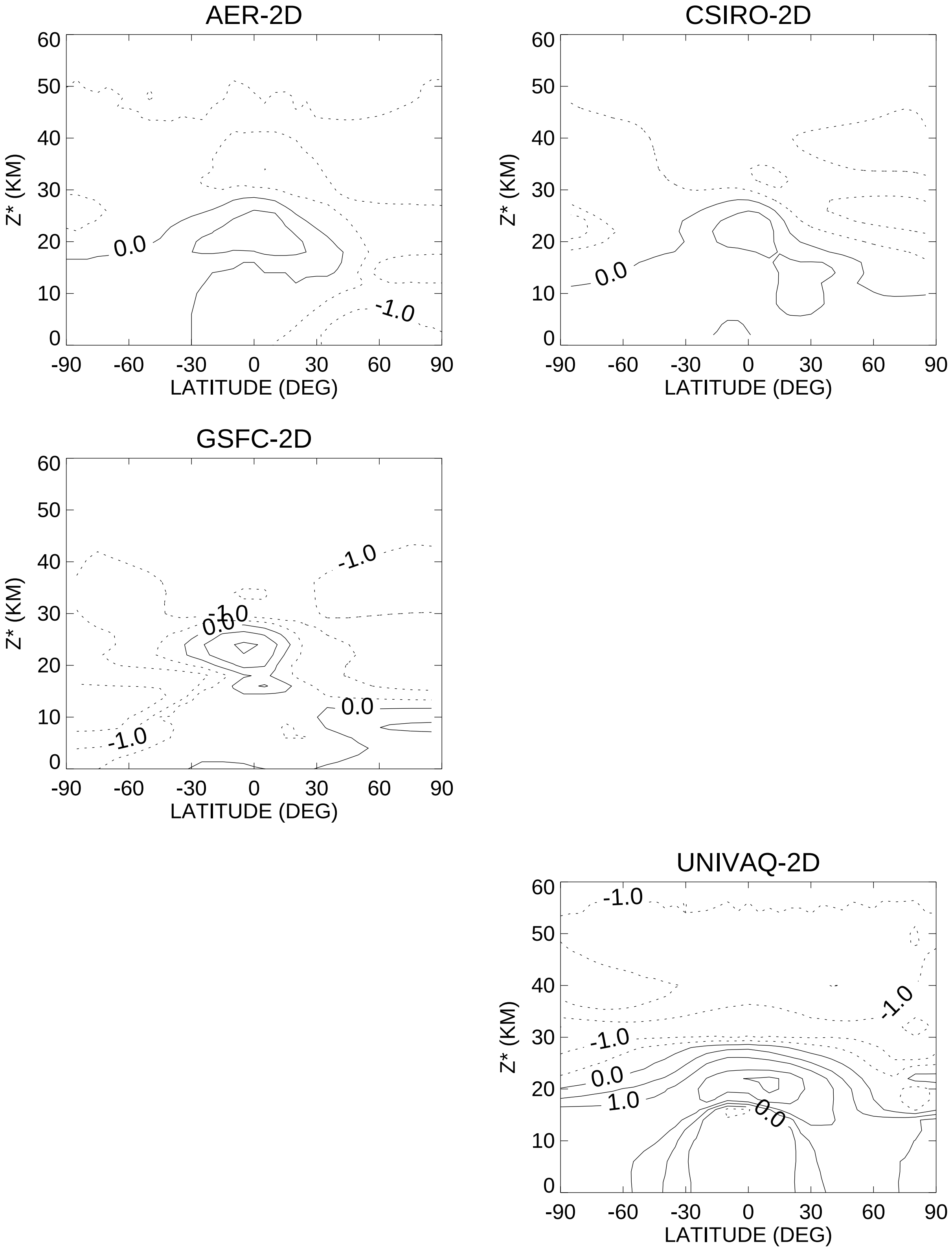

Figure 5.14: Calculated perturbations to O_3 (percent) as a function of latitude and altitude in March of 2050 due to emissions from a fleet of 500 HSCT aircraft with EI(NO_x)=10 under Scenario S9b relative to Scenario D9. Contours are -2, -1, -0.5, 0, 0.5, 1, 2, 3.

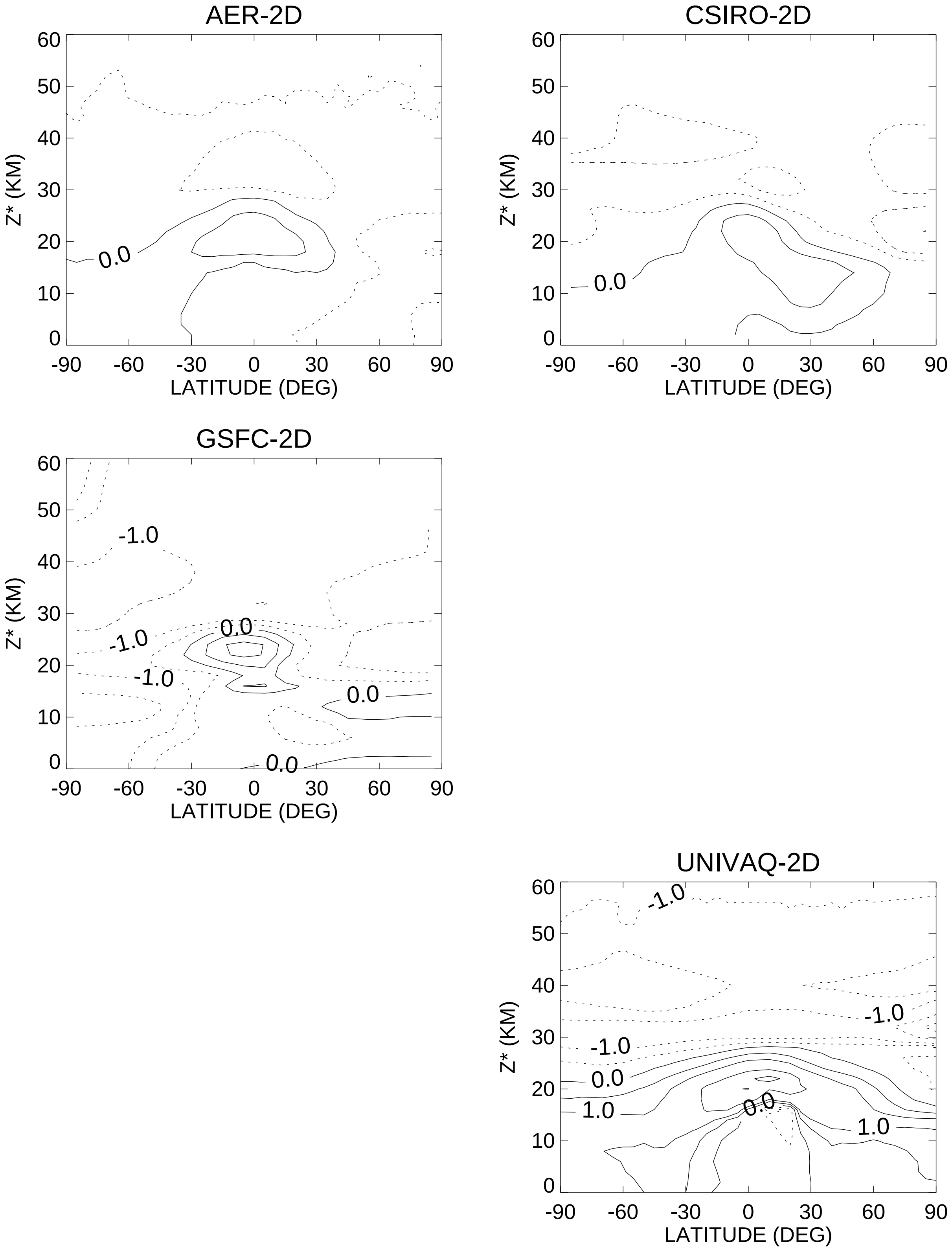

Figure 5.15: Calculated perturbations to O_3 (percent) as a function of latitude and altitude in June of 2050 due to emissions from a fleet of 500 HSCT aircraft with $EI(NO_x)$=10 under Scenario S9b relative to Scenario D9. Contours are -2, -1, -0.5, 0, 0.5, 1, 2, 3.

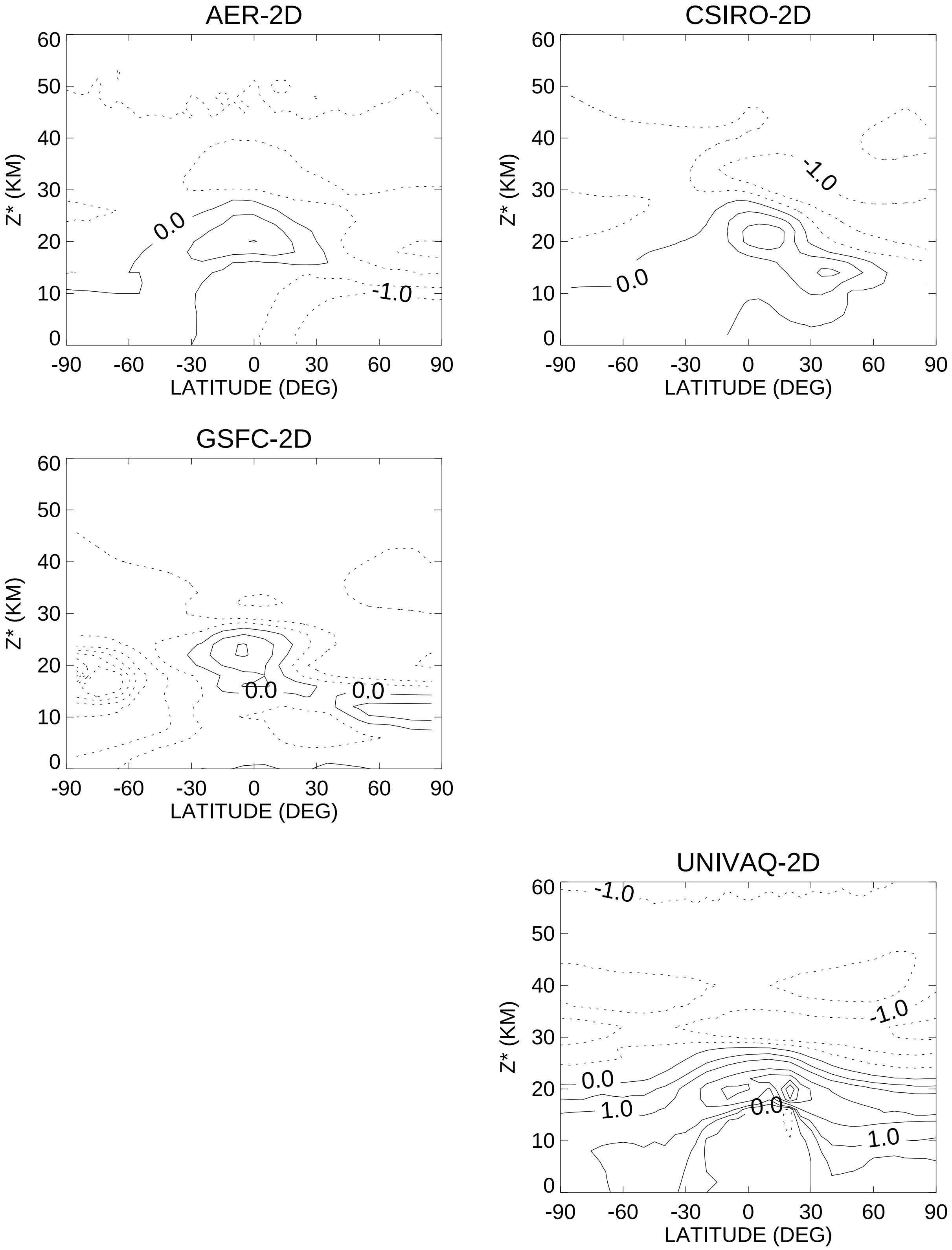

Figure 5.16: Calculated perturbations to O_3 (percent) as a function of latitude and altitude in October of 2050 due to emissions from a fleet of 500 HSCT aircraft with $EI(NO_x)=10$ under Scenario S9b relative to Scenario D9. Contours are -5, -4, -3, -2, -1, -0.5, 0, 0.5, 1, 2, 3, 4, 5.

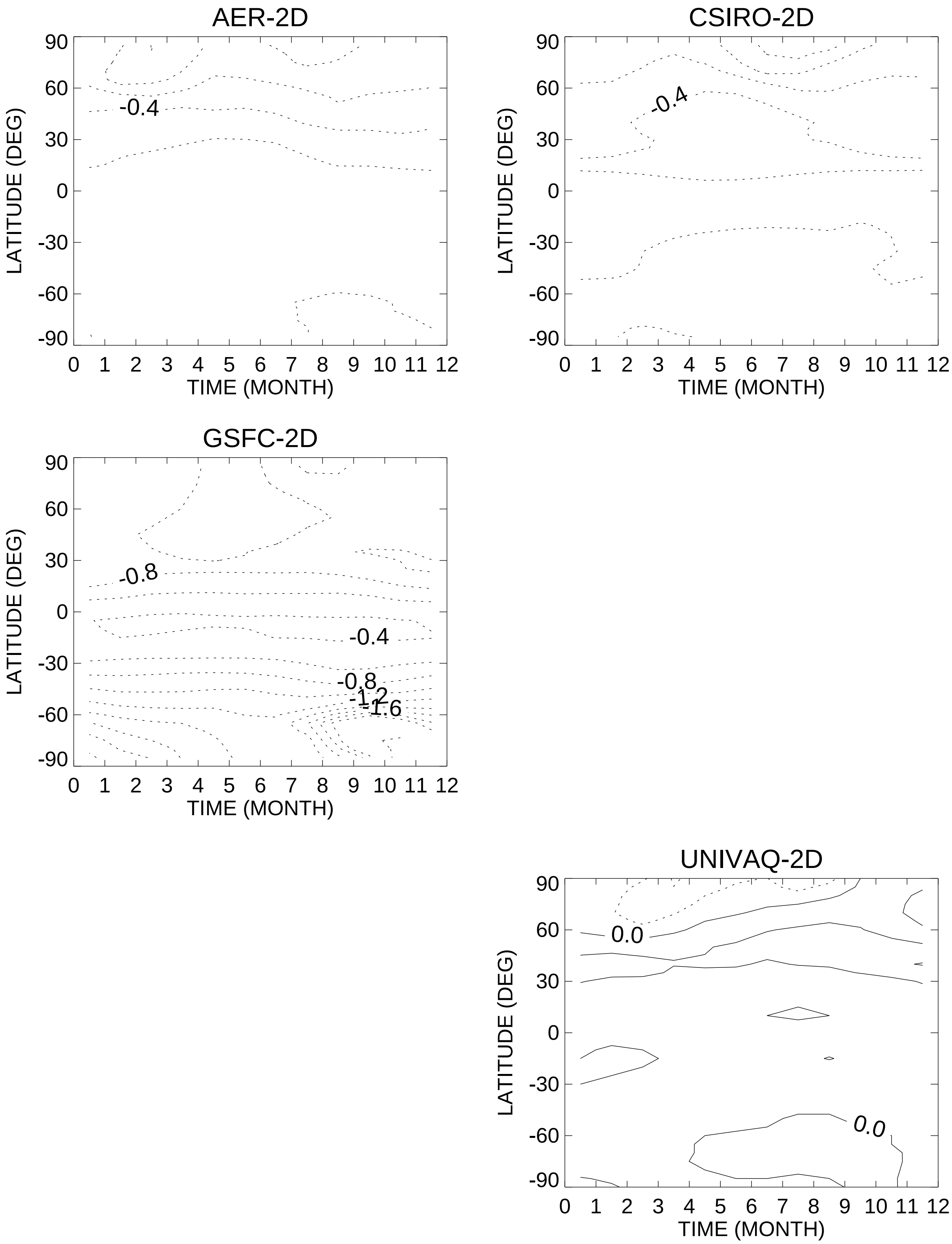

Figure 5.17: Calculated perturbations to column O_3 (percent) as a function of latitude and season in 2050 due to emissions from a fleet of 500 HSCT aircraft with $EI(NO_x)$=10 under Scenario S9b relative to Scenario D9. Contours are -3 and -2 to 0.2 by 0.2.

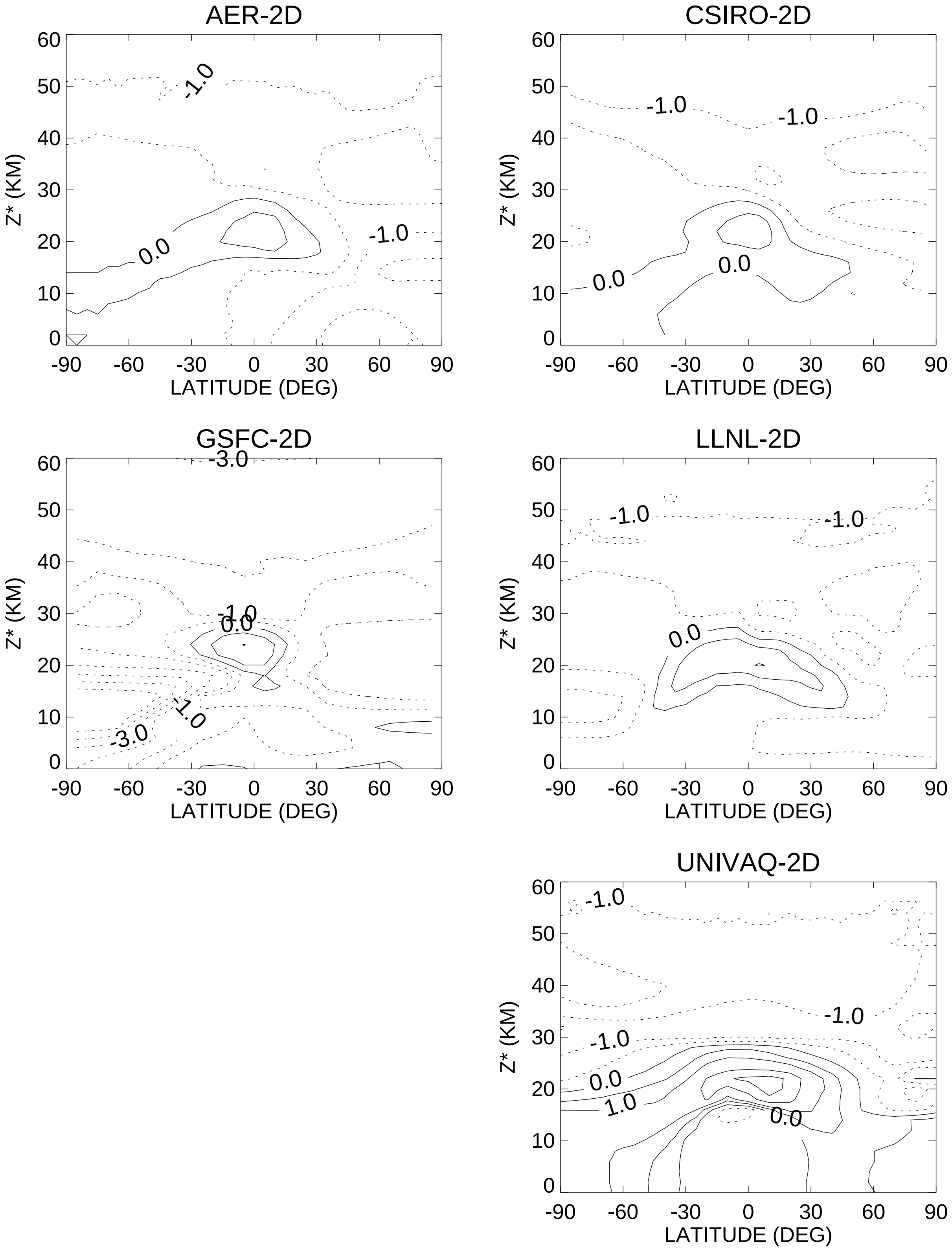

Figure 5.18: Calculated perturbations to O_3 (percent) as a function of latitude and altitude in March of 2050 due to emissions from a fleet of 1000 HSCT aircraft with $EI(NO_x)=5$ under Scenario S9d relative to Scenario D9. Contours are -5, -4, -3, -2, -1, -0.5, 0, 0.5, 1, 2, 3.

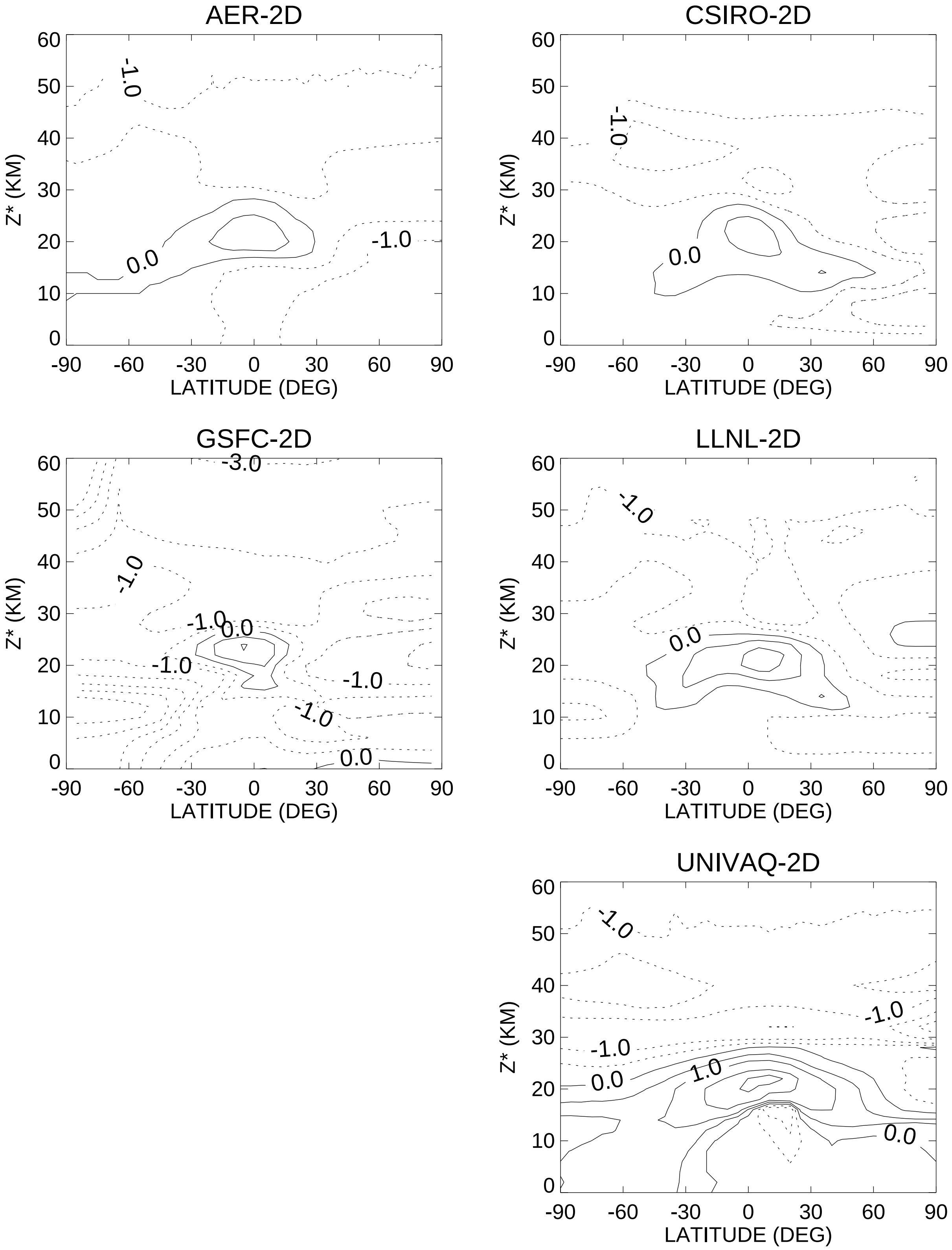

Figure 5.19: Calculated perturbations to O_3 (percent) as a function of latitude and altitude in June of 2050 due to emissions from a fleet of 1000 HSCT aircraft with $EI(NO_x)=5$ under Scenario S9d relative to Scenario D9. Contours are -5, -4, -3, -2, -1, -0.5, 0, 0.5, 1, 2, 3.

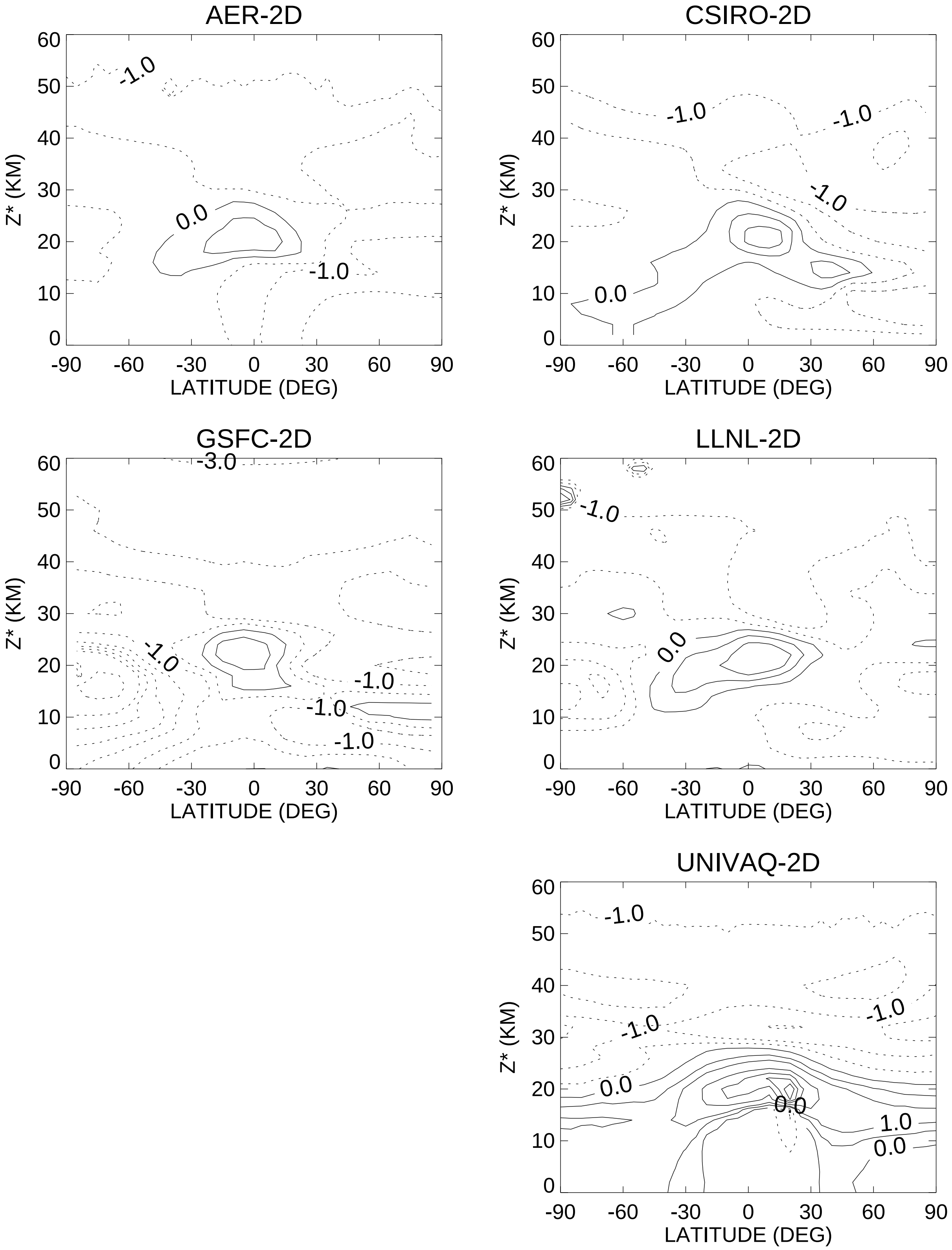

Figure 5.20: Calculated perturbations to O_3 (percent) as a function of latitude and altitude in October of 2050 due to emissions from a fleet of 1000 HSCT aircraft with EI(NO_x)=5 under Scenario S9d relative to Scenario D9. Contours are -10, -5, -4, -3, -2, -1, -0.5, 0, 0.5, 1, 2, 3, 4, 5.

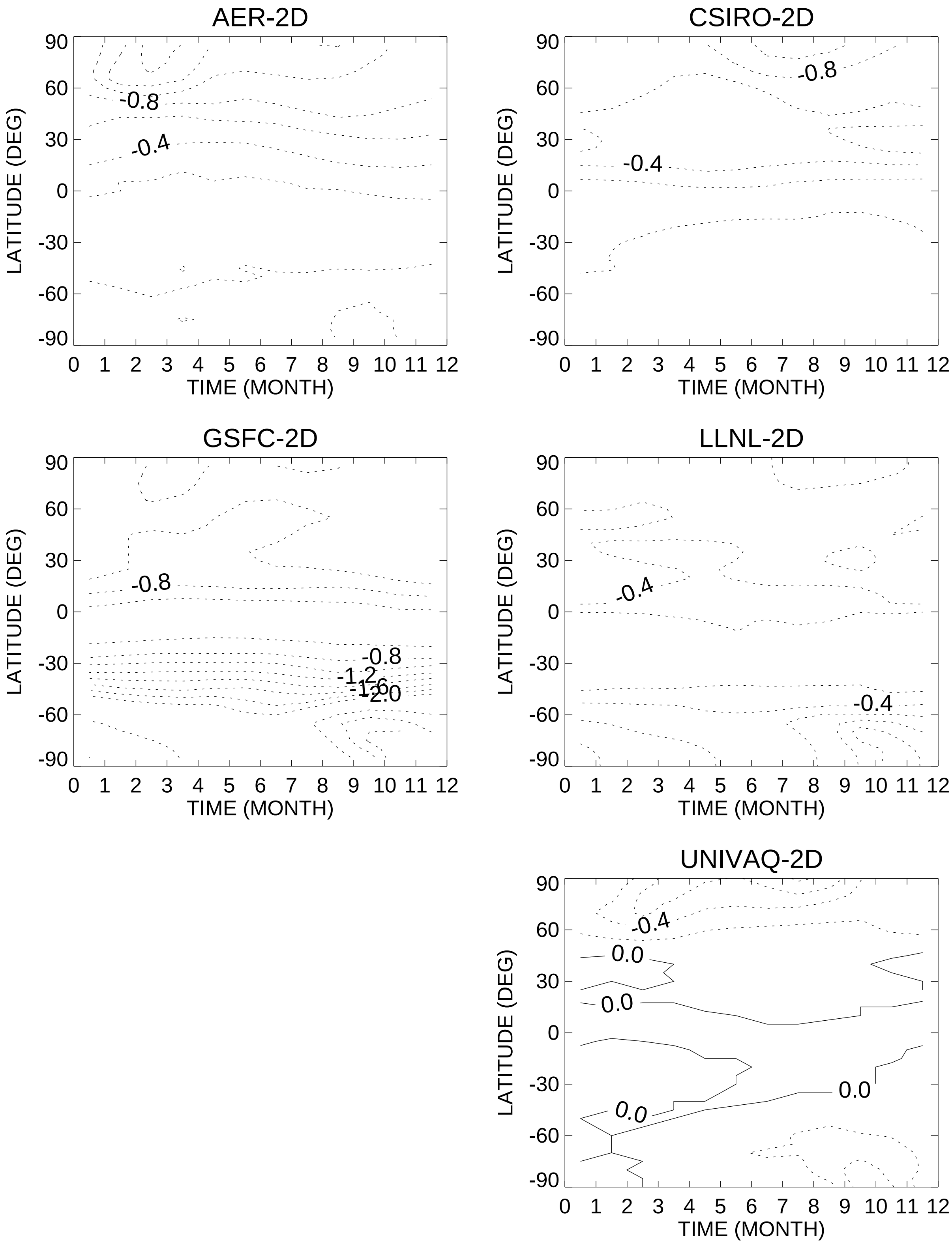

Figure 5.21: Calculated perturbations to column O_3 (percent) as a function of latitude and season in 2050 due to emissions from a fleet of 1000 HSCT aircraft with EI(NO_x)=5 under Scenario S9d relative to Scenario D9. Contours are -5, -4, -3 and -2 to 0 by 0.2.

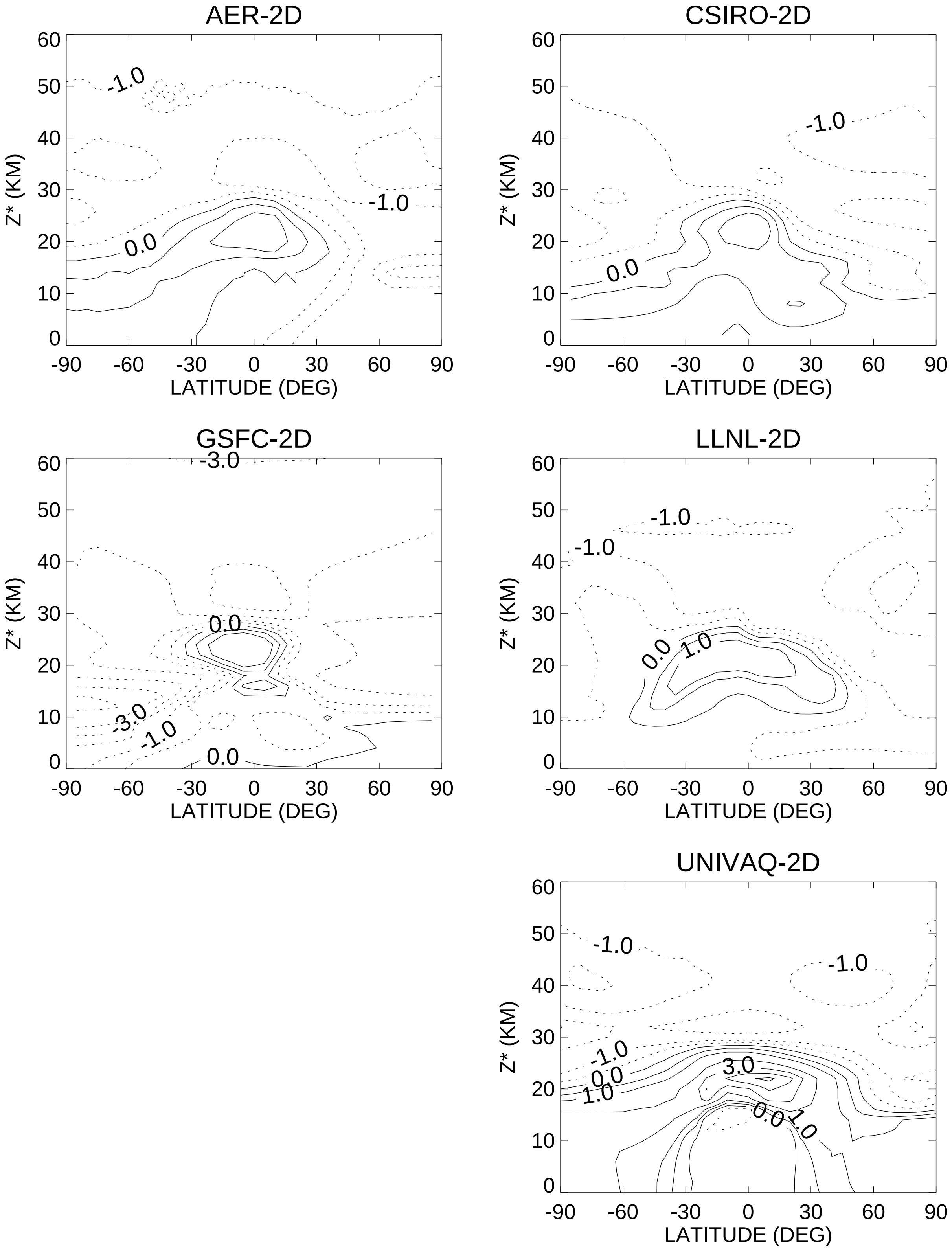

Figure 5.22: Calculated perturbations to O_3 (percent) as a function of latitude and altitude in March of 2050 due to emissions from a fleet of 1000 HSCT aircraft with $EI(NO_x)=10$ under Scenario S9g relative to Scenario D9. Contours are -5, -4, -3, -2, -1, -0.5, 0, 0.5, 1, 2, 3, 4, 5.

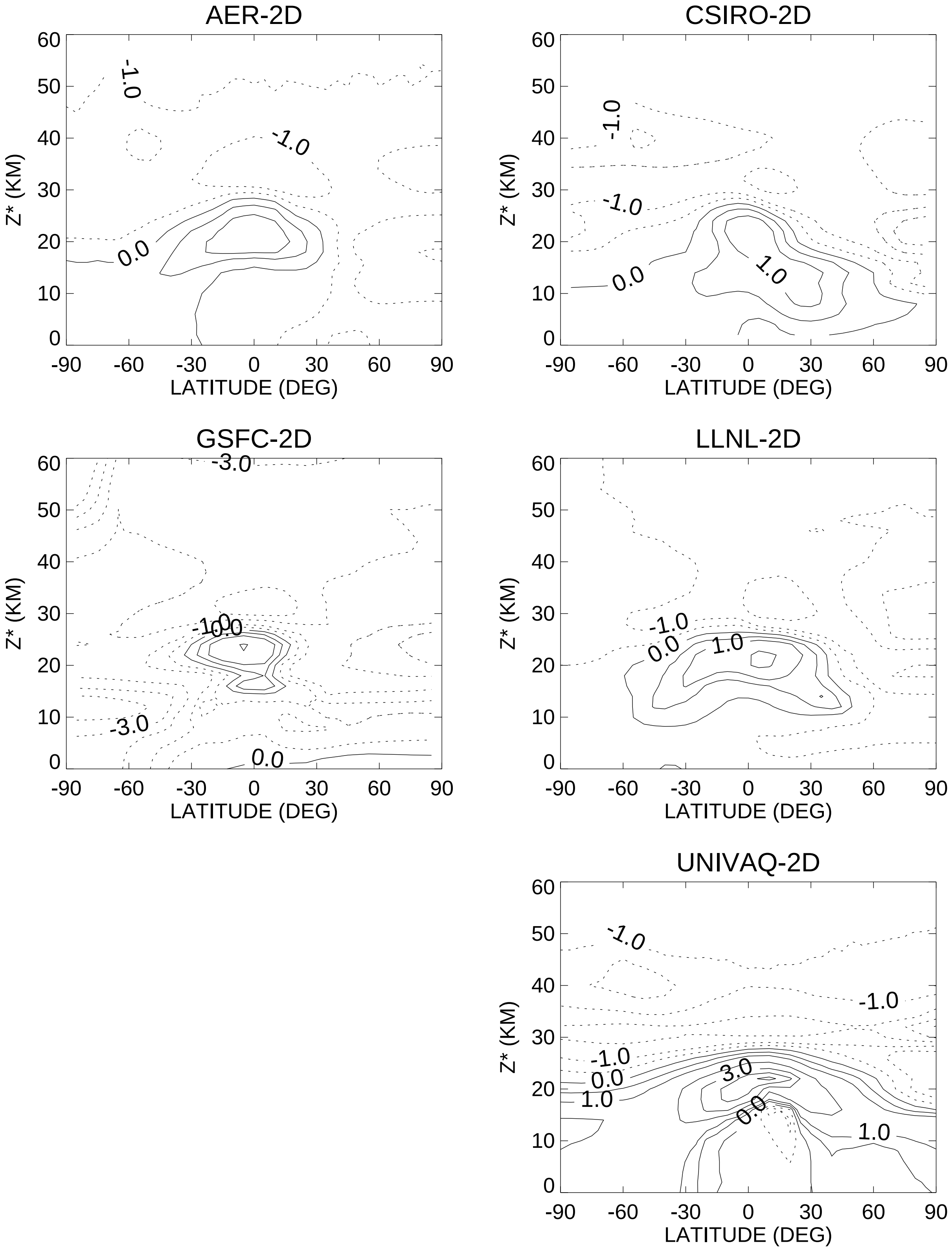

Figure 5.23: Calculated perturbations to O_3 (percent) as a function of latitude and altitude in June of 2050 due to emissions from a fleet of 1000 HSCT aircraft with $EI(NO_x)$=10 under Scenario S9g relative to Scenario D9. Contours are -4, -3, -2, -1, -0.5, 0, 0.5, 1, 2, 3, 4, 5.

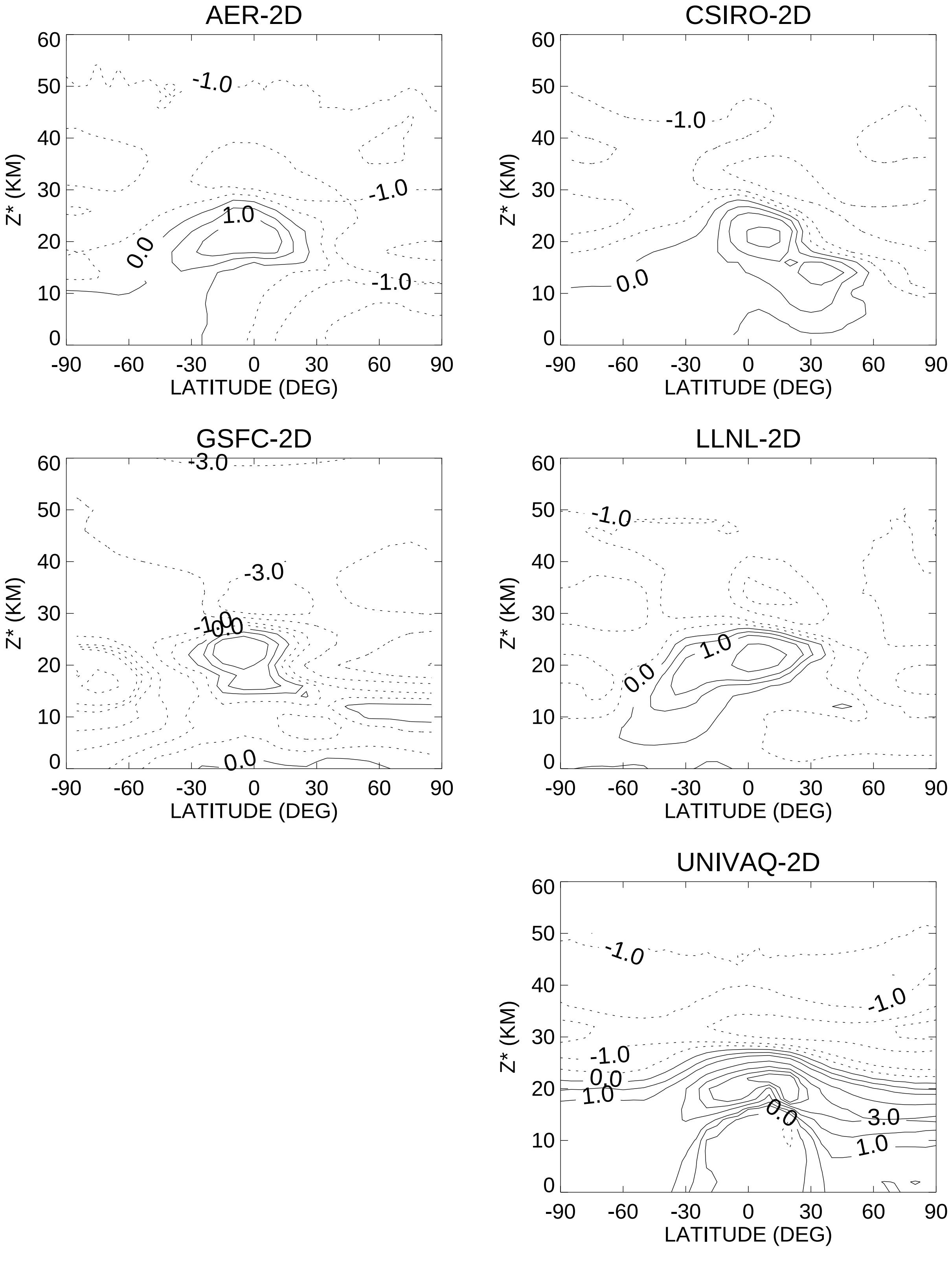

Figure 5.24: Calculated perturbations to O_3 (percent) as a function of latitude and altitude in October of 2050 due to emissions from a fleet of 1000 HSCT aircraft with EI(NO_x)=10 under Scenario S9g relative to Scenario D9. Contours are -10, -5, -4, -3, -2, -1, -0.5, 0, 0.5, 1, 2, 3, 4, 5.

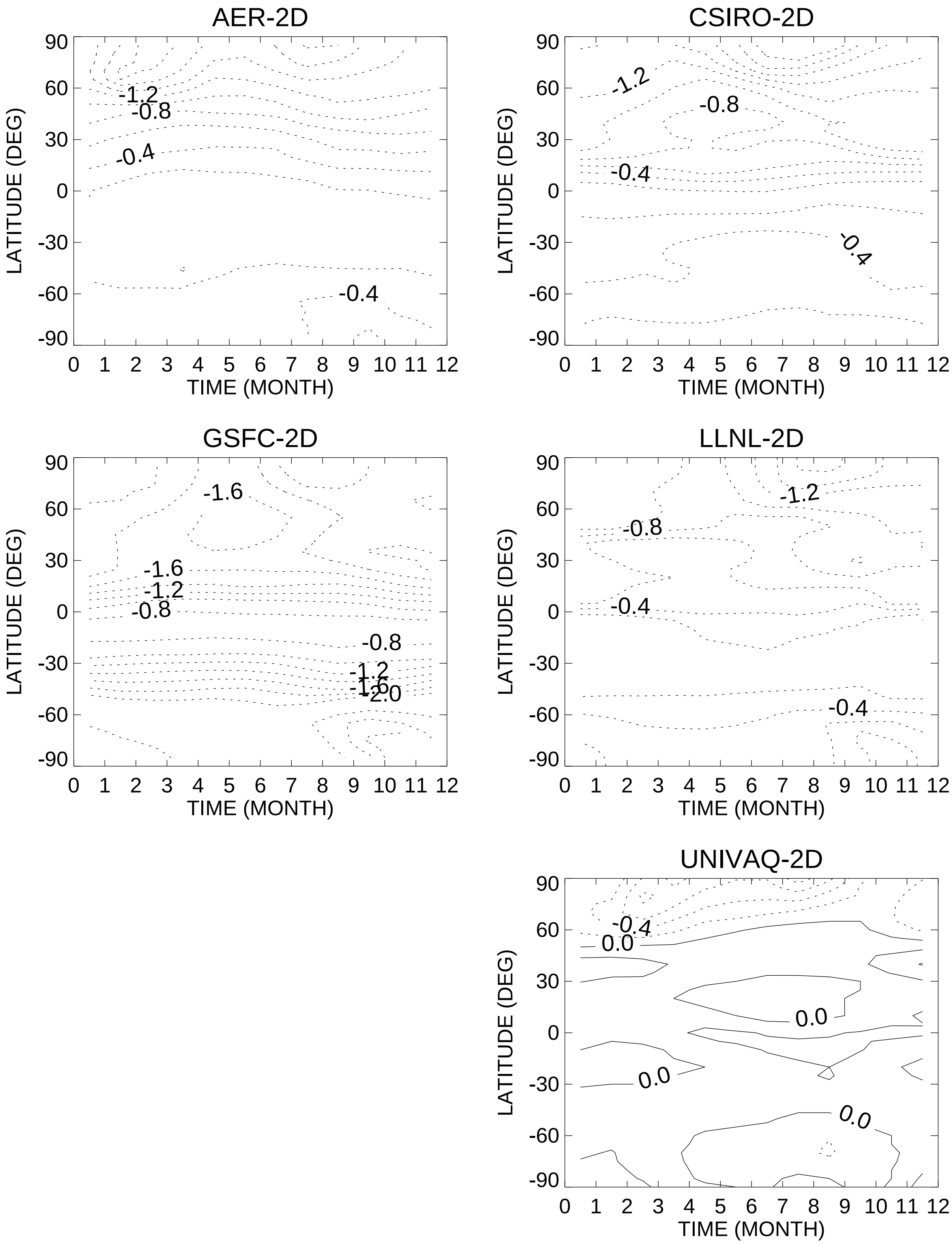

Figure 5.25: Calculated perturbations to column O_3 (percent) as a function of latitude and season in 2050 due to emissions from a fleet of 1000 HSCT aircraft with EI(NO_x)=10 under Scenario S9g relative to Scenario D9. Contours are -5, -4, -3 and -2 to 0.2 by 0.2.

5.3.2 Scenarios with Sulfur Emissions (S9c,e,f,h)

Scenarios S9c, S9e, S9f, and S9h include sulfur emission from HSCT aircraft in 2050. S9c uses a 500 HSCT fleet while the others use a 1000 HSCT fleet. All these scenarios employ an EI(NO_x) of 5 and an EI(SO_2) of 0.4. The gas to particle conversion fraction varies from 10% to 100%.

Scenario S9c uses sulfate surface area SA1, which assumes 50% gas to particle conversion in the plume. The aircraft fleet contains 500 HSCTs with EI(NO_x)=5. Changes in ozone for this scenario relative to scenario D9 are shown in Figures 5.26, 5.27, and 5.28 for March, June, and October, respectively. Compared to Scenario S9a-D9 which omits aircraft sulfur emissions, the ozone change is more negative below 20 km and more positive above. Compared with a similar scenario (S9f-D) in 2015, the ozone depletion is reduced. Figure 5.29 shows changes in ozone column for this scenario. The CSIRO model shows ozone increases in much of the southern hemisphere and ozone decreases of up to 0.6% in the northern hemisphere high latitudes. The AER model shows ozone decreases of greater than 0.8% in the northern hemisphere poleward of 60^oN. The GSFC model shows depletions of up to 1.6% in the northern high latitudes and over 2% in the southern high latitudes. The UNIVAQ model shows ozone increases in the tropics and depletions of up to 0.8% in the northern high latitudes.

Scenario S9e uses a 1000 HSCT fleet and SA2 surface area density, which assumes 50% gas to particle conversion. Figures 5.30, 5.31, and 5.32 show calculated changes in ozone for March, June, and October. Lower stratospheric ozone depletion peaks around 15 km in the northern hemisphere, with up to 3% depletion in the AER and GSFC models, 2% in the LLNL and UNIVAQ models, and 1% in the CSIRO Model. The AER, CSIRO, and LLNL models show ozone increases around 25 km at some extratropical latitudes, due to a decrease in NO_x-catalyzed ozone loss when aerosols are added. Ozone column changes are shown in Figure 5.33. All models calculate more than 1% ozone column depletion in parts of the northern hemisphere, with the AER and UNIVAQ models maximizing at 1.8% and the GSFC model at over 2%.

Scenario S9f uses surface area density SA4, which assumes 100% gas to particle conversion to calculate the maximum possible effect of aircraft sulfur emissions. The fleet consists of 1000 HSCTs. Calculated changes in ozone for this scenario relative to Scenario D9 are shown in Figures 5.34, 5.35, and 5.36. Ozone perturbations are slightly larger than those for S9e-D9. Figure 5.37 shows changes in ozone column. All models show slightly greater ozone column depletion for S9f-D9 than for S9e-D9.

Scenario S9h uses the 1000 HSCT fleet with surface area density SA6. SA6 assumes 10% gas to particle conversion in the plume. Calculated ozone changes for this scenario are shown in Figures 5.38, 5.39, and 5.40 for March, June, and October. Ozone reductions are somewhat greater than for S9d-D9 with SA0, but less than S9e-D9 with SA2. Figure 5.41 shows changes in column ozone for this scenario. Maximum column ozone depletions in the northern hemisphere are 1.8% for GSFC, 1.6% for AER, 1% for CSIRO and UNIVAQ, and 0.8% for LLNL.

The sensitivity of northern hemisphere ozone change to aircraft sulfur emissions in 2050 is depicted graphically in Figure 5.42. The abscissa show percentage increase in SAD in the 14-21 km, 33-90^oN region due to emission of sulfur from 1000 HSCTs relative to an SA0 background. Scenario S9d is used for the 0% change in SAD. Scenario S9h, with 10% gas to particle conversion, corresponds to a 74% increase in SAD. Scenarios S9e and S9f, with 50% and 100% gas to particle conversion, correspond to 124% and 164% increases in SAD, respectively. These scenarios all employ an EI(NO_x) of 5. All models show increasing ozone depletion with increasing SAD perturbation, and the slopes are fairly consistent among the AER, GSFC, LLNL, and UNIVAQ models. The CSIRO model shows a smaller response to aircraft sulfur emissions. The sensitivity to SAD perturbation in 2050 is considerably less than in 2015 (by factors of 2-4) due to the reduced Cl_y concentration.

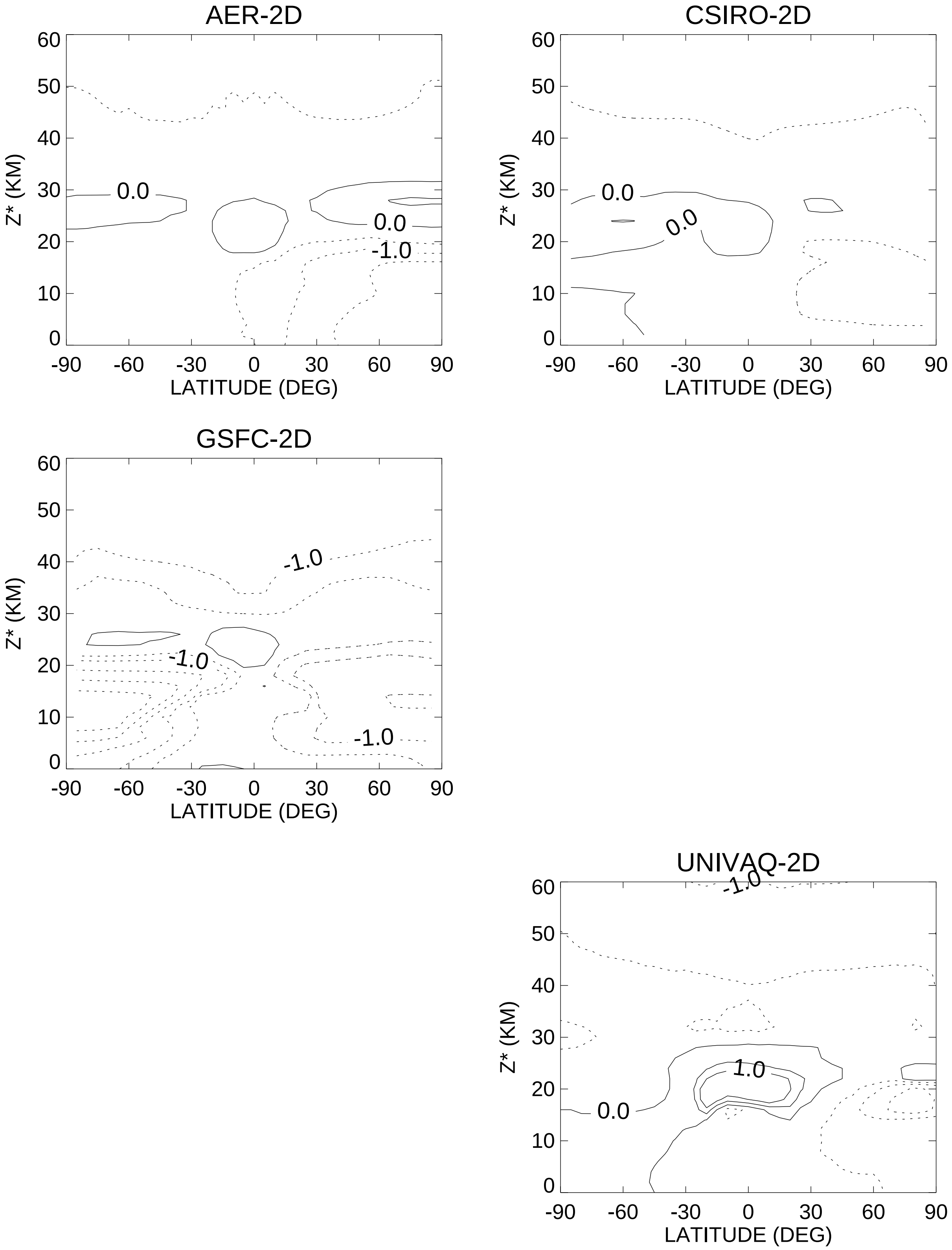

Figure 5.26: Calculated perturbations to O_3 (percent) as a function of latitude and altitude in March of 2050 due to emissions from a fleet of 500 HSCT aircraft with $EI(NO_x)=5$ and SA1 sulfate surface area density under Scenario S9c relative to Scenario D9. Contours are -4, -3, -2, -1, -0.5, 0, 0.5, 1.

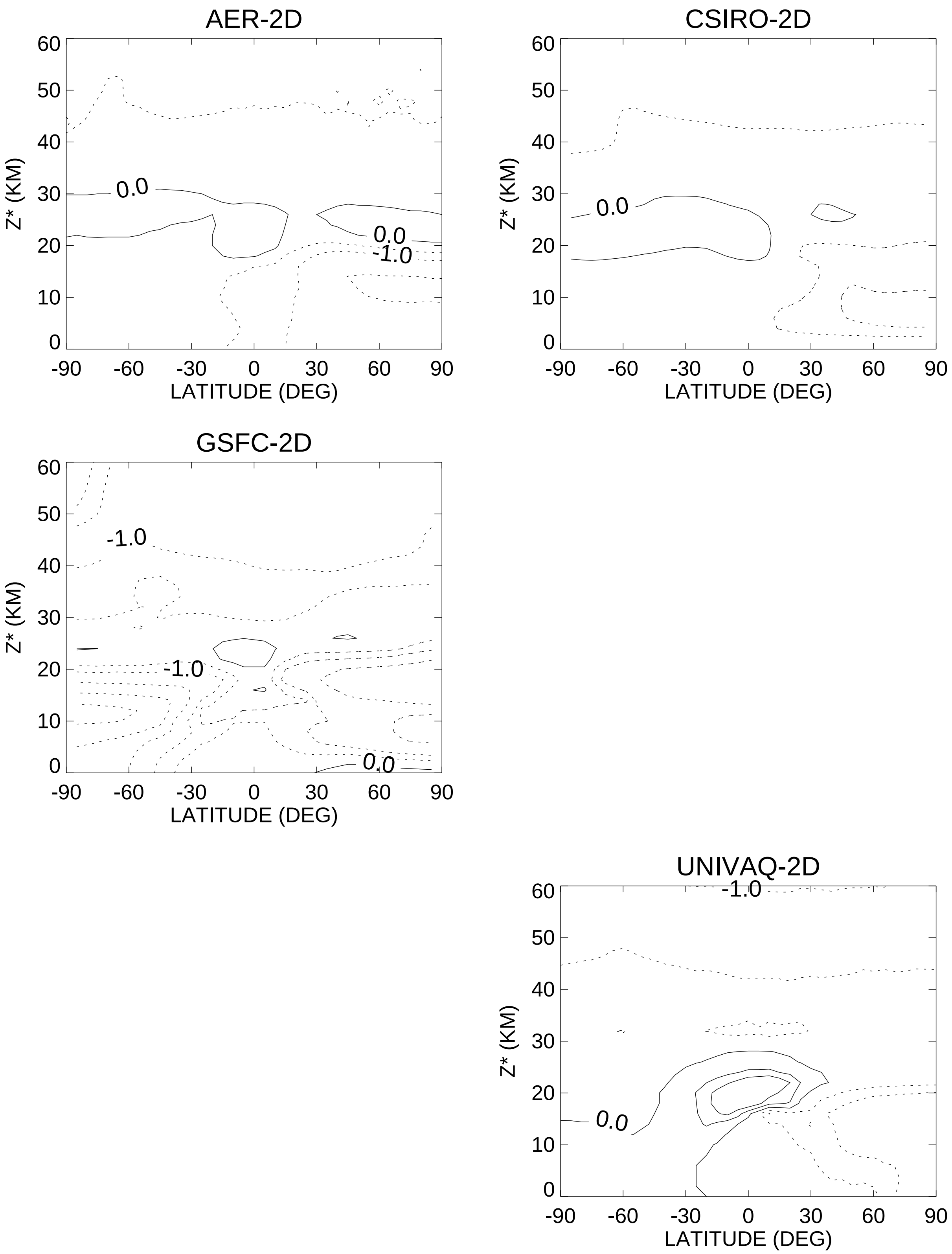

Figure 5.27: Calculated perturbations to O_3 (percent) as a function of latitude and altitude in June of 2050 due to emissions from a fleet of 500 HSCT aircraft with $EI(NO_x)=5$ and SA1 sulfate surface area density under Scenario S9c relative to Scenario D9. Contours are -4, -3, -2, -1, -0.5, 0, 0.5, 1.

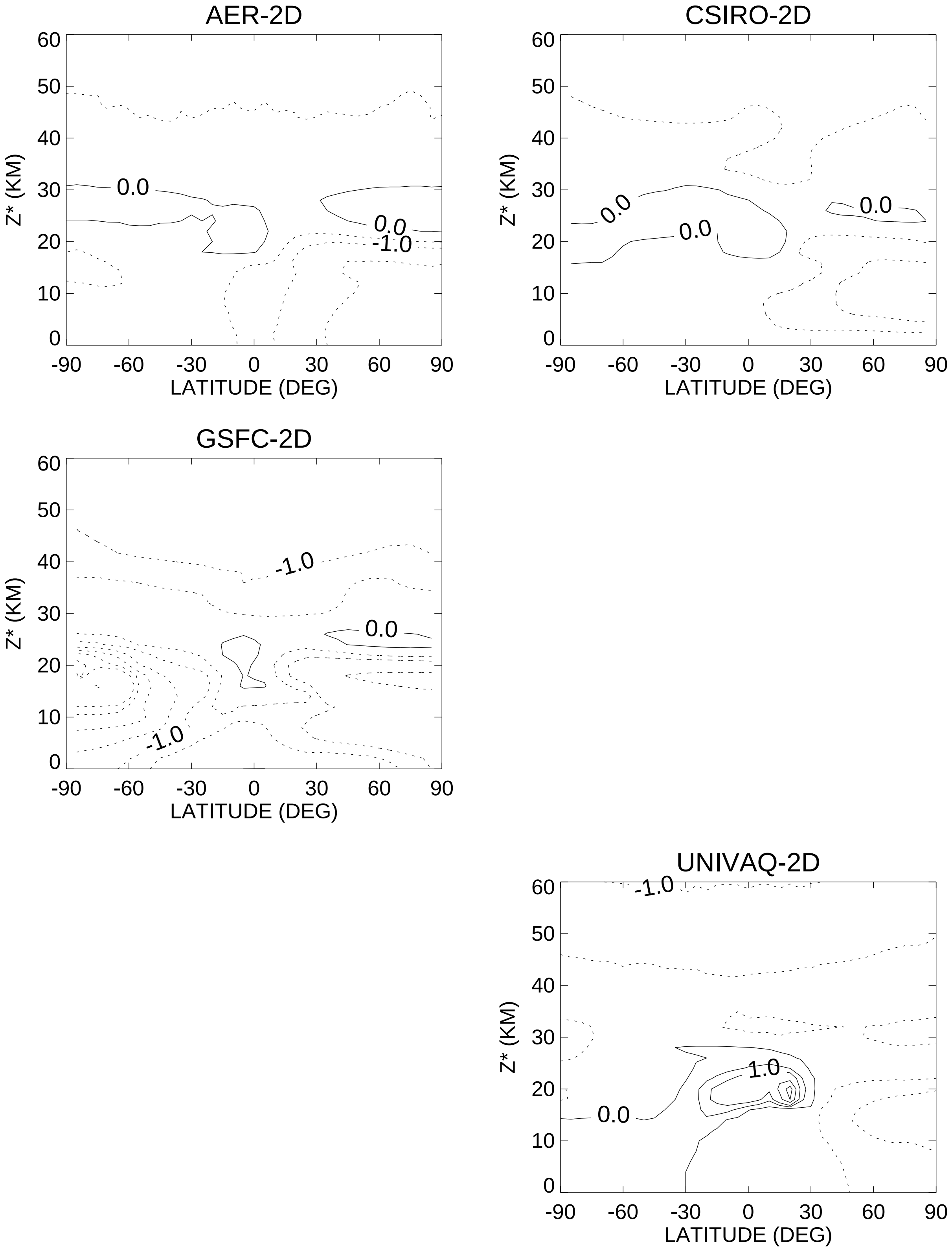

Figure 5.28: Calculated perturbations to O_3 (percent) as a function of latitude and altitude in October of 2050 due to emissions from a fleet of 500 HSCT aircraft with EI(NO_x)=5 and SA1 sulfate surface area density under Scenario S9c relative to Scenario D9. Contours are -10, -5, -4, -3, -2, -1, -0.5, 0, 0.5, 1, 2, 3.

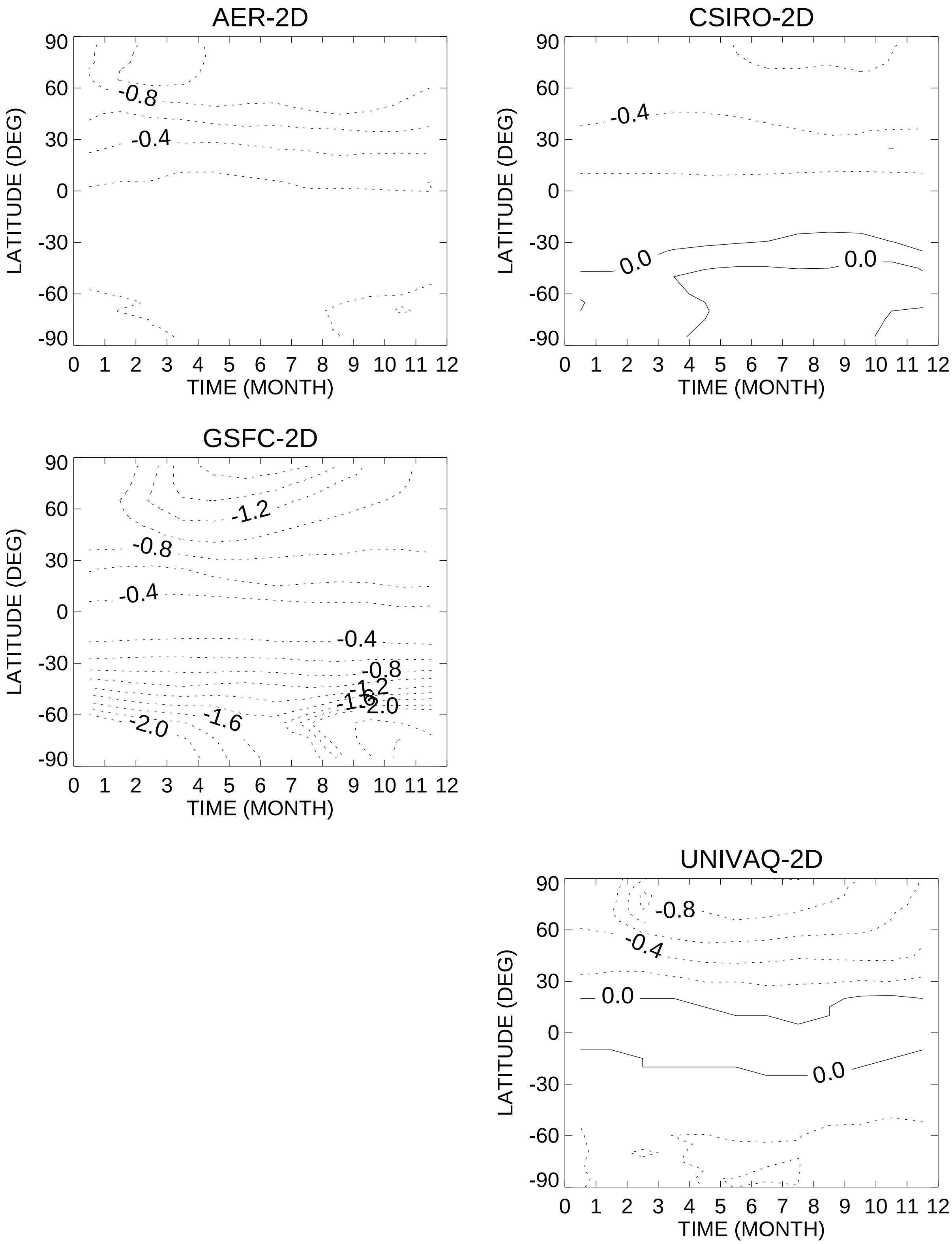

Figure 5.29: Calculated perturbations to column O_3 (percent) as a function of latitude and season in 2050 due to emissions from a fleet of 500 HSCT aircraft with $EI(NO_x)=5$ and SA1 sulfate surface area density under Scenario S9c relative to Scenario D9. Contours are -4, -3 and -2 to 0.2 by 0.2.

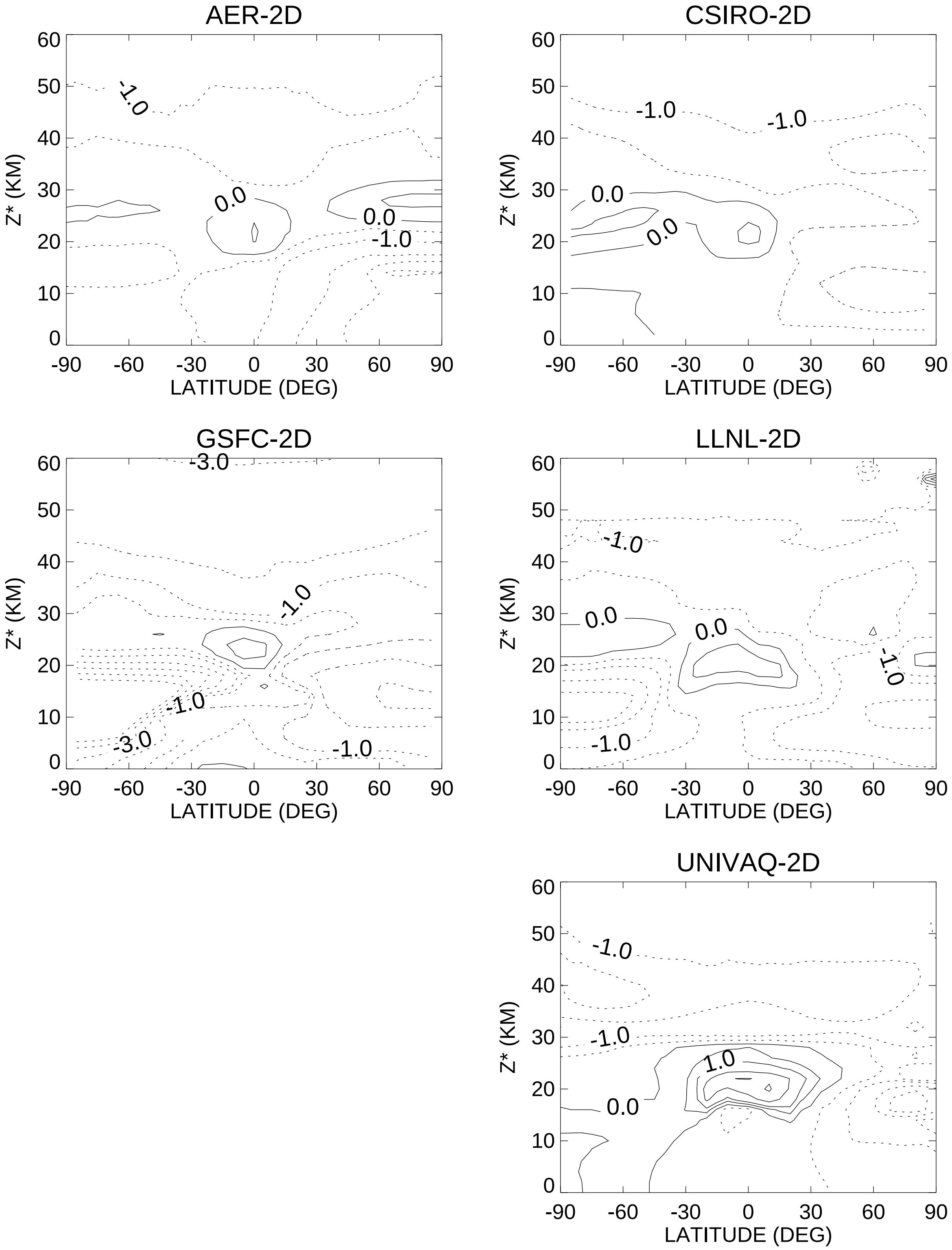

Figure 5.30: Calculated perturbations to O_3 (percent) as a function of latitude and altitude in March of 2050 due to emissions from a fleet of 1000 HSCT aircraft with EI(NO_x)=5 and SA2 sulfate surface area density under Scenario S9e relative to Scenario D9. Contours are -5, -4, -3, -2, -1, -0.5, 0, 0.5, 1, 2, 3.

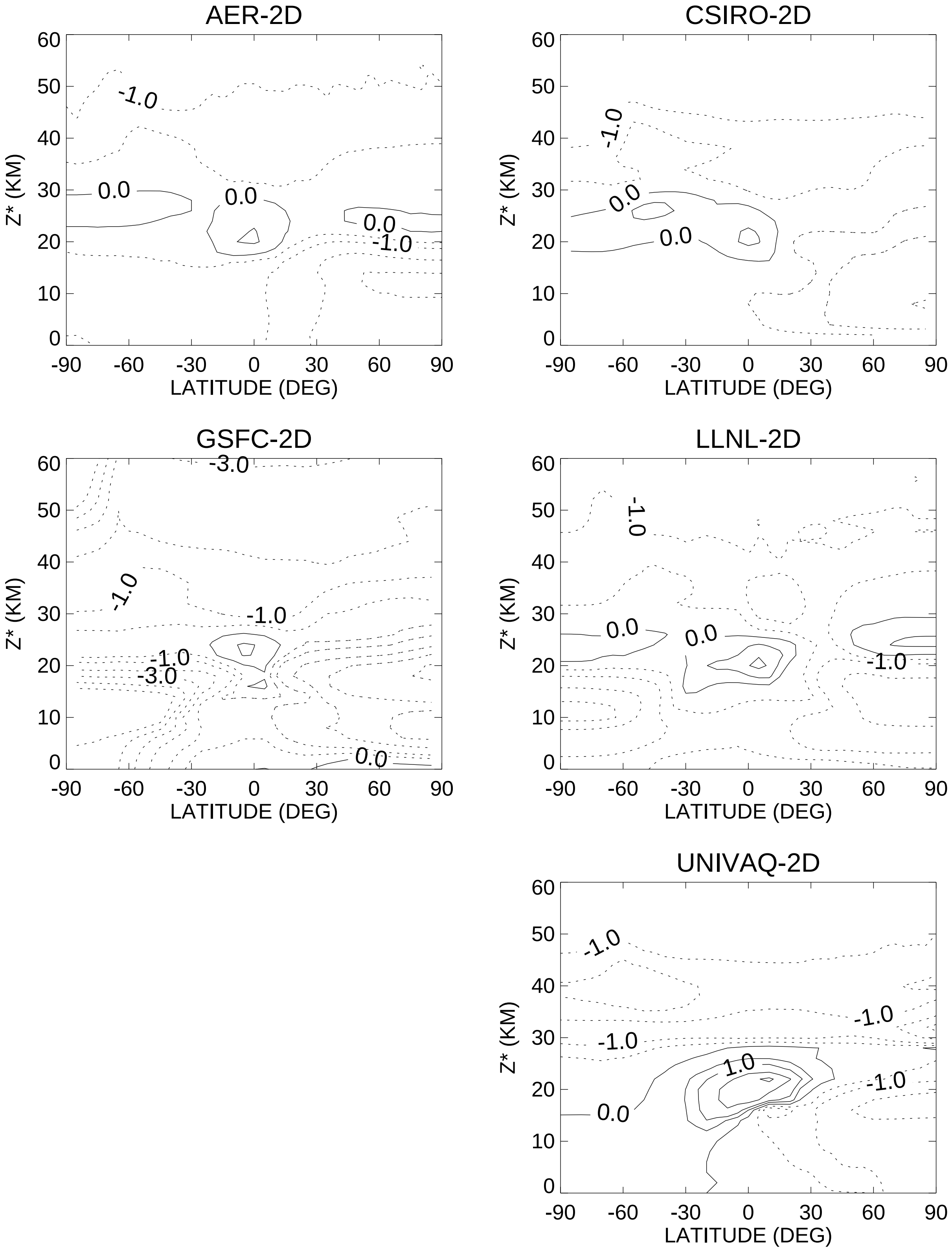

Figure 5.31: Calculated perturbations to O_3 (percent) as a function of latitude and altitude in June of 2050 due to emissions from a fleet of 1000 HSCT aircraft with $EI(NO_x)$=5 and SA2 sulfate surface area density under Scenario S9e relative to Scenario D9. Contours are -5, -4, -3, -2, -1, -0.5, 0, 0.5, 1, 2, 3.

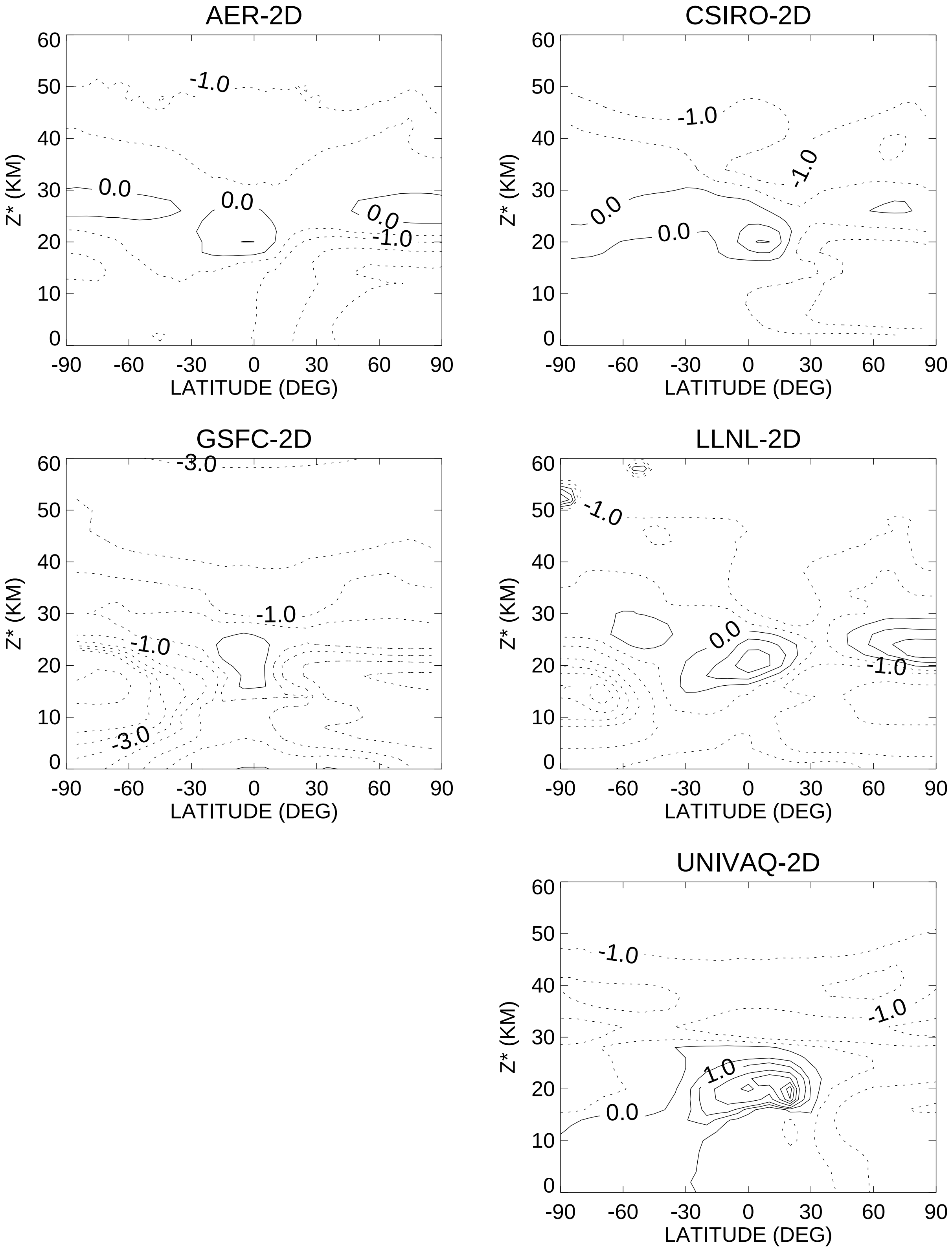

Figure 5.32: Calculated perturbations to O_3 (percent) as a function of latitude and altitude in October of 2050 due to emissions from a fleet of 1000 HSCT aircraft with $EI(NO_x)=5$ and SA2 sulfate surface area density under Scenario S9e relative to Scenario D9. Contours are -10, -5, -4, -3, -2, -1, -0.5, 0, 0.5, 1, 2, 3, 4, 5.

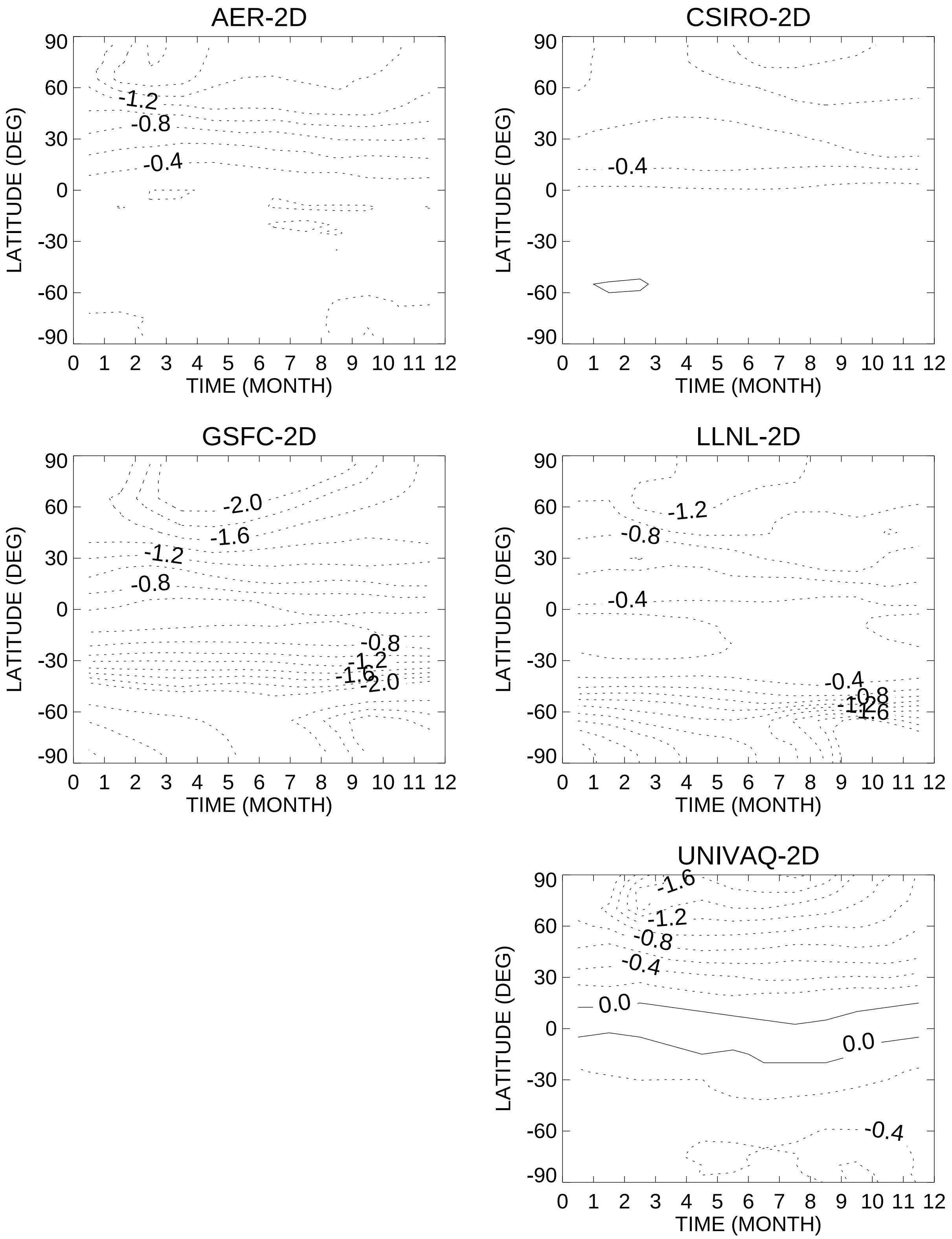

Figure 5.33: Calculated perturbations to column O_3 (percent) as a function of latitude and season in 2050 due to emissions from a fleet of 1000 HSCT aircraft with $EI(NO_x)$=5 and SA2 sulfate surface area density under Scenario S9e relative to Scenario D9. Contours are -5, -4, -3 and -2 to 0 by 0.2.

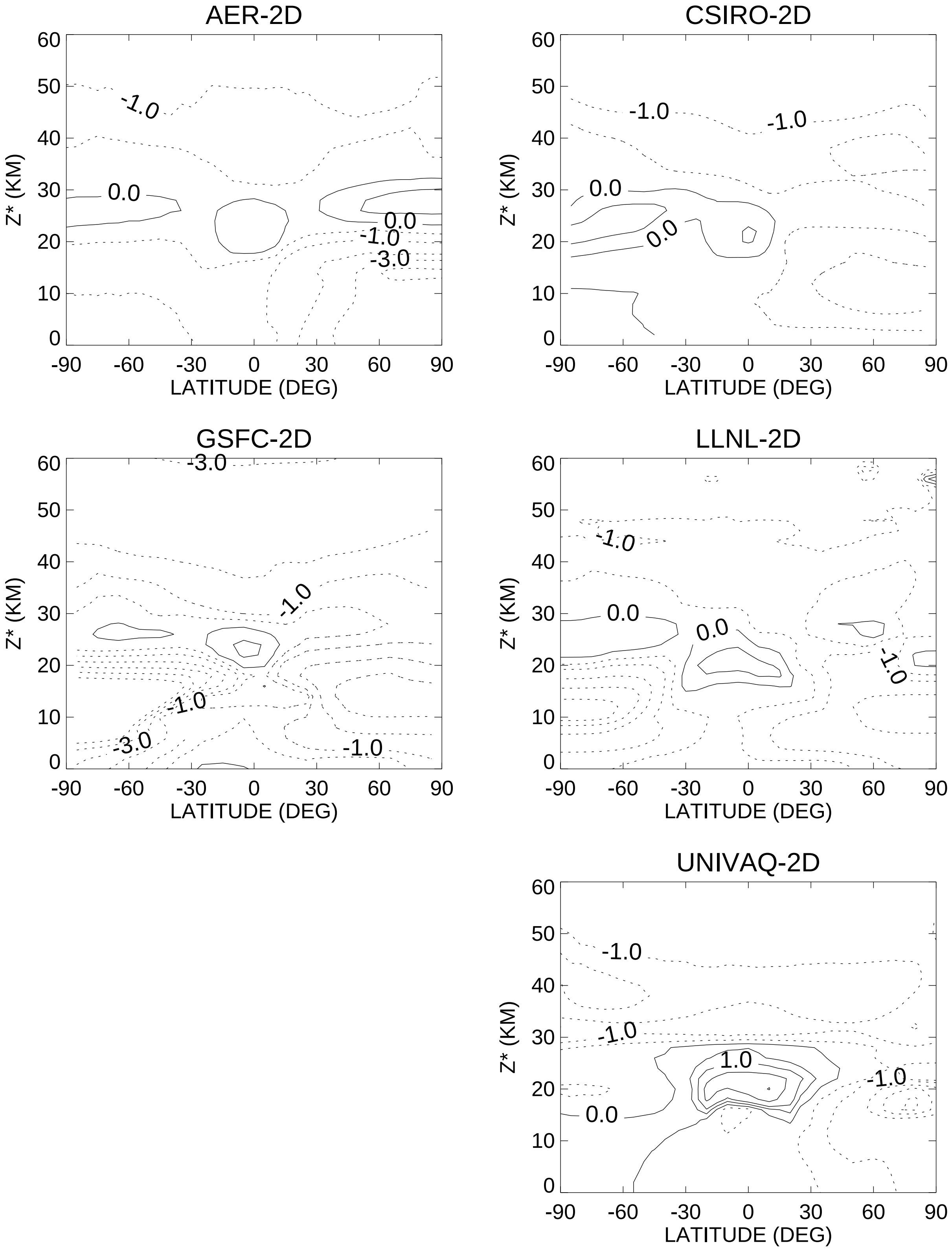

Figure 5.34: Calculated perturbations to O_3 (percent) as a function of latitude and altitude in March of 2050 due to emissions from a fleet of 1000 HSCT aircraft with EI(NO_x)=5 and SA4 sulfate surface area density under Scenario S9f relative to Scenario D9. Contours are -5, -4, -3, -2, -1, -0.5, 0, 0.5, 1, 2, 3.

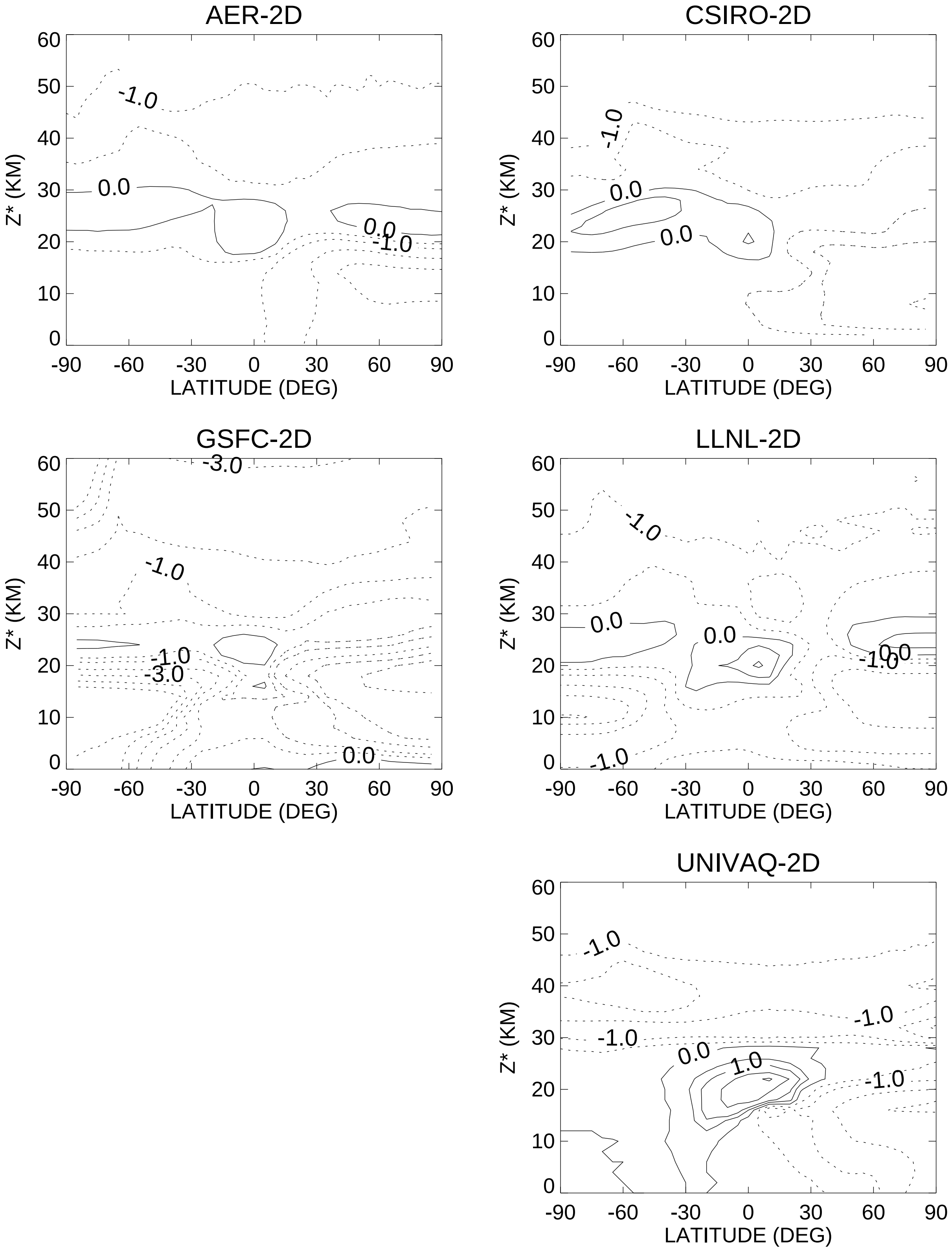

Figure 5.35: Calculated perturbations to O_3 (percent) as a function of latitude and altitude in June of 2050 due to emissions from a fleet of 1000 HSCT aircraft with $EI(NO_x)=5$ and SA4 sulfate surface area density under Scenario S9f relative to Scenario D9. Contours are -5, -4, -3, -2, -1, -0.5, 0, 0.5, 1, 2, 3.

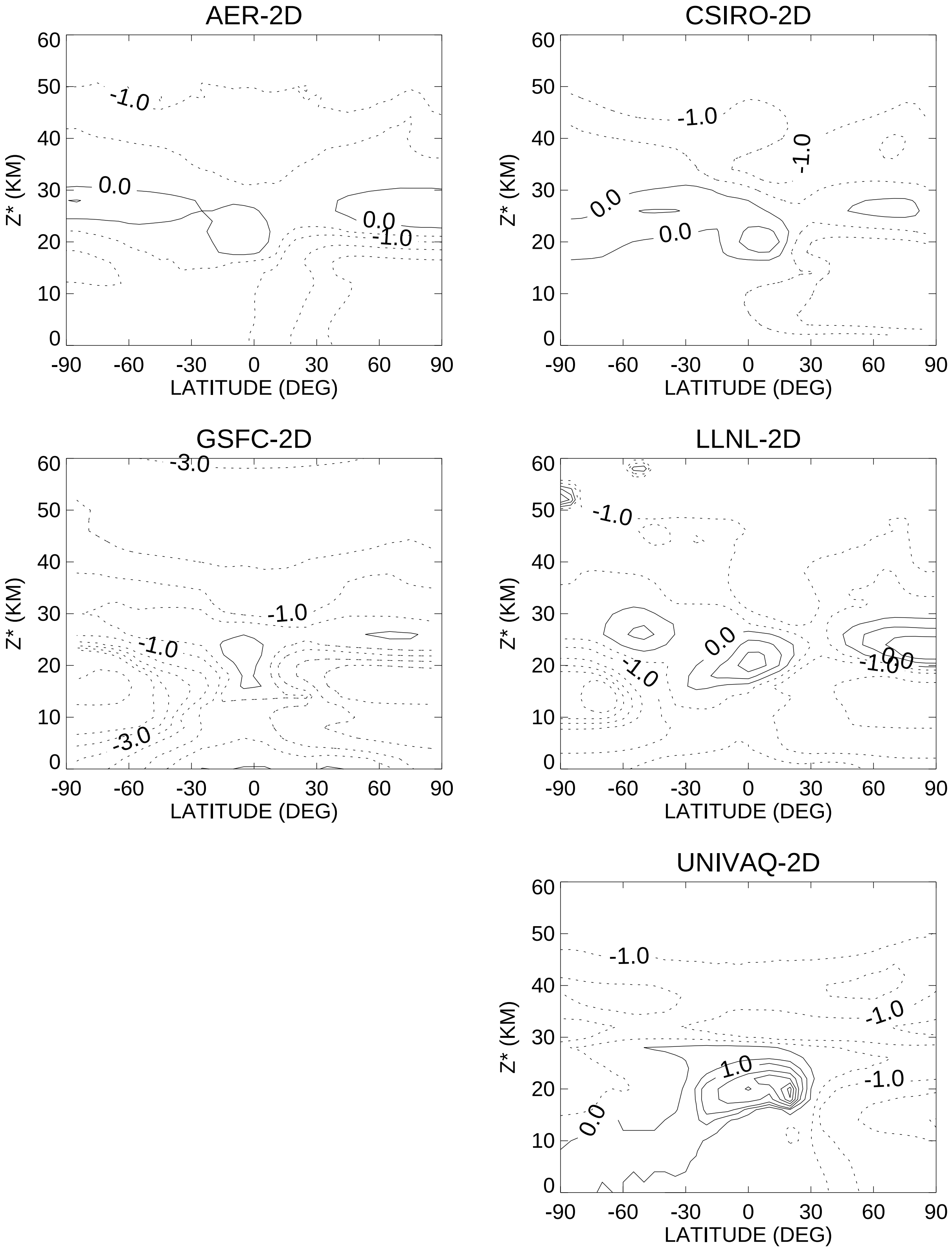

Figure 5.36: Calculated perturbations to O_3 (percent) as a function of latitude and altitude in October of 2050 due to emissions from a fleet of 1000 HSCT aircraft with EI(NO_x)=5 and SA4 sulfate surface area density under Scenario S9f relative to Scenario D9. Contours are -10, -5, -4, -3, -2, -1, -0.5, 0, 0.5, 1, 2, 3, 4, 5.

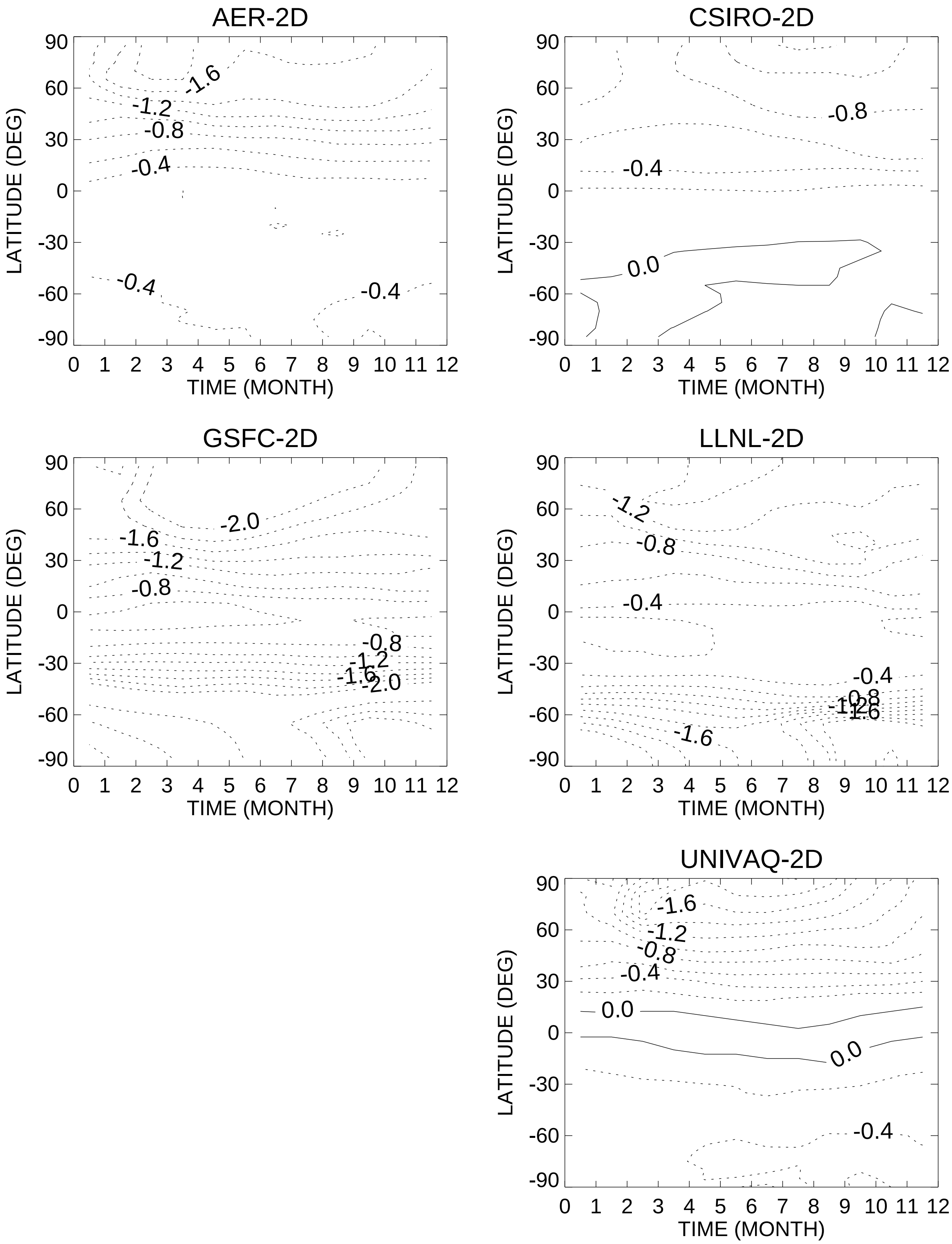

Figure 5.37: Calculated perturbations to column O_3 (percent) as a function of latitude and season in 2050 due to emissions from a fleet of 1000 HSCT aircraft with $EI(NO_x)=5$ and SA4 sulfate surface area density under Scenario S9f relative to Scenario D9. Contours are -5, -4, -3 and -2 to 0 by 0.2.

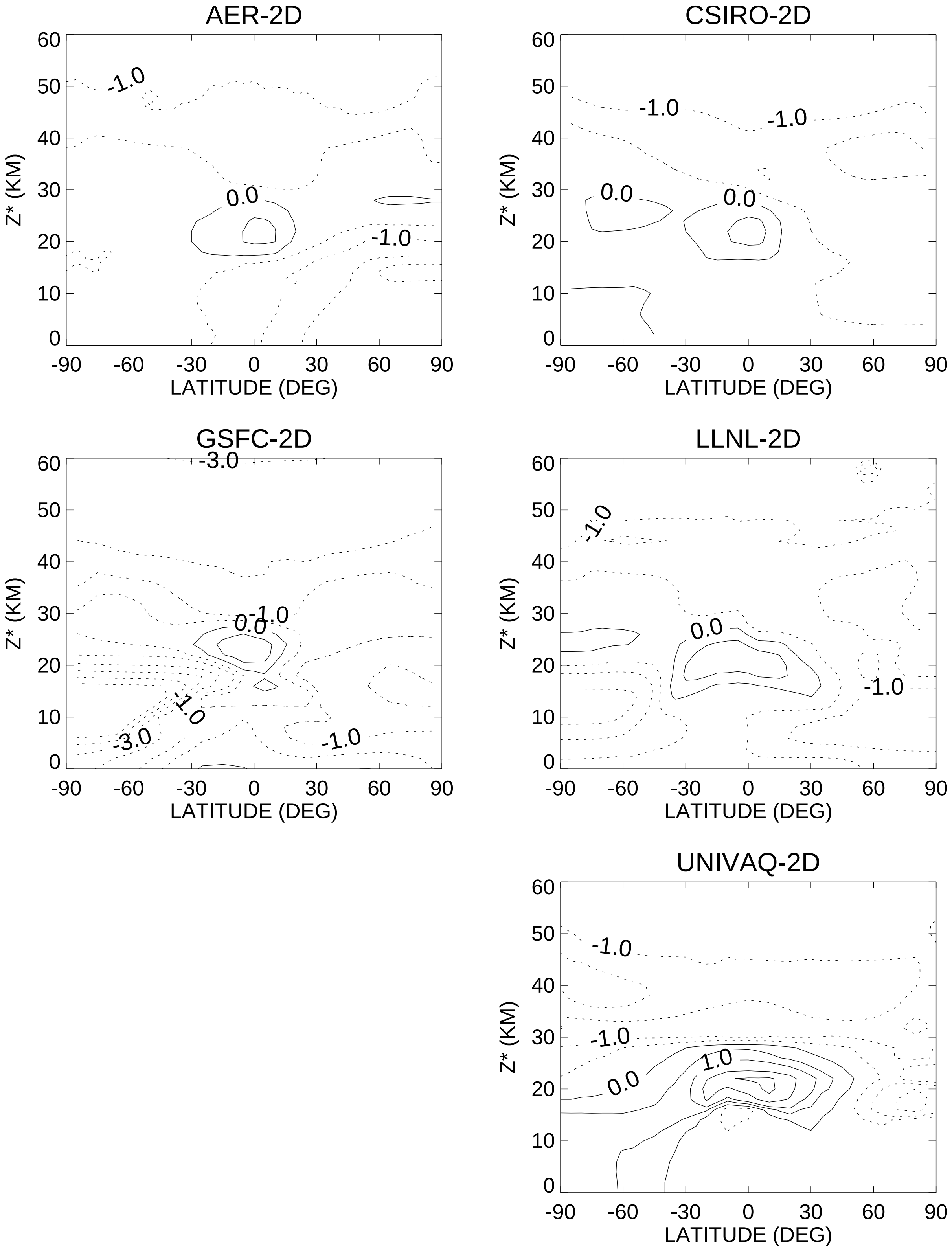

Figure 5.38: Calculated perturbations to O_3 (percent) as a function of latitude and altitude in March of 2050 due to emissions from a fleet of 1000 HSCT aircraft with $EI(NO_x)=5$ and SA6 sulfate surface area density under Scenario S9h relative to Scenario D9. Contours are -5, -4, -3, -2, -1, -0.5, 0, 0.5, 1, 2, 3.

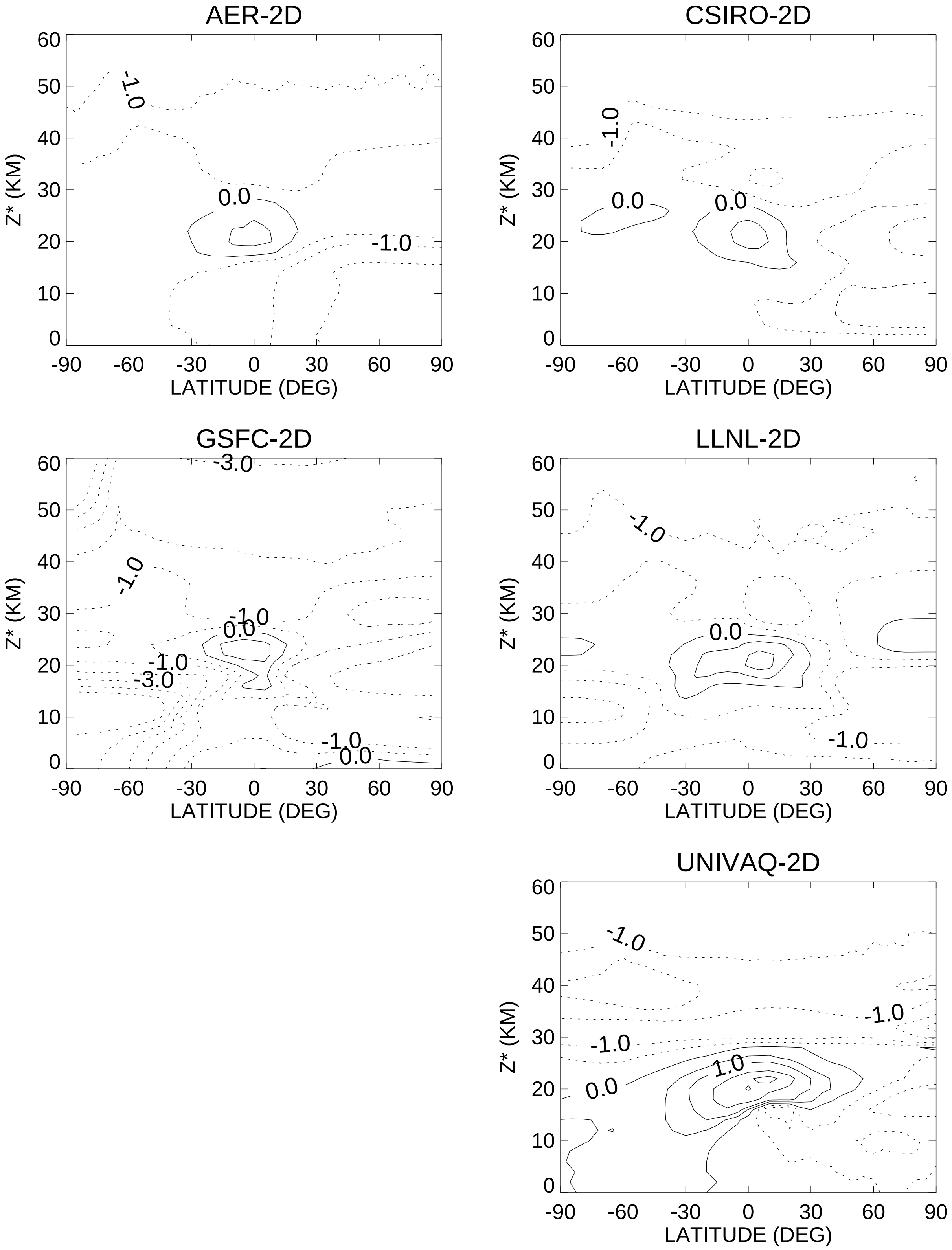

Figure 5.39: Calculated perturbations to O_3 (percent) as a function of latitude and altitude in June of 2050 due to emissions from a fleet of 1000 HSCT aircraft with $EI(NO_x)=5$ and SA6 sulfate surface area density under Scenario S9h relative to Scenario D9. Contours are -5, -4, -3, -2, -1, -0.5, 0, 0.5, 1, 2, 3.

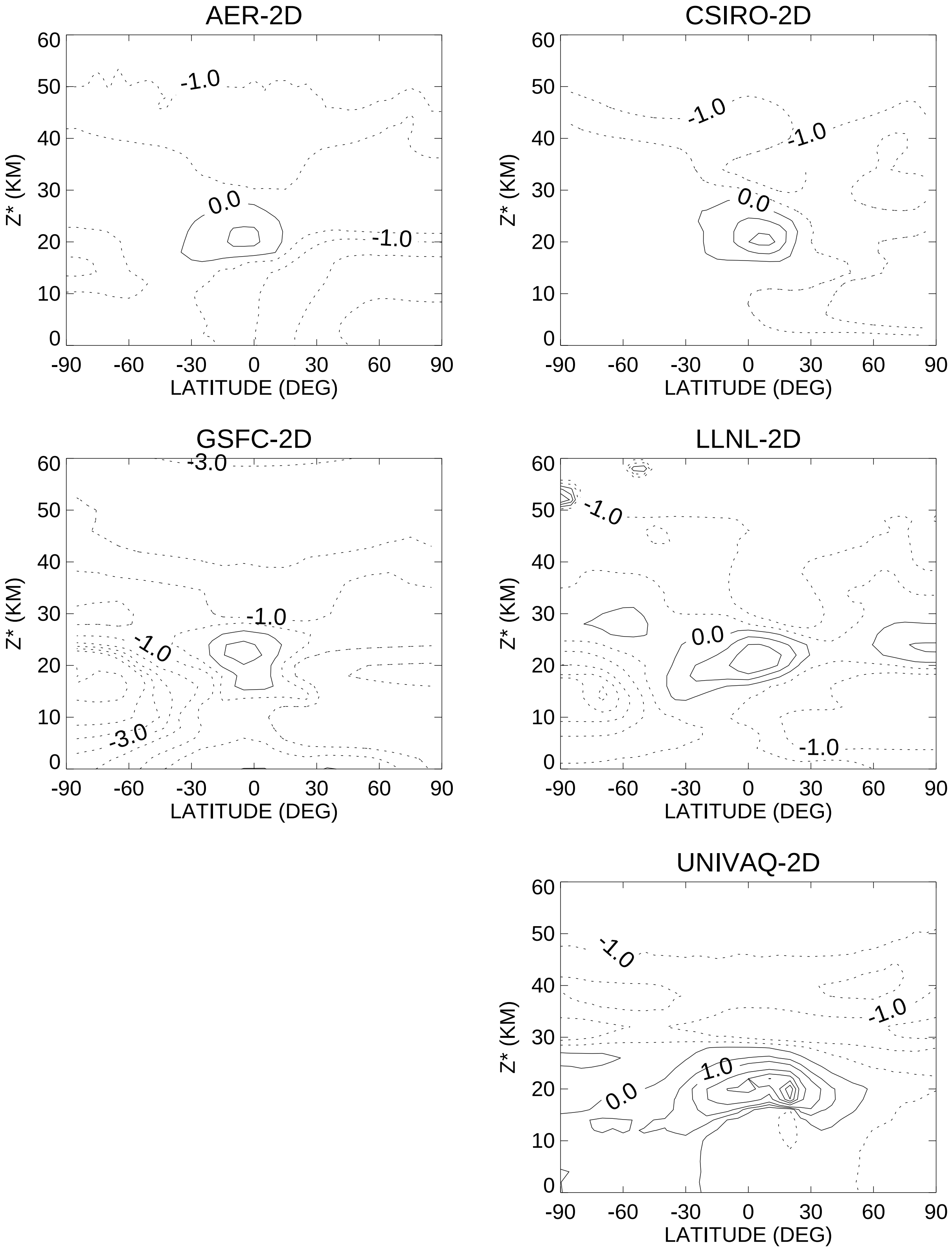

Figure 5.40: Calculated perturbations to O_3 (percent) as a function of latitude and altitude in October of 2050 due to emissions from a fleet of 1000 HSCT aircraft with $EI(NO_x)=5$ and SA6 sulfate surface area density under Scenario S9h relative to Scenario D9. Contours are -10, -5, -4, -3, -2, -1, -0.5, 0, 0.5, 1, 2, 3, 4, 5.

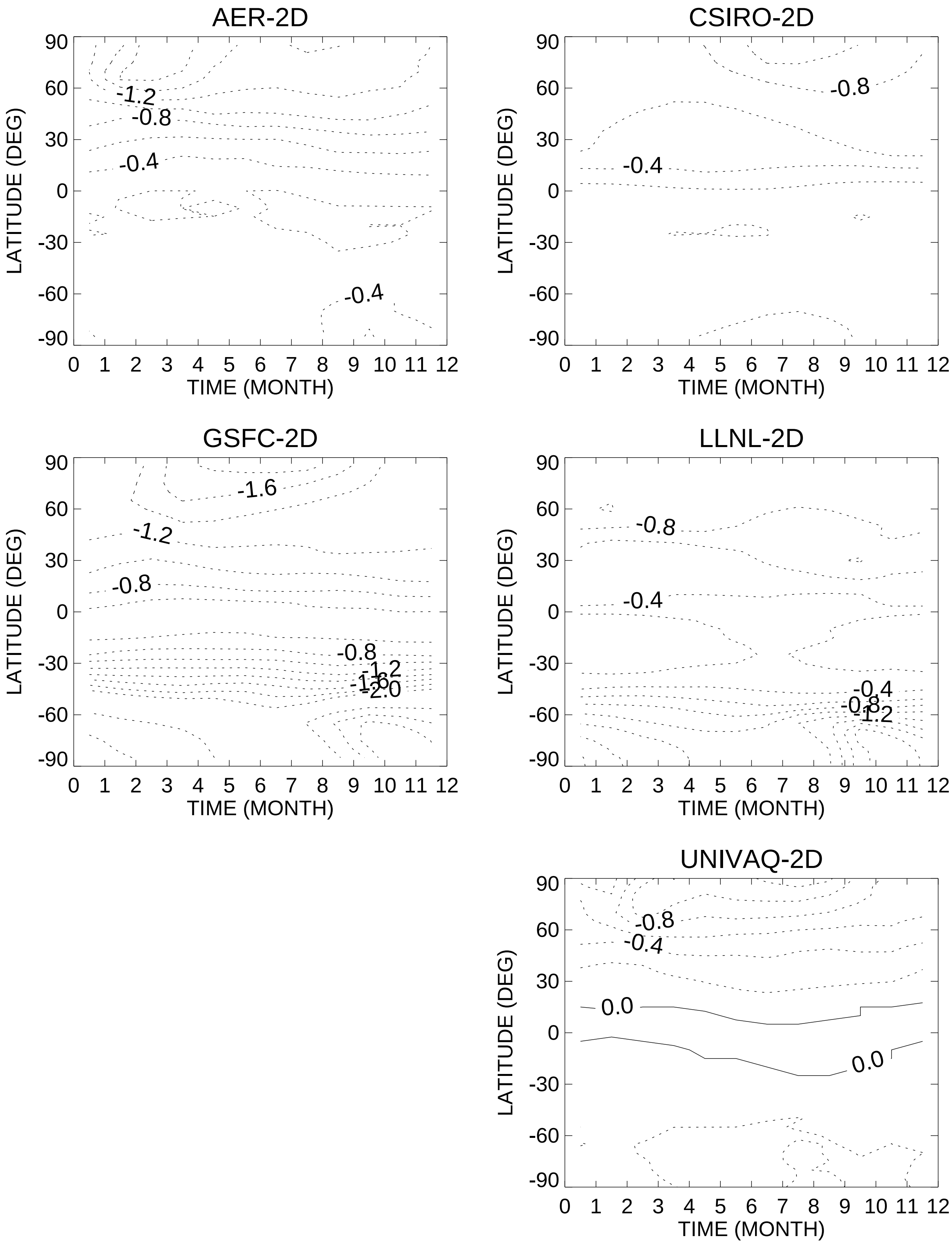

Figure 5.41: Calculated perturbations to column O_3 (percent) as a function of latitude and season in 2050 due to emissions from a fleet of 1000 HSCT aircraft with $EI(NO_x)=5$ and SA6 sulfate surface area density under Scenario S9h relative to Scenario D9. Contours are -5, -4, -3 and -2 to 0 by 0.2.

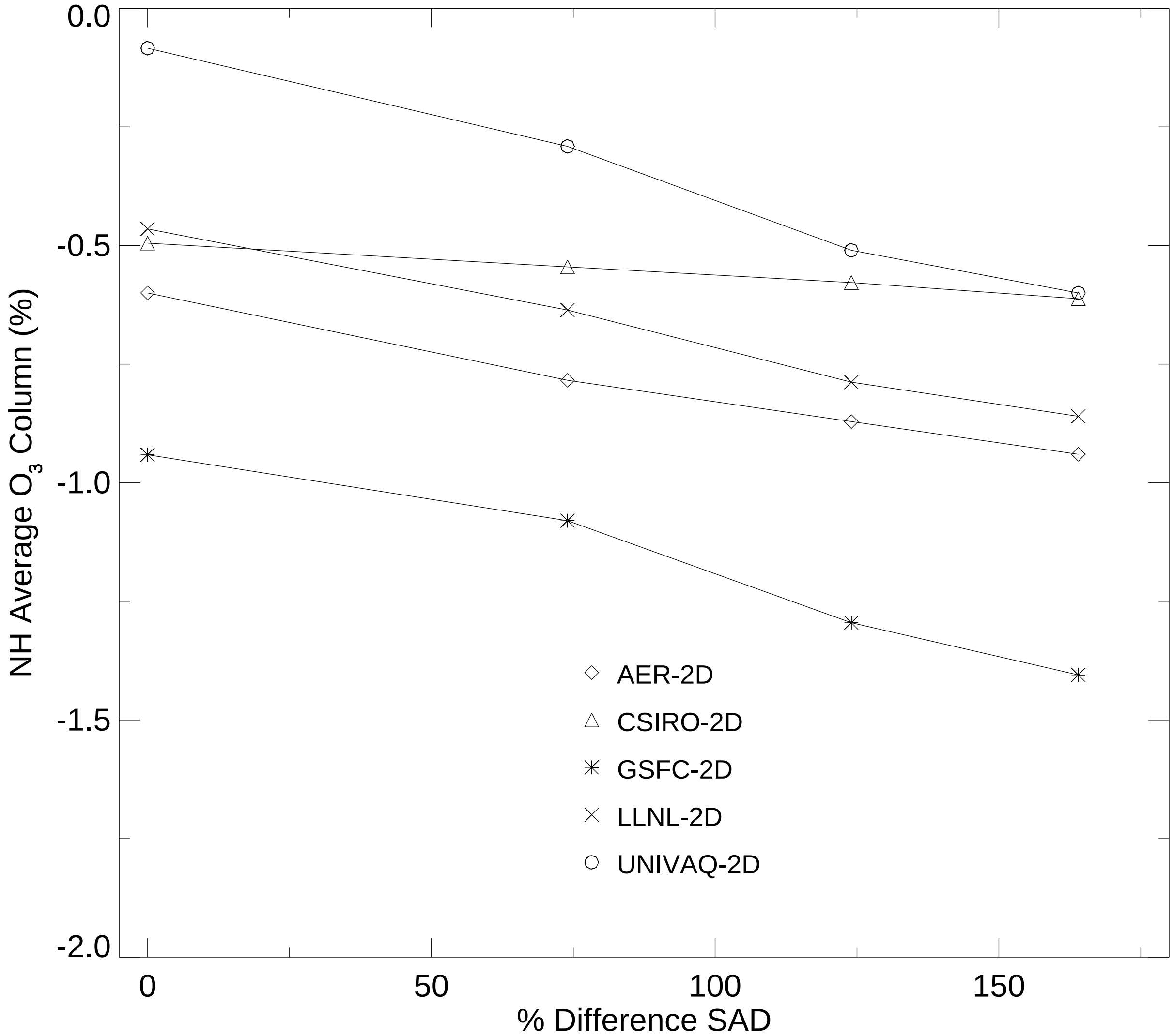

Figure 5.42: Northern hemisphere annual average total O_3 column change (percent) as a function of the percent change in aerosol surface area density in the region from 14 to 21 km and from 33^{o}N to 90^{o}N. The HSCT fleet consisted of 1000 aircraft with EI(NO_x)=5 operating in 2050 and assuming a background surface area density of SA0.

5.3.3 Scenarios with Modified Cruise Altitude (S10a-d)

Scenarios with modified cruise altitude are covered in this section. These 4 scenarios all use a supersonic fleet for which the cruise altitude is shifted downward by 2 km. Scenario S10a represents a fleet of 1000 HSCTs in 2015 with EI(NO_x)=5. Calculated changes in ozone as a function of latitude and altitude for March, June, and October are shown in Figures 5.43, 5.44, and 5.45. These ozone perturbations are similar to those for Scenario S2e-D, which represents the same aircraft fleet in 2015. Major differences are seen only in the October plot at high southern latitudes and in the GSFC model northern hemisphere lowermost stratosphere. And as with the 2015 scenarios, reducing the HSCT cruise altitude decreases the calculated ozone perturbation in the stratosphere very substantially. Changes in ozone column for Scenario S10a relative to Scenario D9 are shown in Figure 5.46. The CSIRO, LLNL, and UNIVAQ models show ozone column changes of 0.2% or less everywhere. The AER model shows maximum ozone column changes of -0.4% in the northern high latitudes, while the GSFC model shows ozone column changes of up to -1.6% in the high southern latitudes.

Scenario S10b represents 1000 HSCTs operating in 2050 at 2 km below the nominal cruise altitude with EI(NO_x)=10. Figures 5.47, 5.48, and 5.49 show calculated changes in ozone for this scenario relative to Scenario D9 for March, June, and October. Calculated changes in column ozone are shown in Figure 5.50. The AER, CSIRO and LLNL models show more of an ozone increase in the tropics and southern hemisphere and more of an ozone decrease at high latitudes for this scenario than for S10a. The GSFC model shows an increase in ozone depletion near 30^{o}N and a decrease in the southern hemisphere poleward of 60^{o}N. The UNIVAQ model show ozone column increases due to HSCT emissions over most latitudes and seasons with this scenario.

Scenarios S10c and S10d include aircraft sulfur emissions along with emissions of H_2O and NO_x with EI(NO_x)=5. S10c uses aerosol scenario SA6-2km, which assumes 10% gas to particle conversion for a fleet of 1000 HSCTs cruising at 2 km below the nominal cruise altitude. Ozone perturbations for this scenario relative to Scenario D9 are shown in Figures 5.51, 5.52, and 5.53. The effect of the aircraft SO_x emissions is to increase ozone depletion (or reduce ozone increases) in the extratropics below 20 km (compare with S10a-D9). Calculated perturbations to ozone column for Scenario 10c are shown in Figure 5.54. Ozone column depletions are larger than for S10a-D9.

Aerosol scenario SA2-2km is used for Scenario S10d. This scenario assumes 50% gas to particle conversion from 1000 HSCTs cruising at 2 km below the nominal altitude. Figures 5.55, 5.56, and 5.57 show calculated ozone changes for March, June, and October. Compared with S10c, ozone depletions are larger in the extratropics below 20 km and smaller from 20-30 km. Ozone column changes are shown in Figure 5.58. Ozone column depletion is increased slightly over S10c-D9, with the GSFC model showing the largest northern hemisphere increases due to the additional particle production.

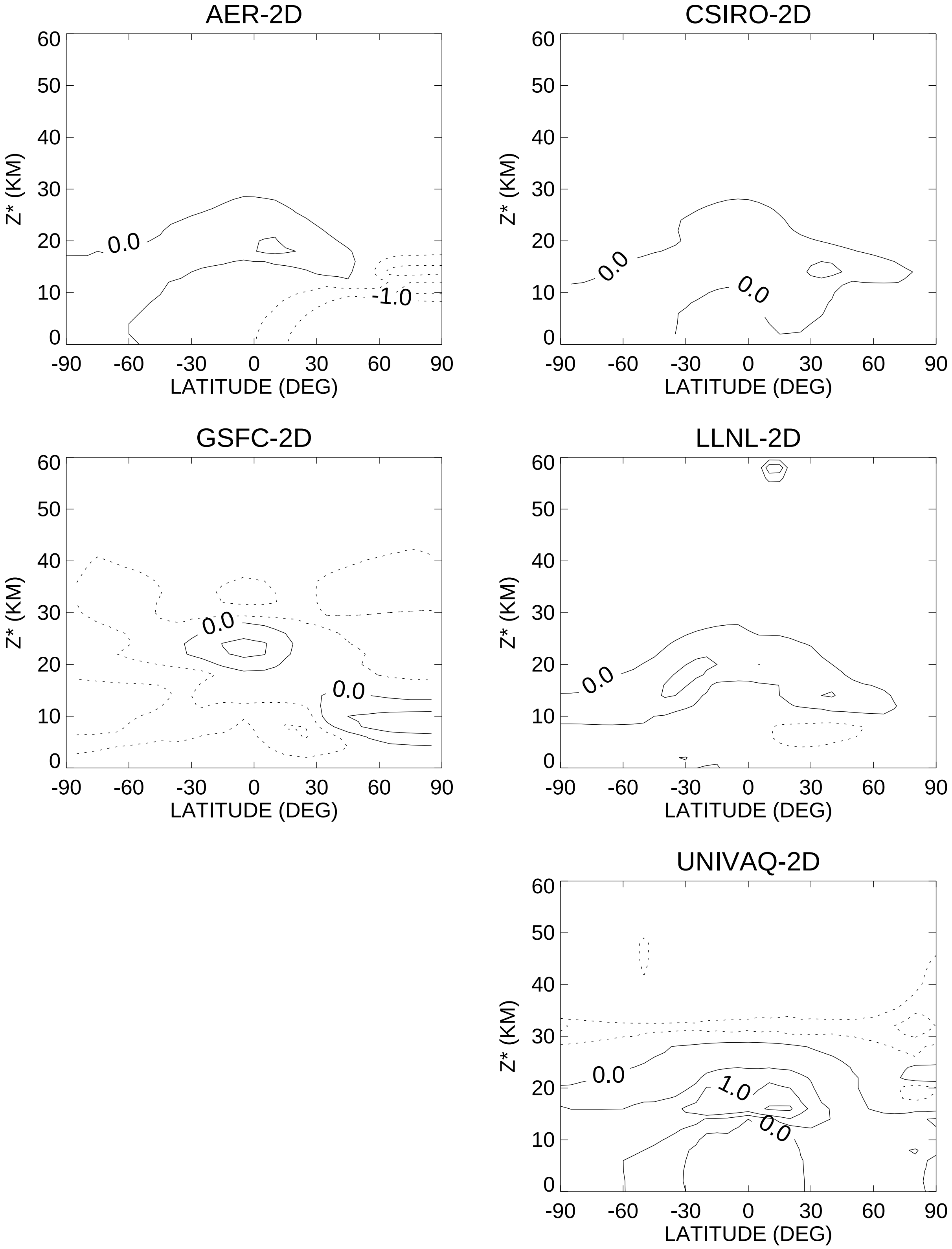

Figure 5.43: Calculated perturbations to O_3 (percent) as a function of latitude and altitude in March of 2050 due to emissions from a fleet of 1000 HSCT aircraft operating at 2 km below nominal cruise altitude with EI(NO_x)=5 under Scenario S10a relative to Scenario D9. Contours are -1, -0.5, 0, 0.5, 1, 2.

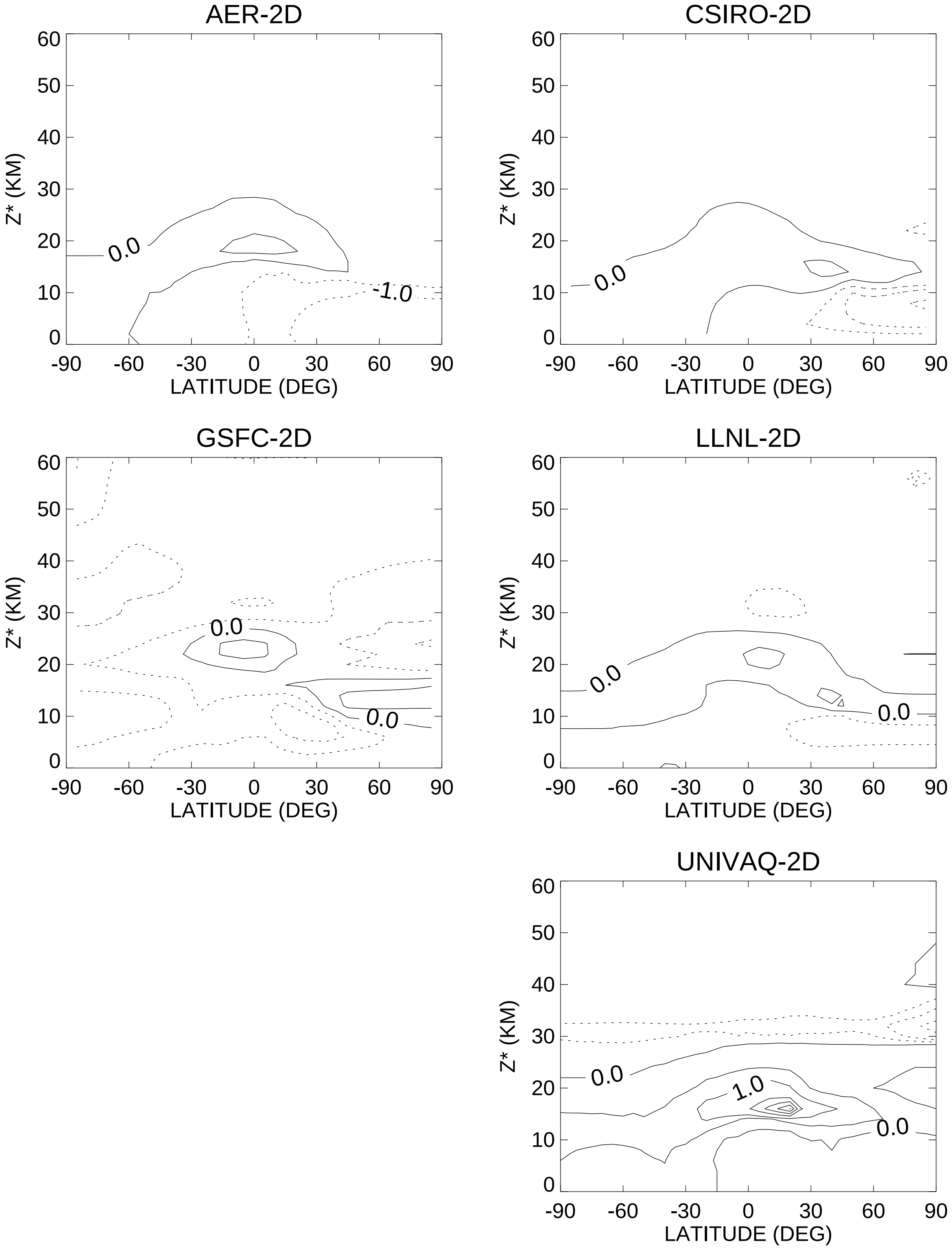

Figure 5.44: Calculated perturbations to O_3 (percent) as a function of latitude and altitude in June of 2050 due to emissions from a fleet of 1000 HSCT aircraft operating at 2 km below nominal cruise altitude with $EI(NO_x)=5$ under Scenario S10a relative to Scenario D9. Contours are -2, -1, -0.5, 0, 0.5, 1, 2, 3, 4, 5.

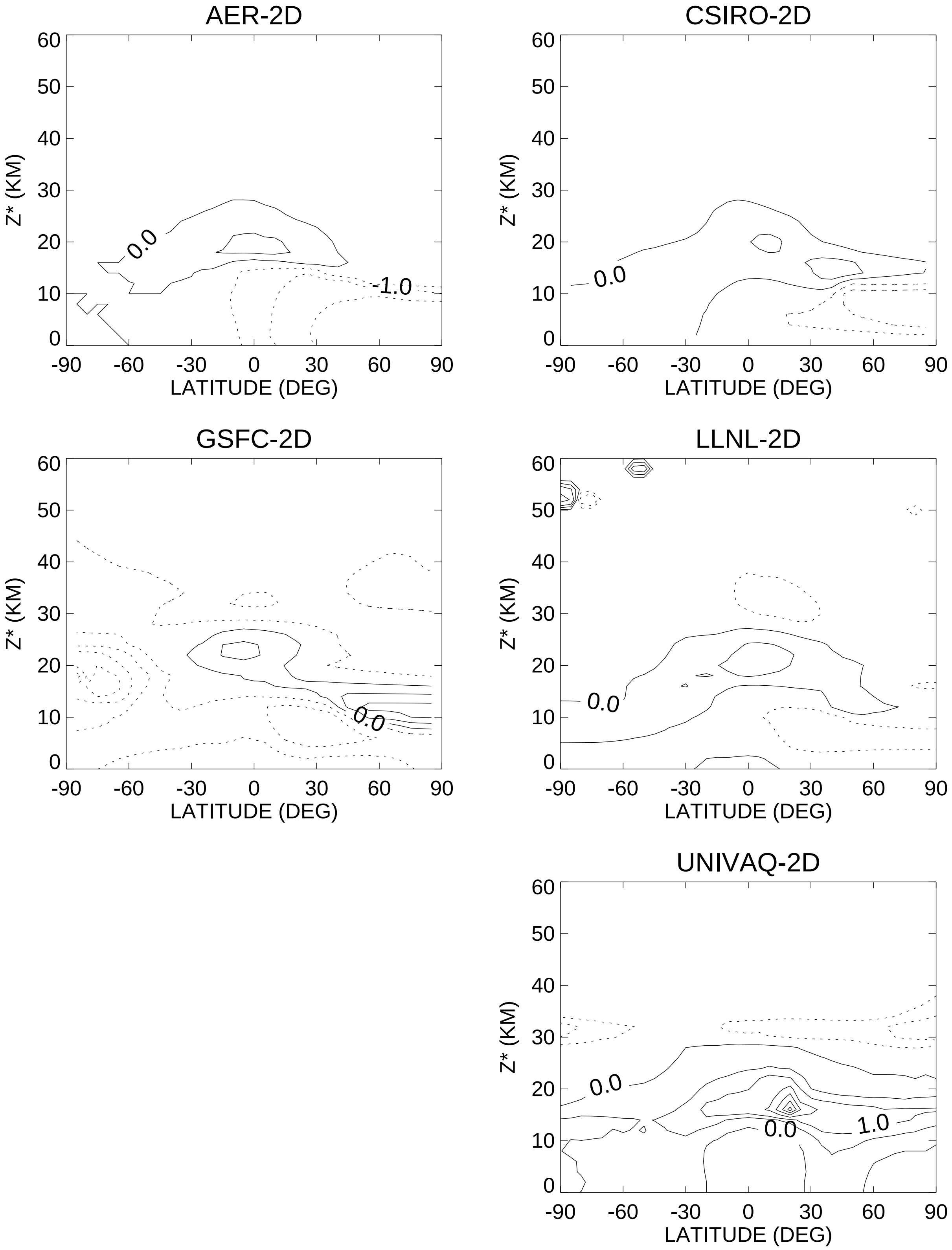

Figure 5.45: Calculated perturbations to O_3 (percent) as a function of latitude and altitude in October of 2050 due to emissions from a fleet of 1000 HSCT aircraft operating at 2 km below nominal cruise altitude with EI(NO_x)=5 under Scenario S10a relative to Scenario D9. Contours are -3, -2, -1, -0.5, 0, 0.5, 1, 2, 3, 4, 5.

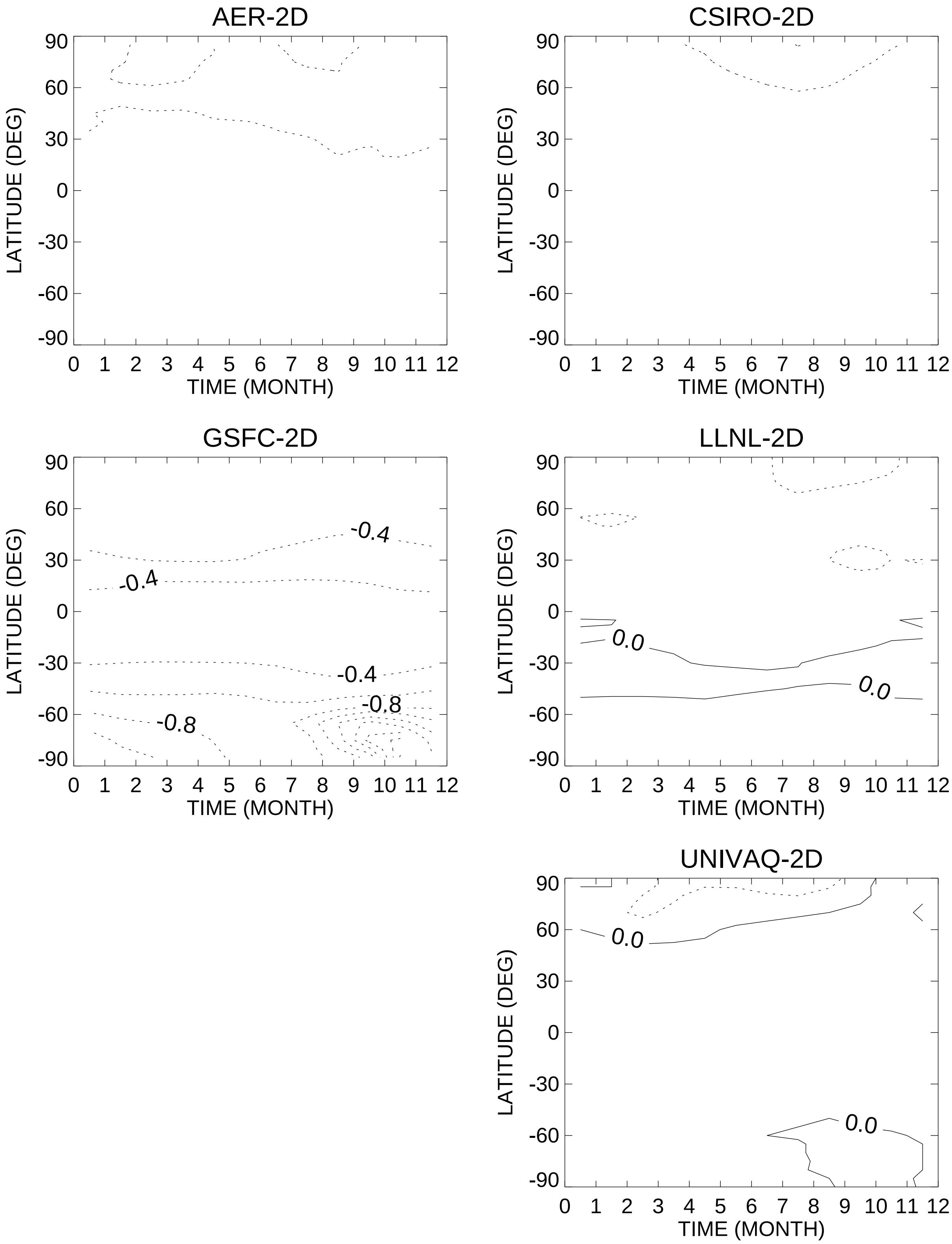

Figure 5.46: Calculated perturbations to column O_3 (percent) as a function of latitude and season in 2050 due to emissions from a fleet of 1000 HSCT aircraft operating at 2 km below nominal cruise altitude with $EI(NO_x)=5$ under Scenario S10a relative to Scenario D9. Contours are -1.6 to 0 by 0.2.

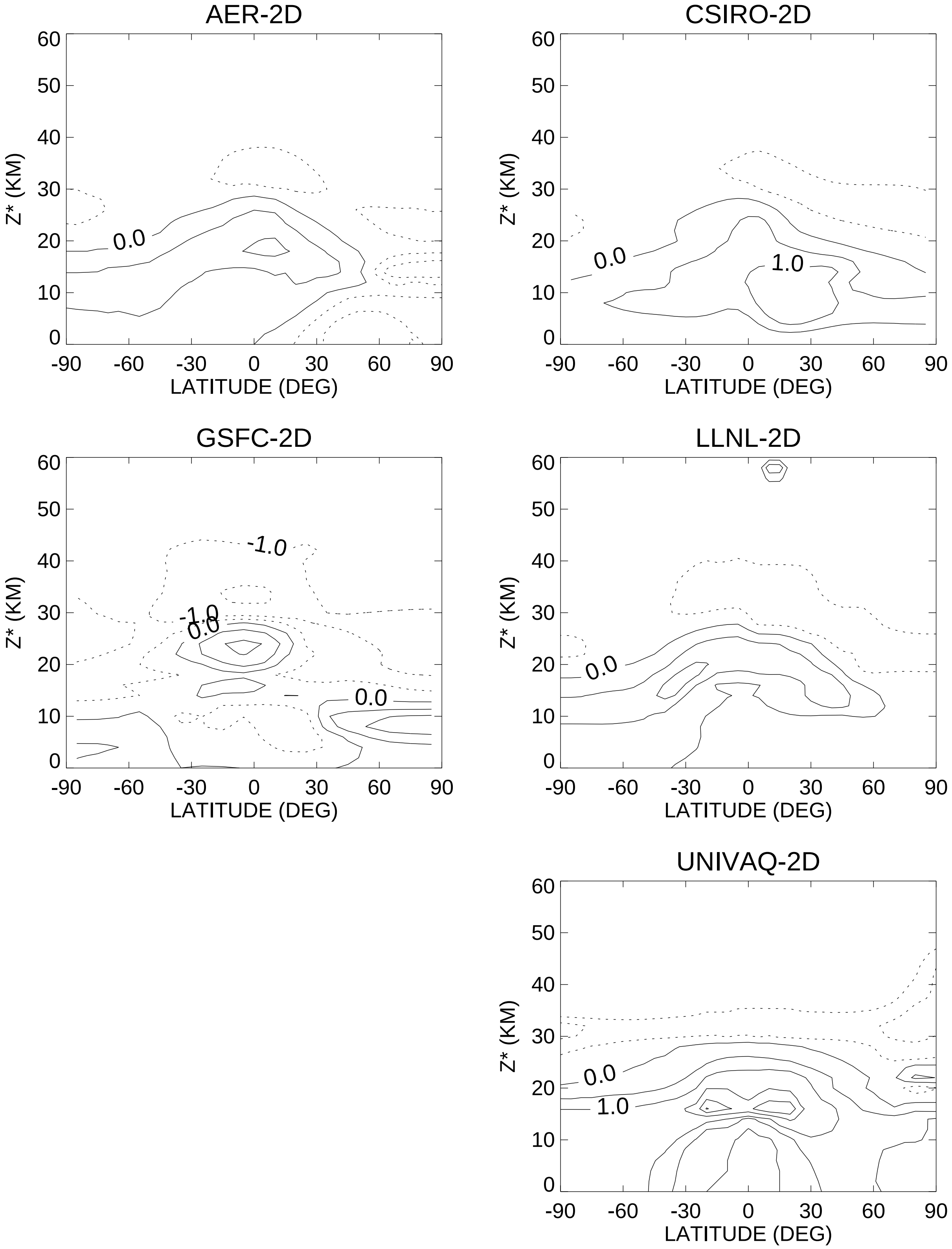

Figure 5.47: Calculated perturbations to O_3 (percent) as a function of latitude and altitude in March of 2050 due to emissions from a fleet of 1000 HSCT aircraft operating at 2 km below nominal cruise altitude with EI(NO_x)=10 under Scenario S10b relative to Scenario D9. Contours are -2, -1, -0.5, 0, 0.5, 1, 2, 3, 4.

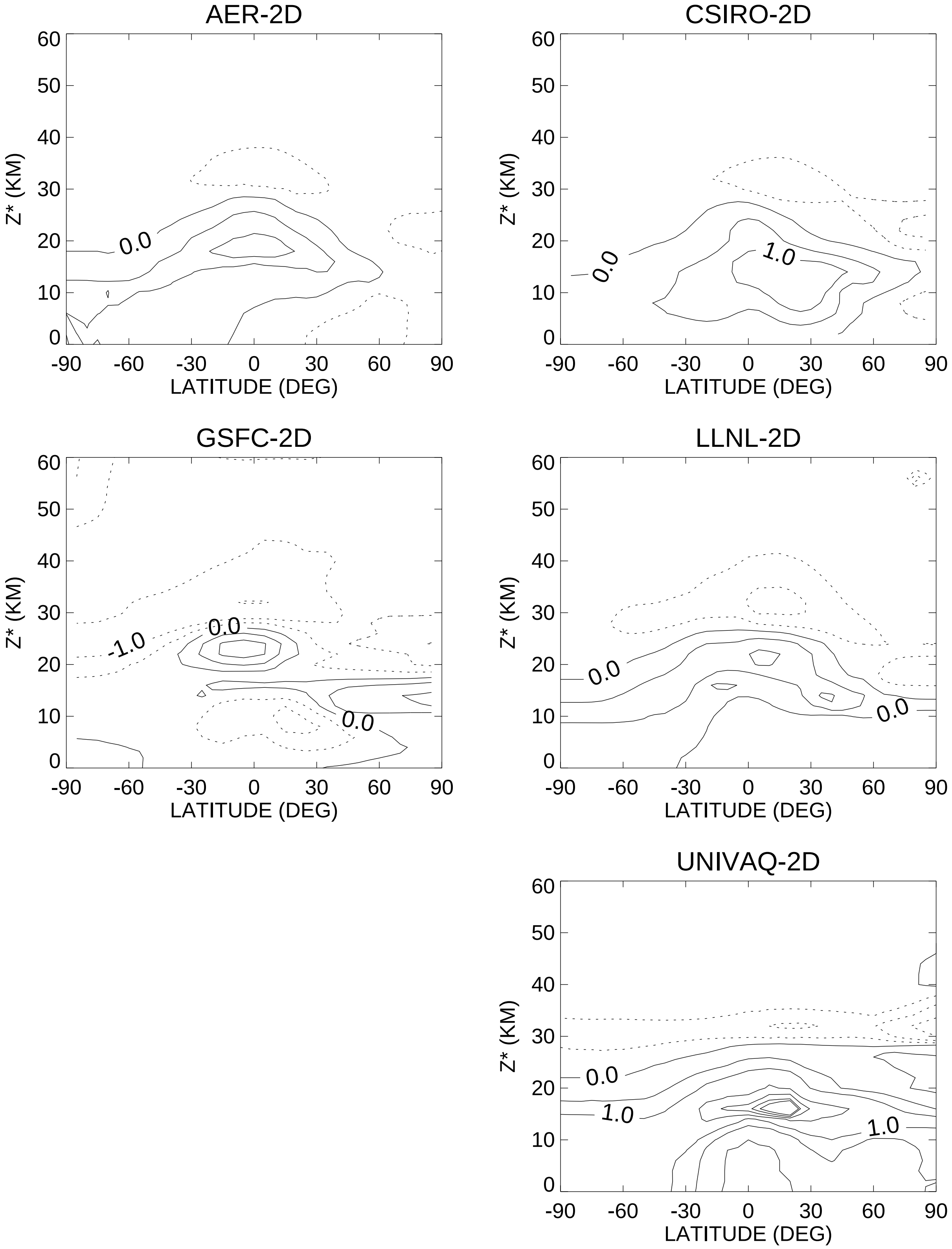

Figure 5.48: Calculated perturbations to O_3 (percent) as a function of latitude and altitude in June of 2050 due to emissions from a fleet of 1000 HSCT aircraft operating at 2 km below nominal cruise altitude with $EI(NO_x)$=10 under Scenario S10b relative to Scenario D9. Contours are -2, -1, -0.5, 0, 0.5, 1, 2, 3, 4, 5.

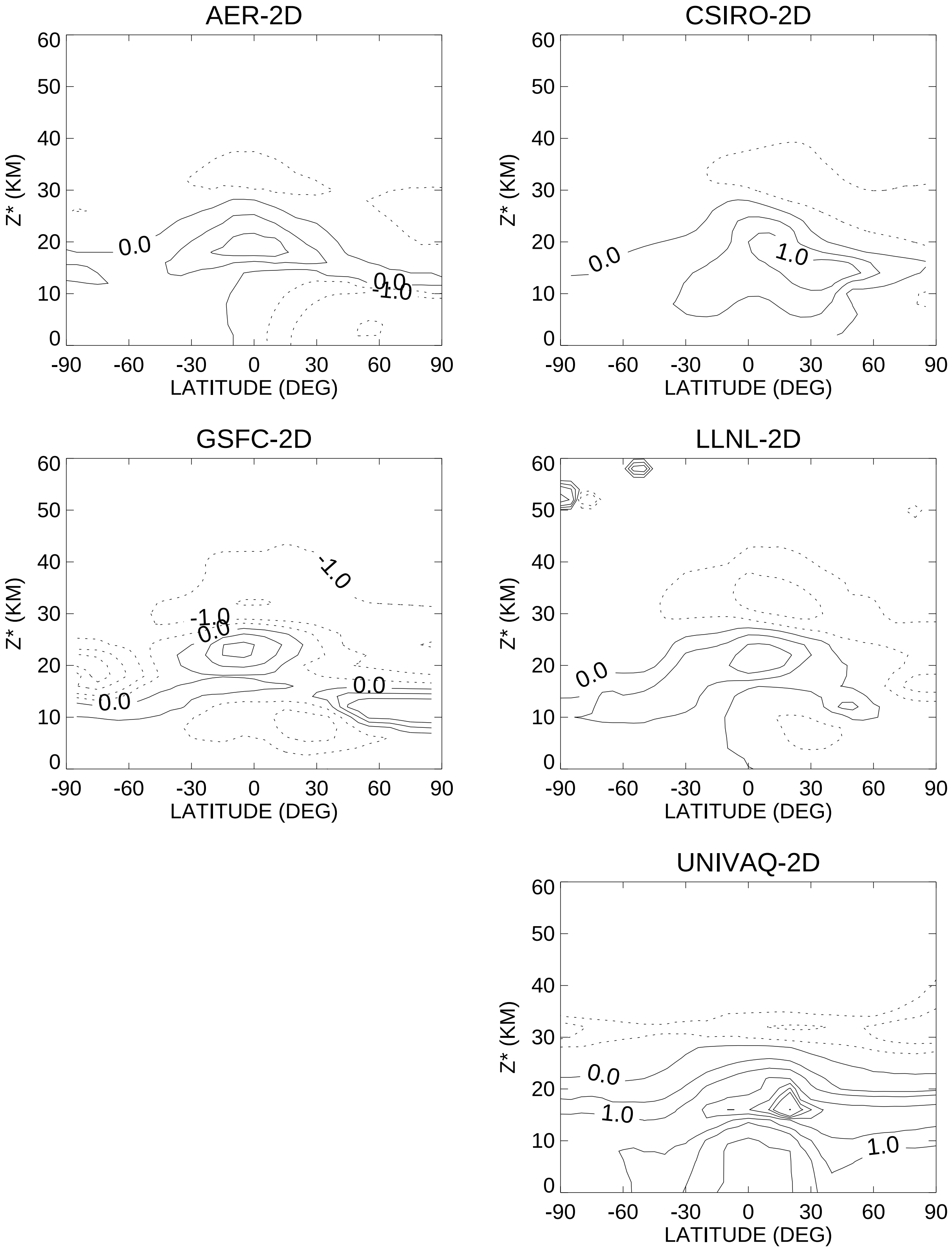

Figure 5.49: Calculated perturbations to O_3 (percent) as a function of latitude and altitude in October of 2050 due to emissions from a fleet of 1000 HSCT aircraft operating at 2 km below nominal cruise altitude with EI(NO_x)=10 under Scenario S10b relative to Scenario D9. Contours are -3, -2, -1, -0.5, 0, 0.5, 1, 2, 3, 4, 5, 6.

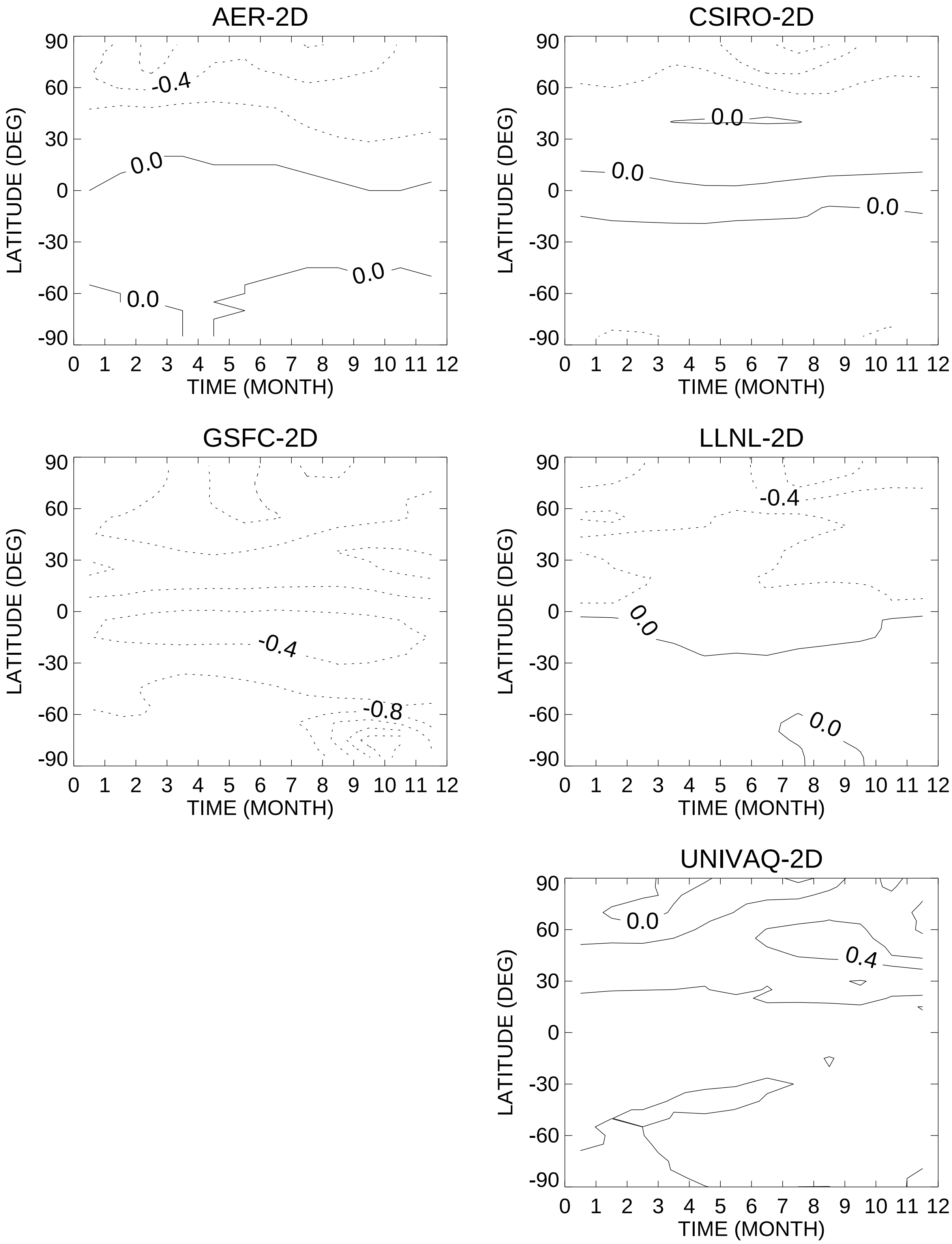

Figure 5.50: Calculated perturbations to column O_3 (percent) as a function of latitude and season in 2050 due to emissions from a fleet of 1000 HSCT aircraft operating at 2 km below nominal cruise altitude with EI(NO_x)=10 under Scenario S10b relative to Scenario D9. Contours are -1.4 to 0.4 by 0.2.

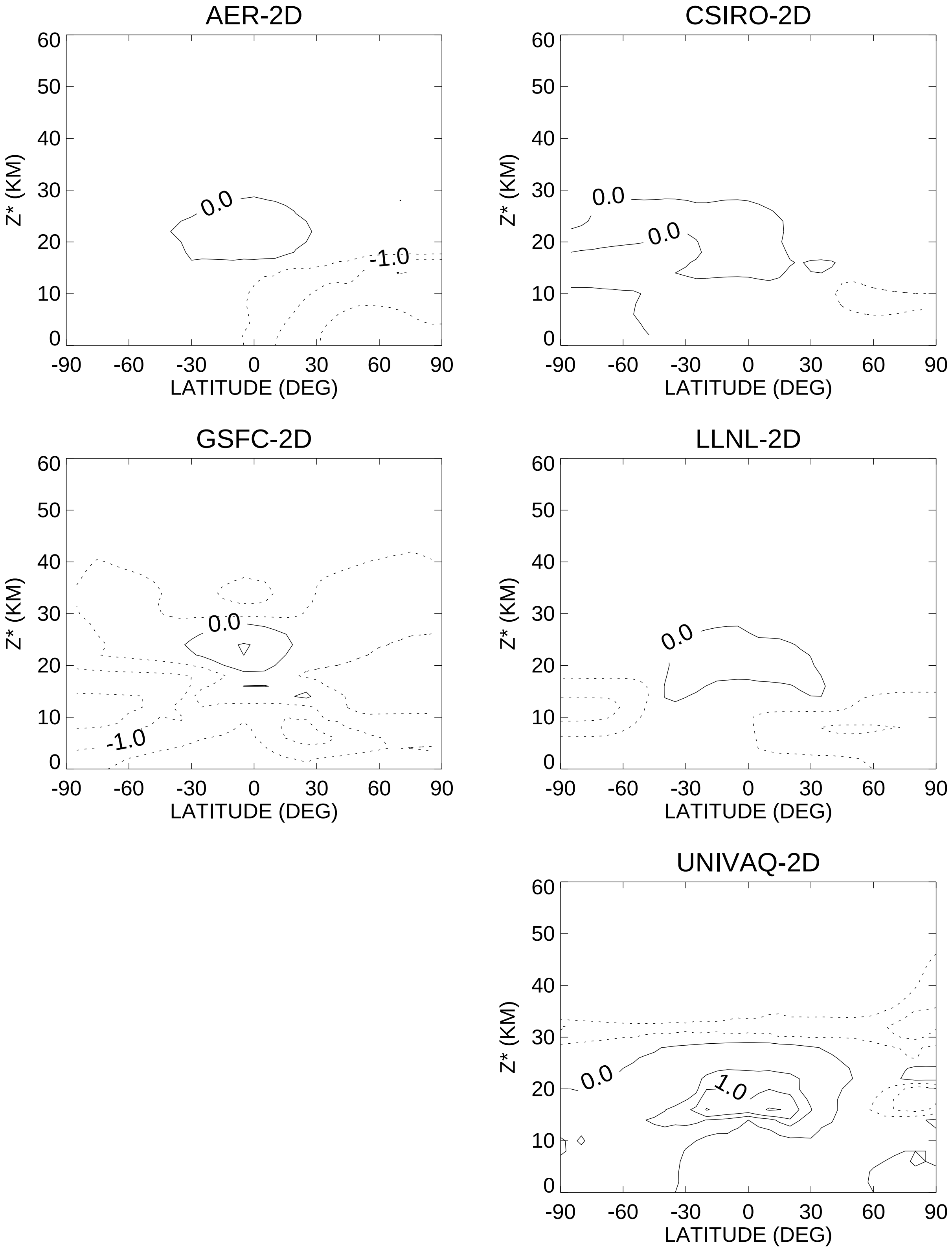

Figure 5.51: Calculated perturbations to O_3 (percent) as a function of latitude and altitude in March of 2050 due to emissions from a fleet of 1000 HSCT aircraft operating at 2 km below nominal cruise altitude with EI(NO_x)=5 with SA6-2km sulfate surface area density under Scenario S10c relative to Scenario D9. Contours are -2, -1, -0.5, 0, 0.5, 1, 2.

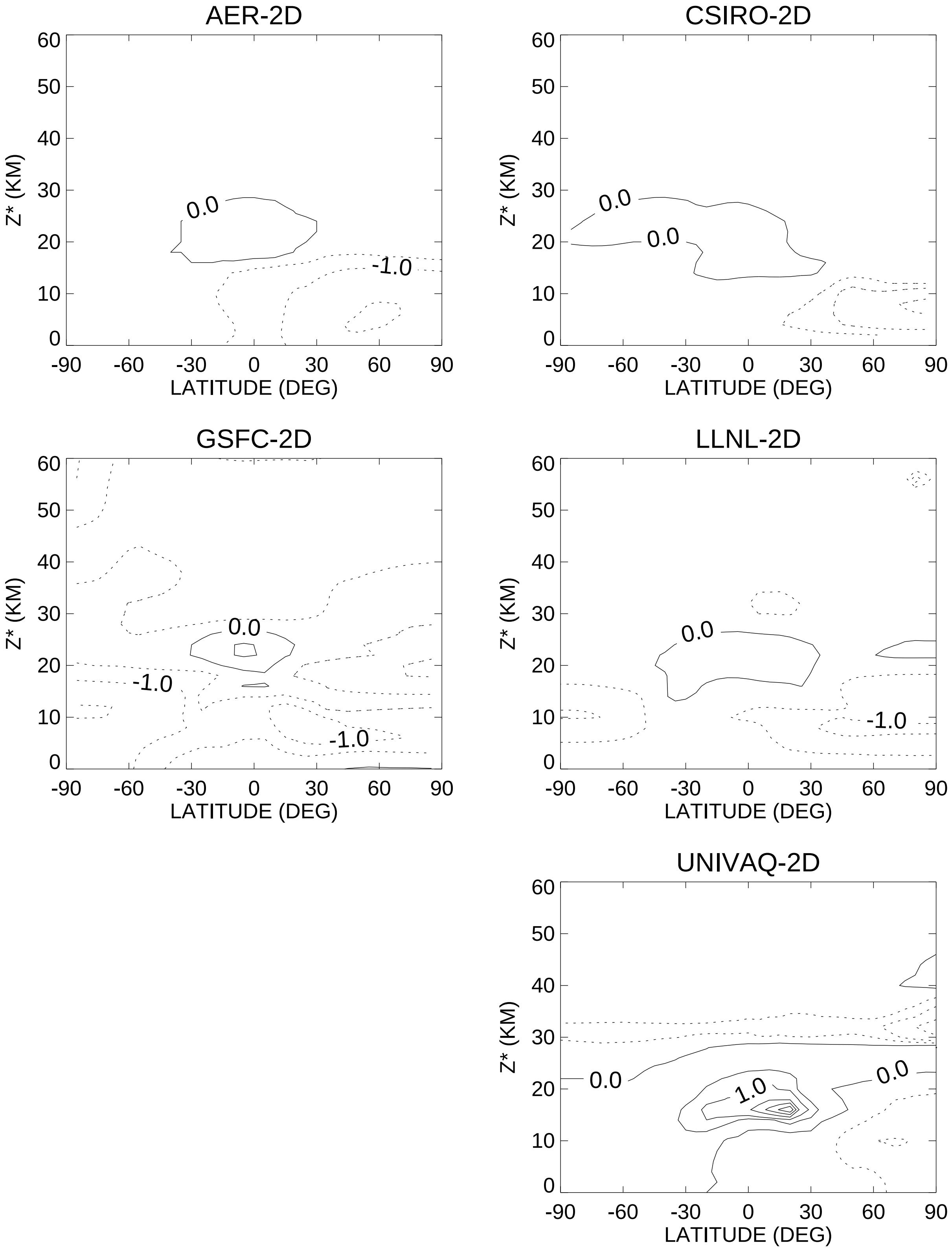

Figure 5.52: Calculated perturbations to O_3 (percent) as a function of latitude and altitude in June of 2050 due to emissions from a fleet of 1000 HSCT aircraft operating at 2 km below nominal cruise altitude with EI(NO_x)=5 with SA6-2km sulfate surface area density under Scenario S10c relative to Scenario D9. Contours are -2, -1, -0.5, 0, 0.5, 1, 2, 3, 4.

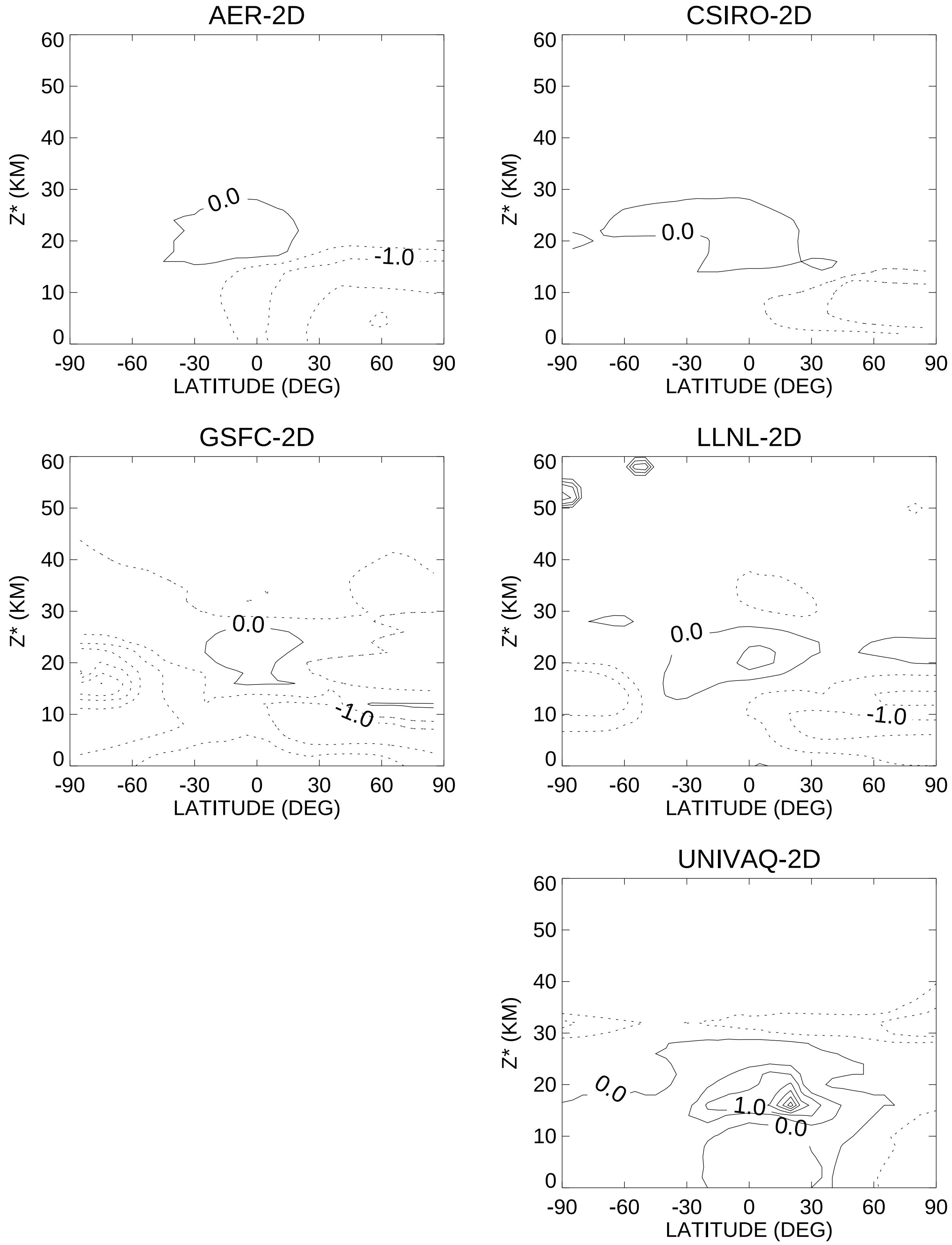

Figure 5.53: Calculated perturbations to O_3 (percent) as a function of latitude and altitude in October of 2050 due to emissions from a fleet of 1000 HSCT aircraft operating at 2 km below nominal cruise altitude with EI(NO_x)=5 with SA6-2km sulfate surface area density under Scenario S10c relative to Scenario D9. Contours are -5, -4, -3, -2, -1, -0.5, 0, 0.5, 1, 2, 3, 4, 5.

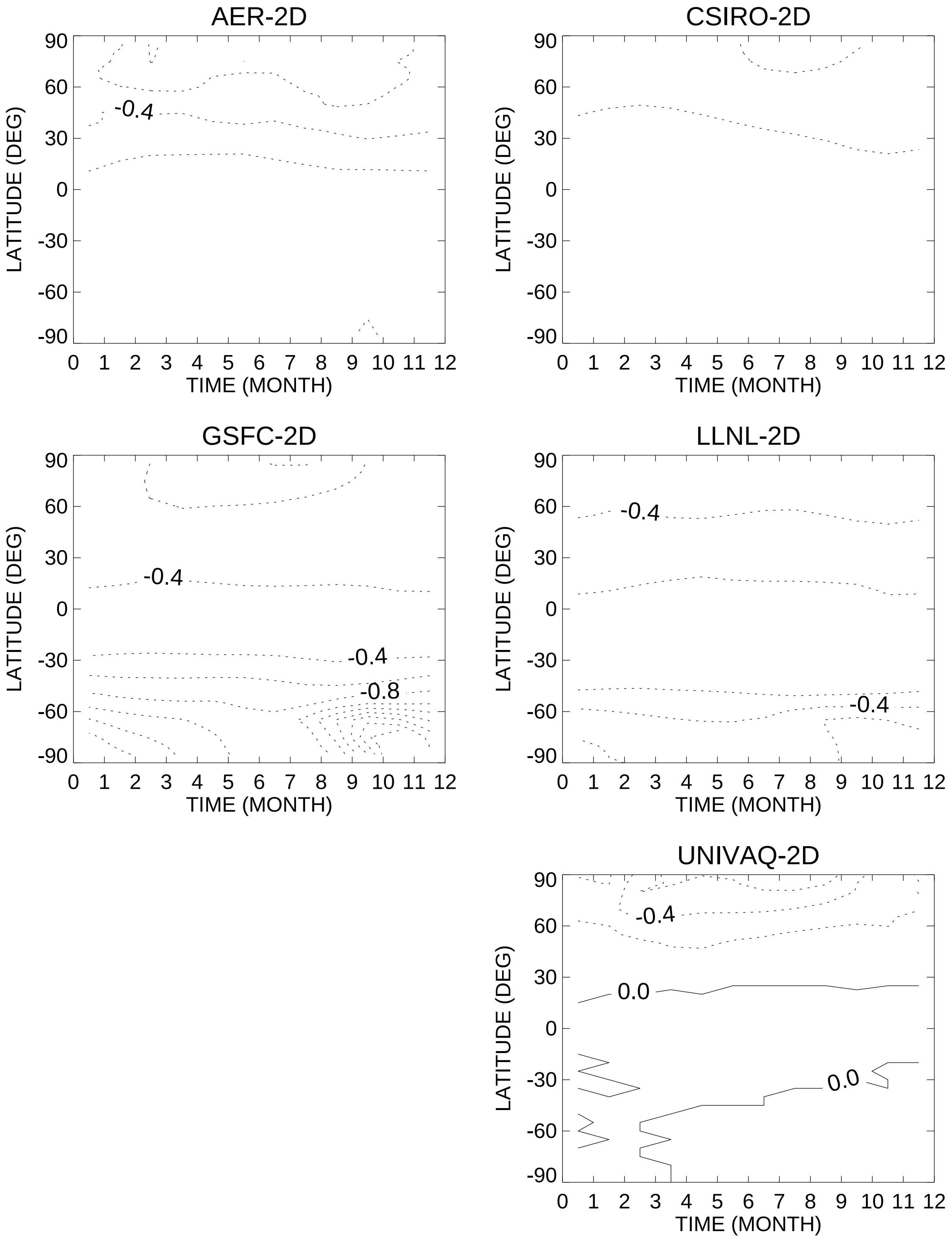

Figure 5.54: Calculated perturbations to column O_3 (percent) as a function of latitude and season in 2050 due to emissions from a fleet of 1000 HSCT aircraft operating at 2 km below nominal cruise altitude with $EI(NO_x)=5$ with SA6-2km sulfate surface area density under Scenario S10c relative to Scenario D9. Contours are -2.0 to 0 by 0.2.

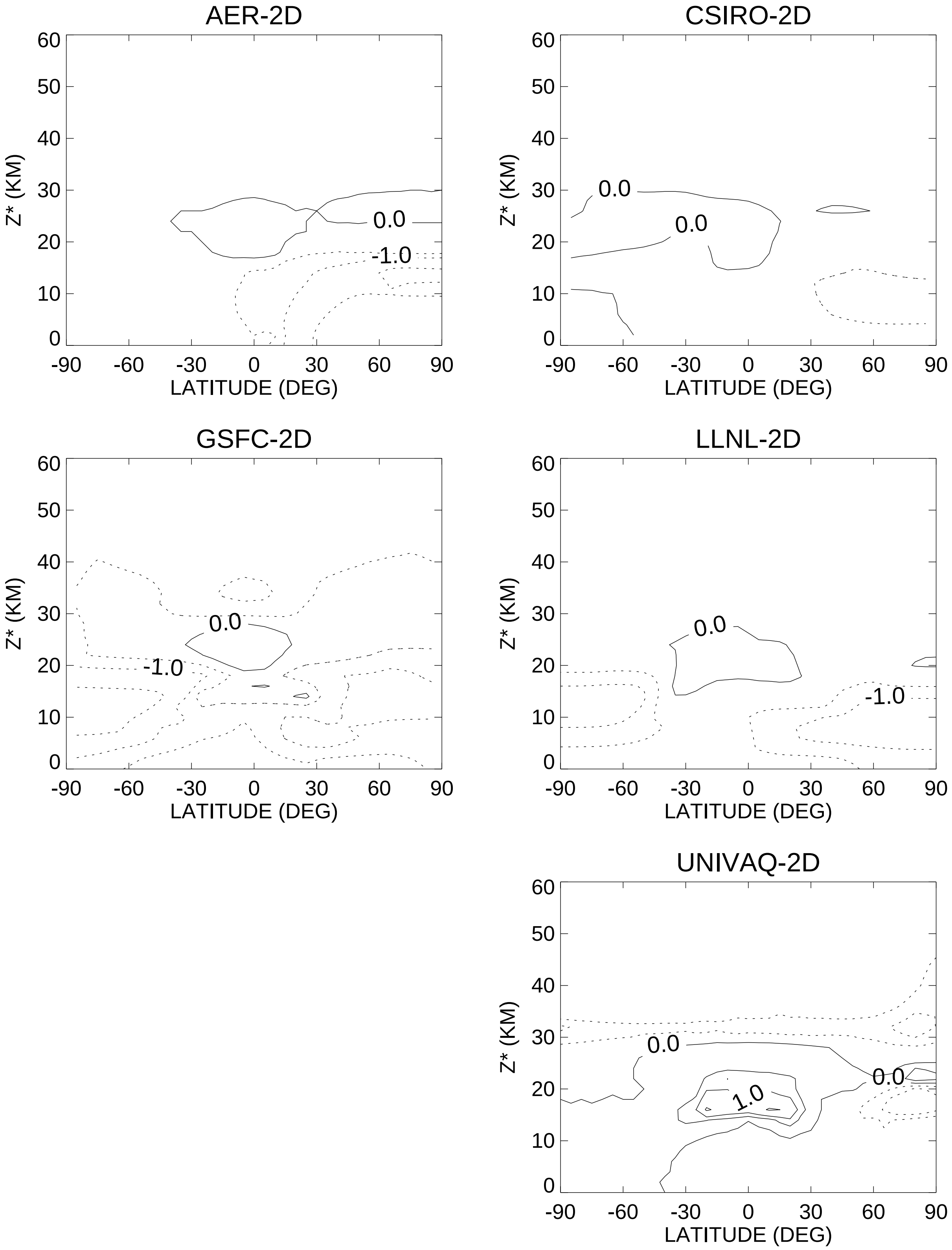

Figure 5.55: Calculated perturbations to O_3 (percent) as a function of latitude and altitude in March of 2050 due to emissions from a fleet of 1000 HSCT aircraft operating at 2 km below nominal cruise altitude with EI(NO_x)=5 with SA2-2km sulfate surface area density under Scenario S10d relative to Scenario D9. Contours are -2, -1, -0.5, 0, 0.5, 1, 2.

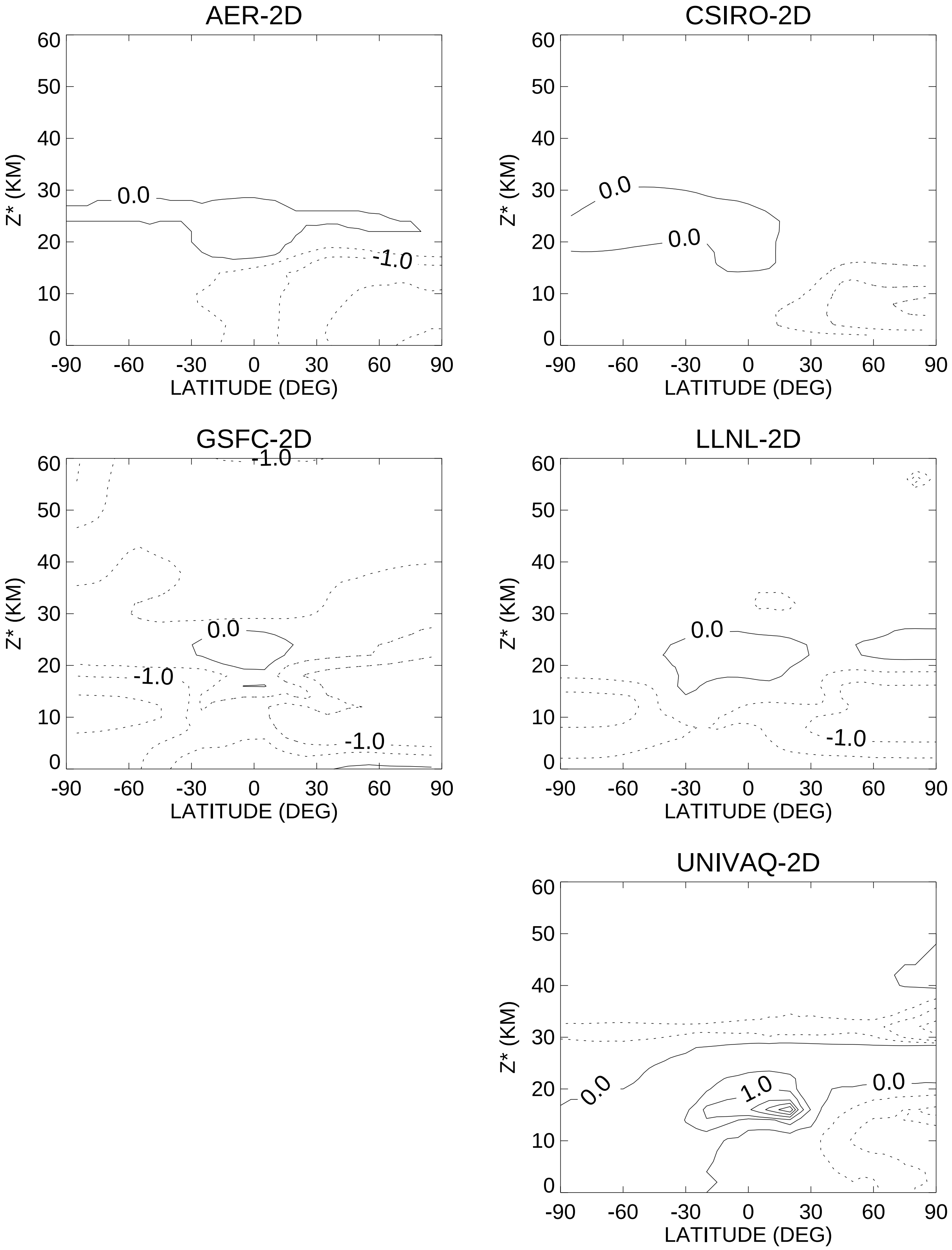

Figure 5.56: Calculated perturbations to O_3 (percent) as a function of latitude and altitude in June of 2050 due to emissions from a fleet of 1000 HSCT aircraft operating at 2 km below nominal cruise altitude with EI(NO_x)=5 with SA2-2km sulfate surface area density under Scenario S10d relative to Scenario D9. Contours are -3, -2, -1, -0.5, 0, 0.5, 1, 2, 3, 4.

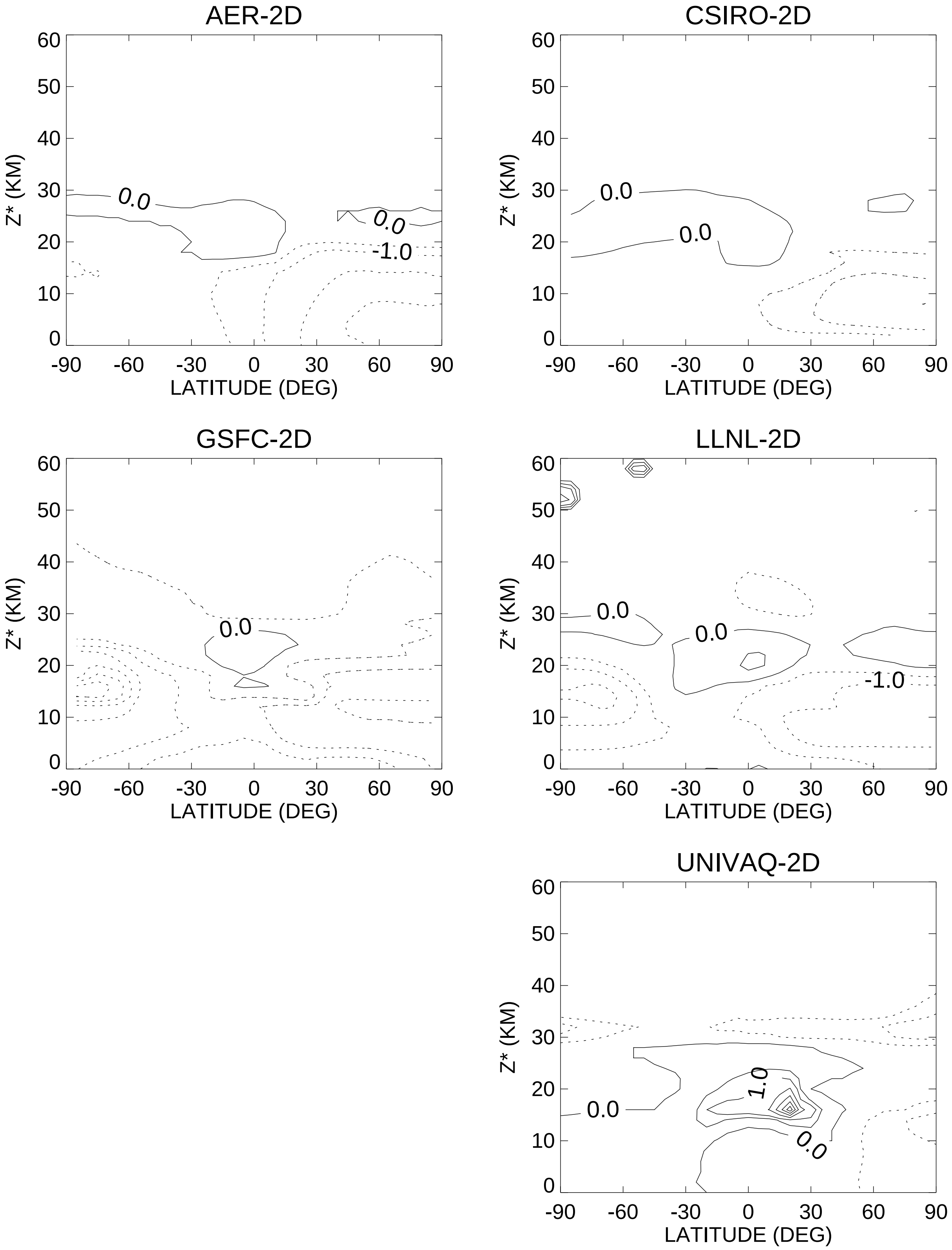

Figure 5.57: Calculated perturbations to O_3 (percent) as a function of latitude and altitude in October of 2050 due to emissions from a fleet of 1000 HSCT aircraft operating at 2 km below nominal cruise altitude with EI(NO_x)=5 with SA2-2km sulfate surface area density under Scenario S10d relative to Scenario D9. Contours are -5, -4, -3, -2, -1, -0.5, 0, 0.5, 1, 2, 3, 4, 5.

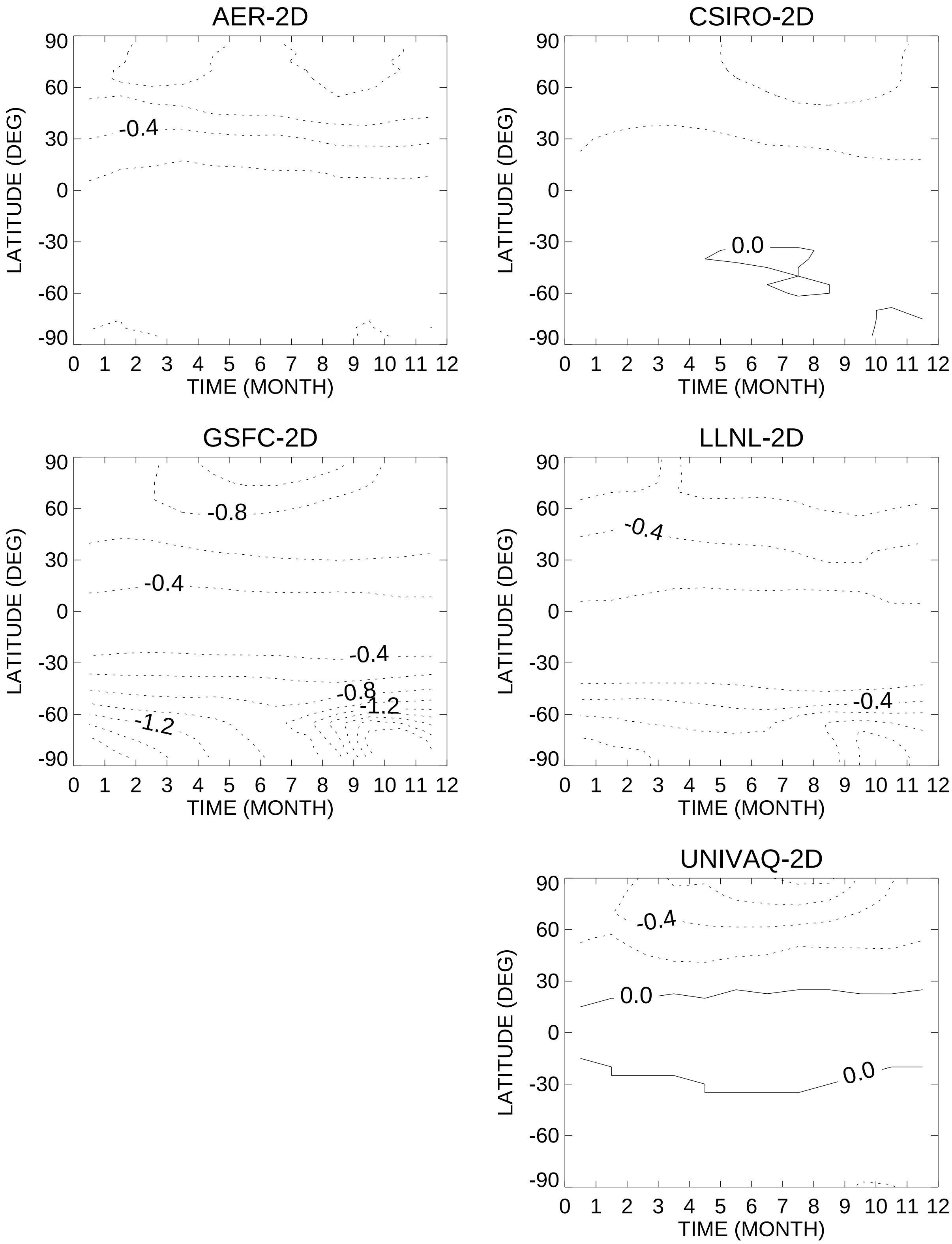

Figure 5.58: Calculated perturbations to column O_3 (percent) as a function of latitude and season in 2050 due to emissions from a fleet of 1000 HSCT aircraft operating at 2 km below nominal cruise altitude with $EI(NO_x)=5$ with SA2-2km sulfate surface area density under Scenario S10d relative to Scenario D9. Contours are -2.0 to 0 by 0.2.

5.3.4 Scenarios with Modified Subsonic Fleets (S11a, S12a)

Scenarios S11a and S12a use subsonic fleets projected to 2050 based on various assumptions regarding economic growth in the intervening years. The other scenarios for 2050 used the same subsonic fleet as was used for the 2015 scenarios. The IS92a subsonic fleet is used for Scenario S11a which includes 1000 HSCTs and for Scenario F which uses only subsonic aircraft. The IS92a subsonic fleet uses 50% more fuel per year than the 2015 subsonic fleet. Calculated ozone depletions for Scenario S11a relative to Scenario F are shown in Figures 5.59, 5.60, and 5.61. Differences due to the subsonic fleet are found mostly below 10 km, as can be seen by comparing this results with that for Scenario S10d-D9. Perturbations to column ozone for S11a are shown in Figure 5.62. Differences between this result and S10d-D9 are small.

Scenario S12a uses the IS92e high demand subsonic scenario. Subsonic fuel usage for IS92e high demand is a factor of 2.4 times greater than for the 2015 subsonic scenario. Figures 5.63, 5.64, and 5.65 show calculated changes in ozone for Scenario S12a relative to Scenario G. Stratospheric ozone perturbations are changed very little by the greatly increased subsonic fleet. Figure 5.66 shows changes in calculated column ozone. These column ozone changes are virtually identical to those for S11a-F and S10d-D9.

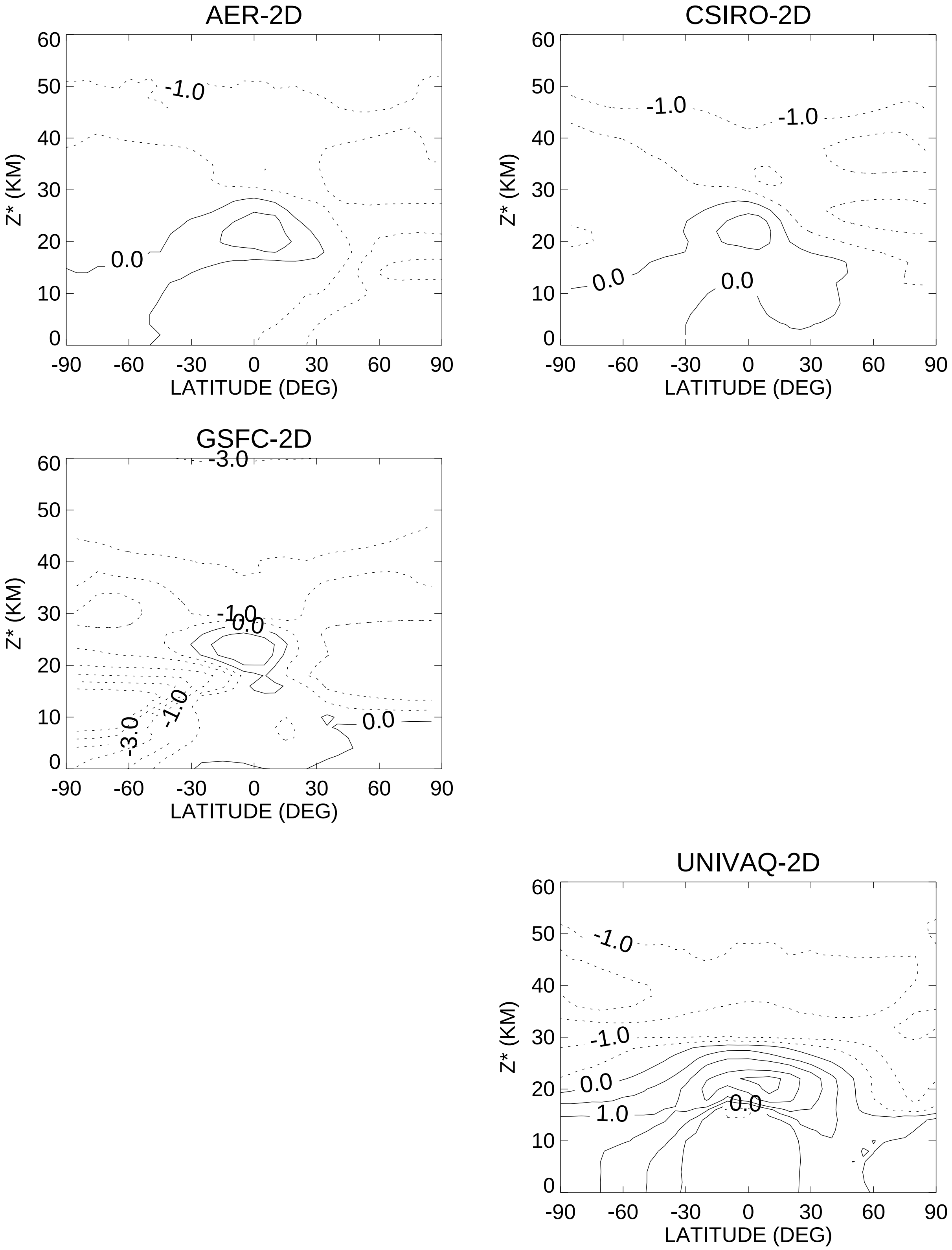

Figure 5.59: Calculated perturbations to O_3 (percent) as a function of latitude and altitude in March of 2050 due to emissions from a fleet of 1000 HSCT aircraft with $EI(NO_x)=5$ and utilizing the IS92a subsonic fleet under Scenario S11a relative to Scenario F. Contours are -5, -4, -3, -2, -1, -0.5, 0, 0.5, 1, 2, 3.

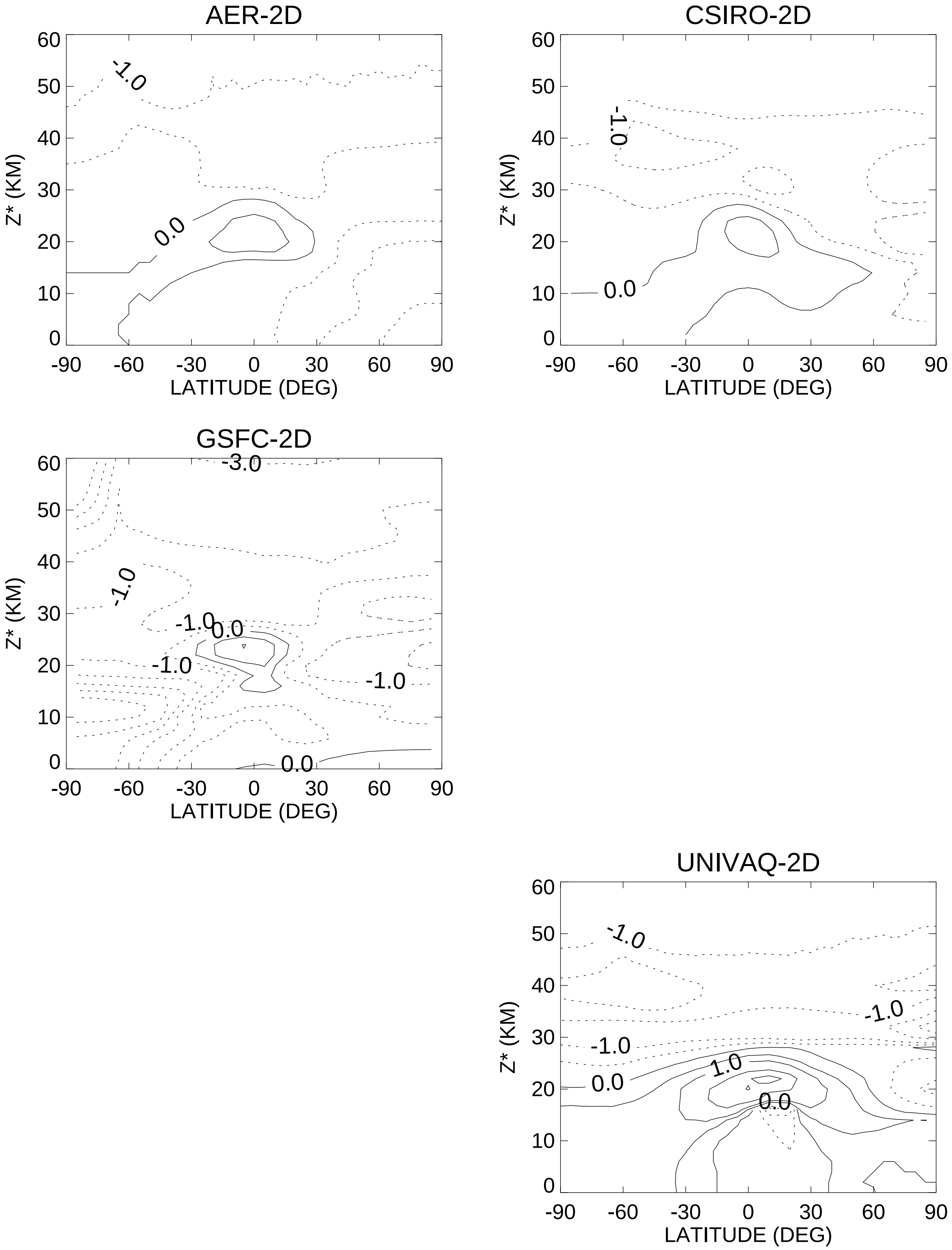

Figure 5.60: Calculated perturbations to O_3 (percent) as a function of latitude and altitude in June of 2050 due to emissions from a fleet of 1000 HSCT aircraft with $EI(NO_x)=5$ and utilizing the IS92a subsonic fleet under Scenario S11a relative to Scenario F. Contours are -5, -4, -3, -2, -1, -0.5, 0, 0.5, 1, 2, 3.

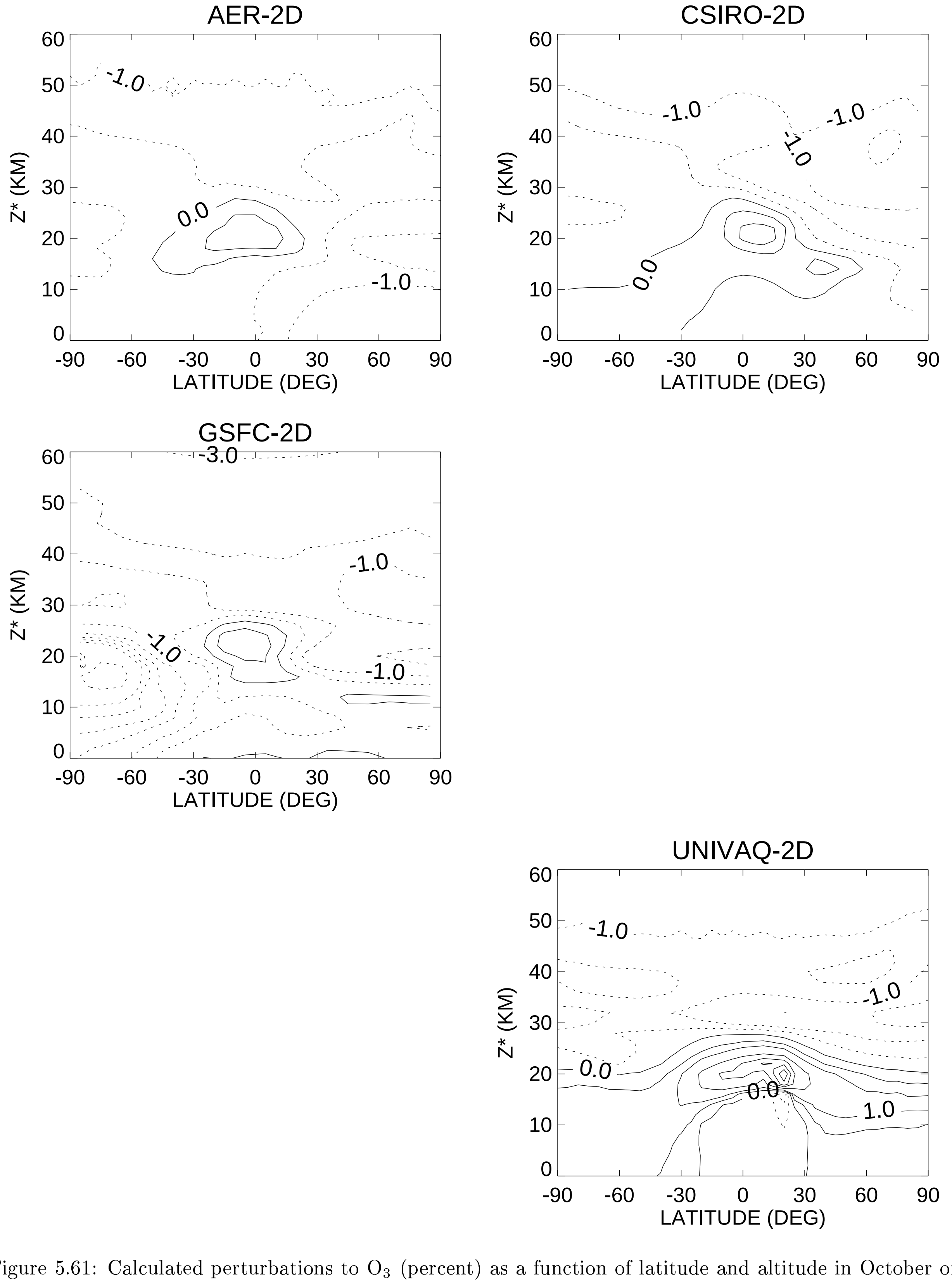

Figure 5.61: Calculated perturbations to O_3 (percent) as a function of latitude and altitude in October of 2050 due to emissions from a fleet of 1000 HSCT aircraft with EI(NO_x)=5 and utilizing the IS92a subsonic fleet under Scenario S11a relative to Scenario F. Contours are -10, -5, -4, -3, -2, -1, -0.5, 0, 0.5, 1, 2, 3, 4, 5.

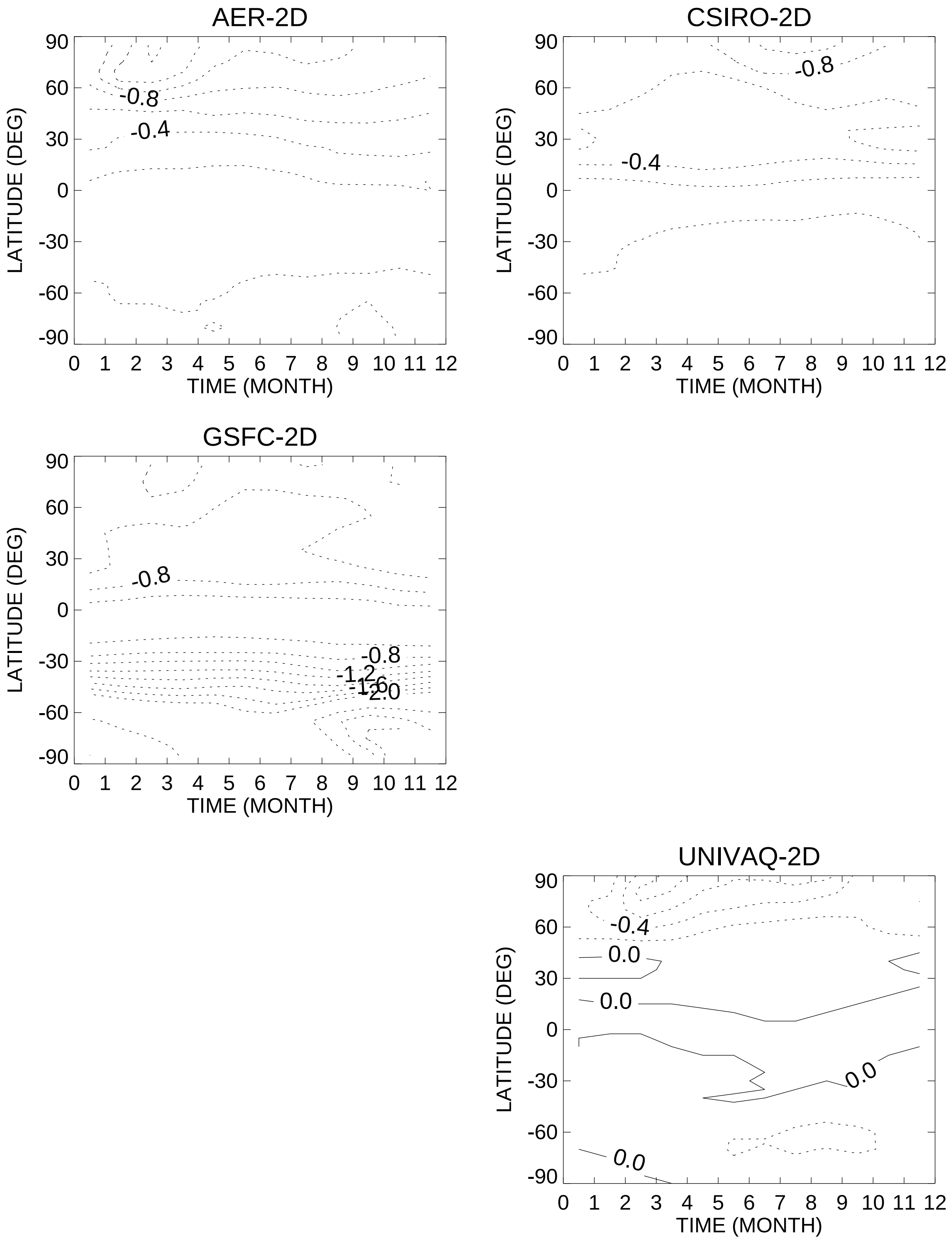

Figure 5.62: Calculated perturbations to column O_3 (percent) as a function of latitude and season in 2050 due to emissions from a fleet of 1000 HSCT aircraft with $EI(NO_x)=5$ and utilizing the IS92a subsonic fleet under Scenario S11a relative to Scenario F. Contours are -5, -4, -3, and -2.0 to 0 by 0.2.

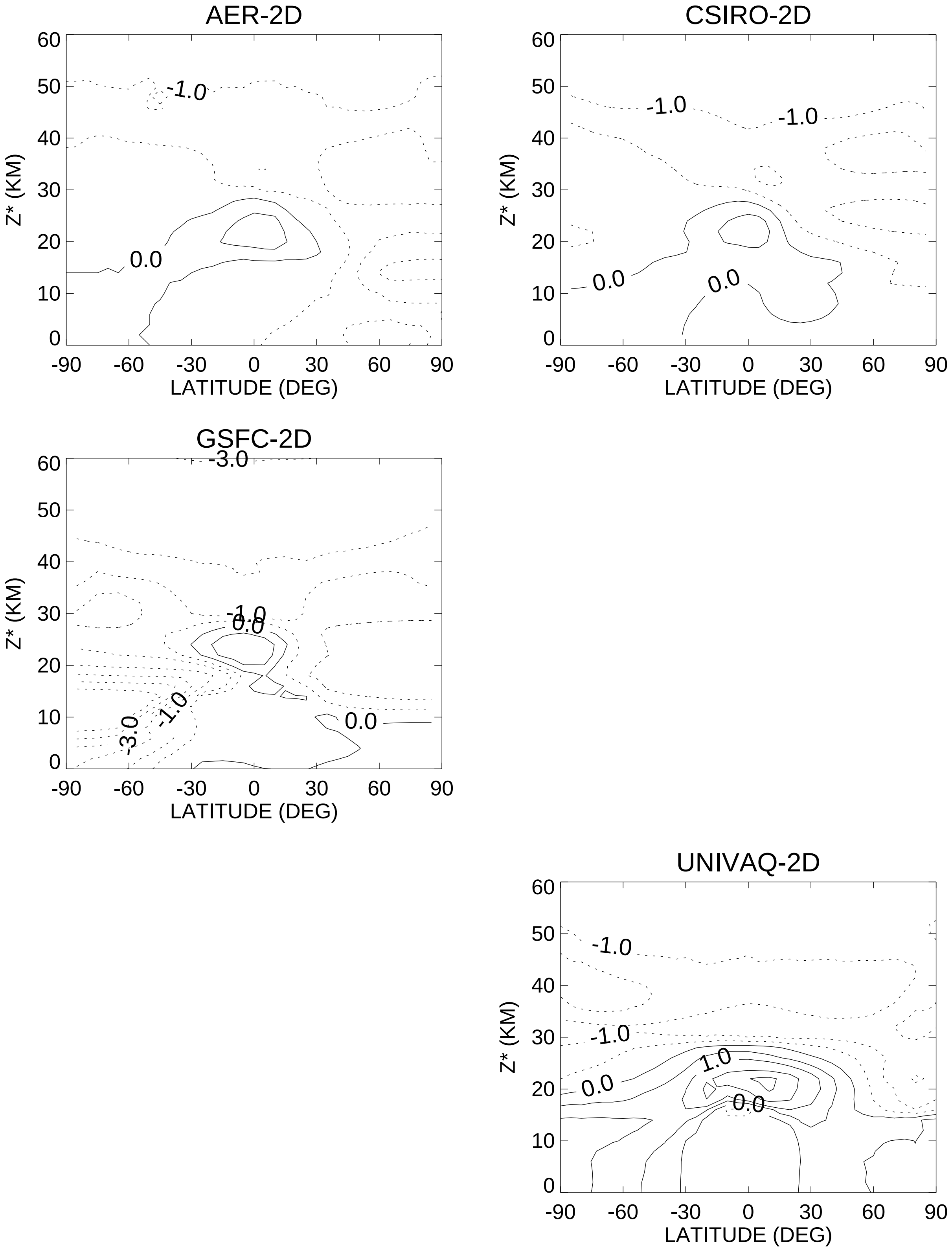

Figure 5.63: Calculated perturbations to O_3 (percent) as a function of latitude and altitude in March of 2050 due to emissions from a fleet of 1000 HSCT aircraft with $EI(NO_x)=5$ and utilizing the IS92e high demand subsonic fleet under Scenario S12a relative to Scenario G. Contours are -5, -4, -3, -2, -1, -0.5, 0, 0.5, 1, 2, 3.

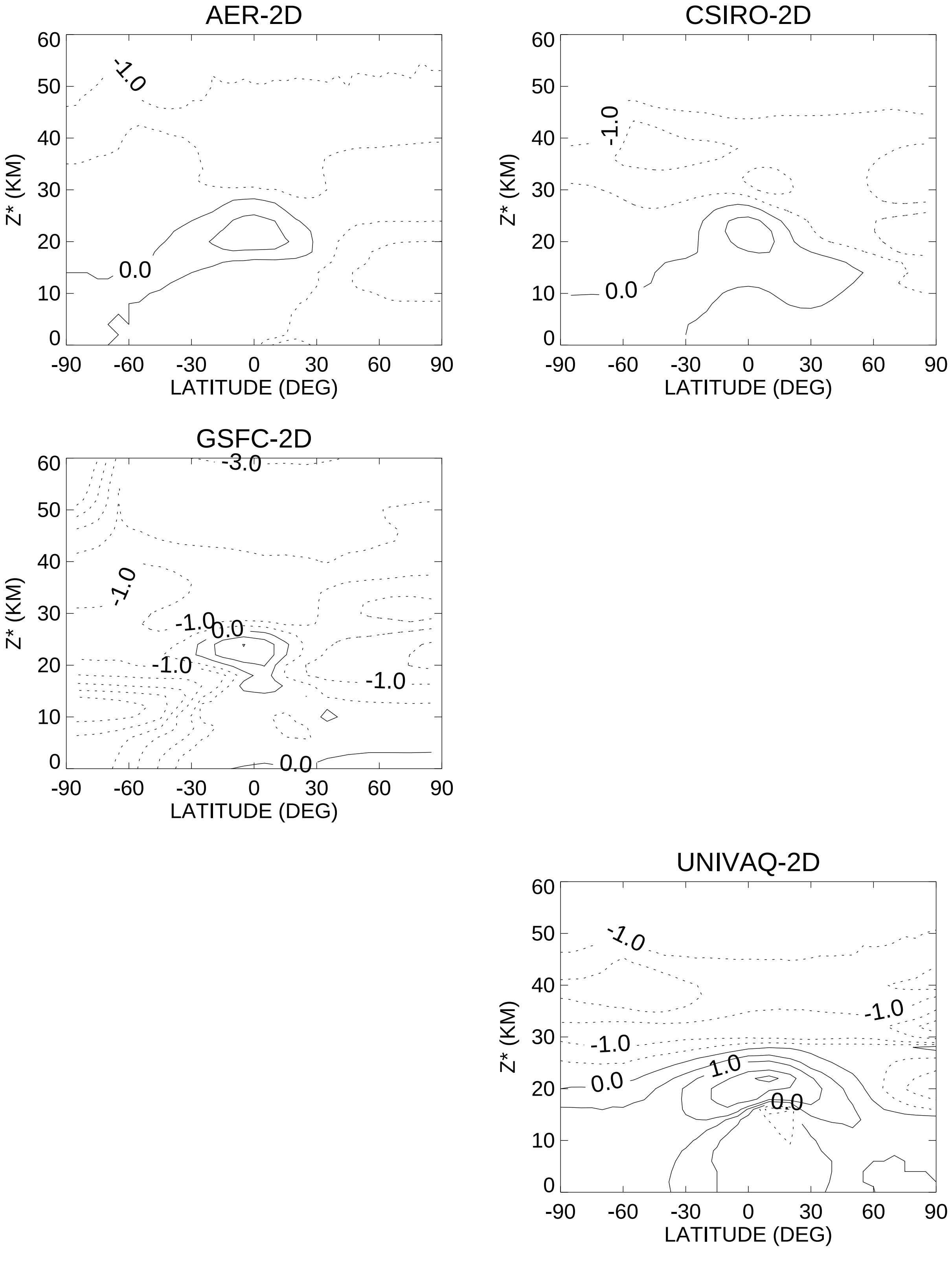

Figure 5.64: Calculated perturbations to O_3 (percent) as a function of latitude and altitude in June of 2050 due to emissions from a fleet of 1000 HSCT aircraft with $EI(NO_x)=5$ and utilizing the IS92e high demand subsonic fleet under Scenario S12a relative to Scenario G. Contours are -5, -4, -3, -2, -1, -0.5, 0, 0.5, 1, 2, 3.

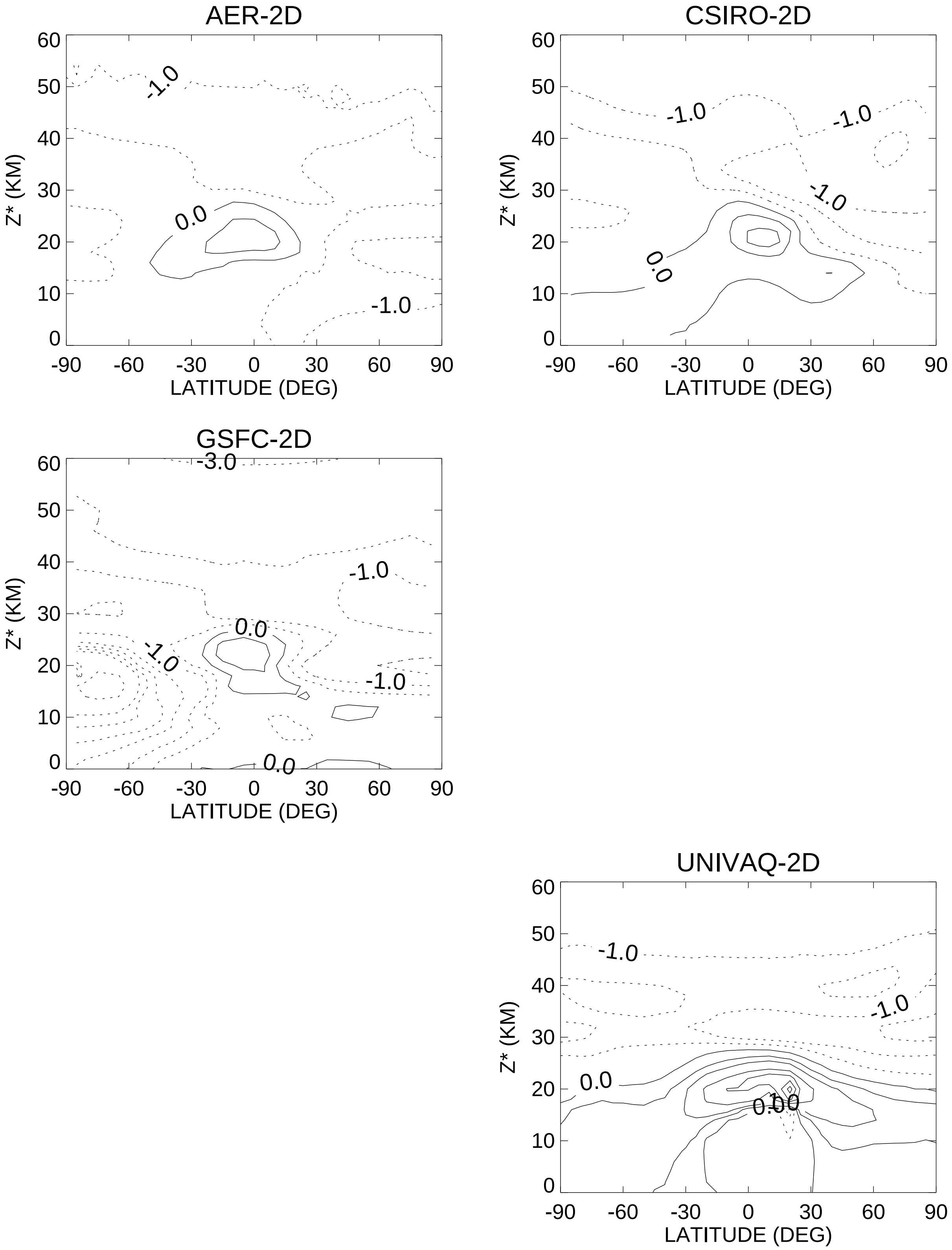

Figure 5.65: Calculated perturbations to O_3 (percent) as a function of latitude and altitude in October of 2050 due to emissions from a fleet of 1000 HSCT aircraft with $EI(NO_x)=5$ and utilizing the IS92e high demand subsonic fleet under Scenario S12a relative to Scenario G. Contours are -10, -5, -4, -3, -2, -1, -0.5, 0, 0.5, 1, 2, 3, 4, 5.

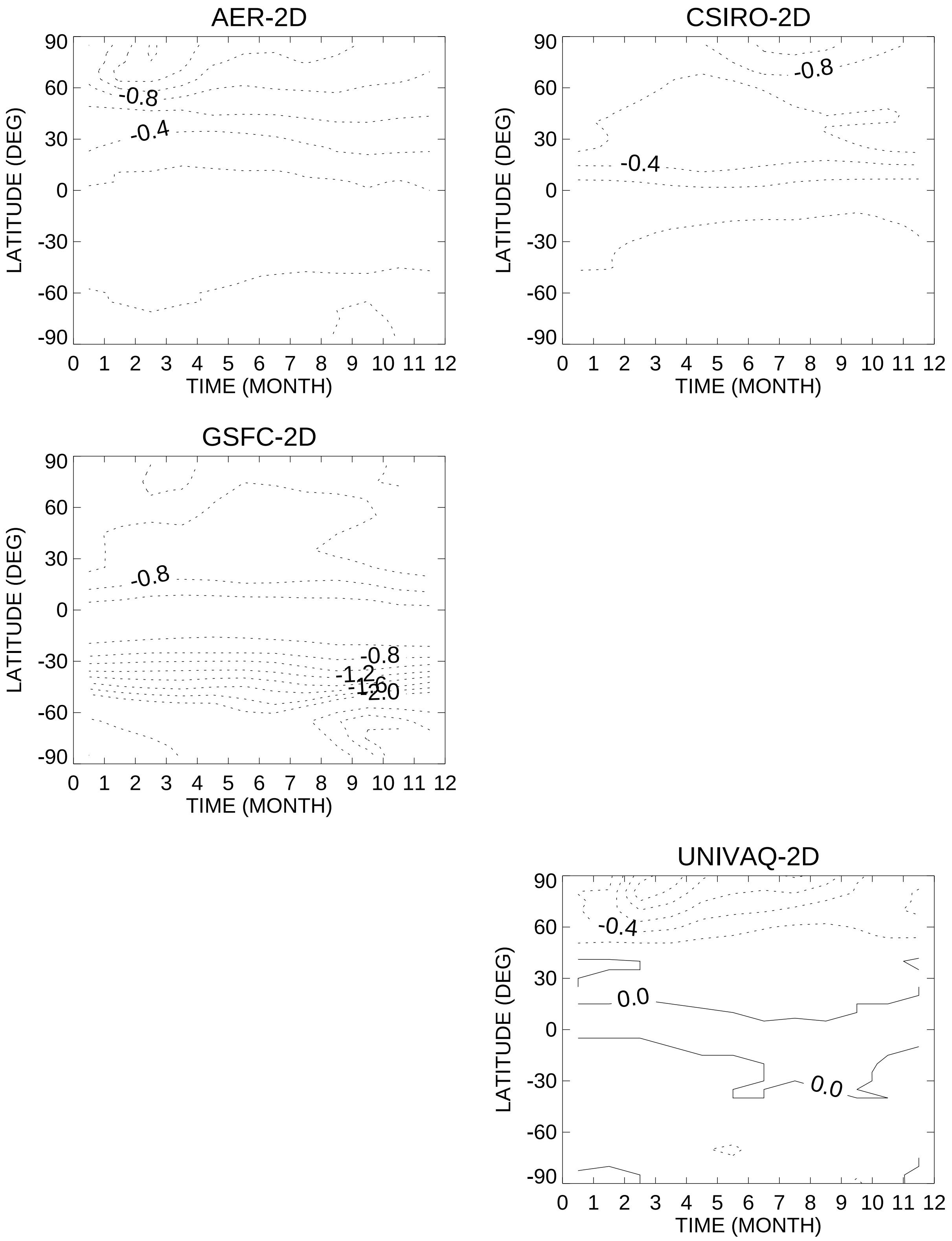

Figure 5.66: Calculated perturbations to column O_3 (percent) as a function of latitude and season in 2050 due to emissions from a fleet of 1000 HSCT aircraft with $EI(NO_x)=5$ and utilizing the IS92e high demand subsonic fleet under Scenario S12a relative to Scenario G. Contours are -5, -4, -3, and -2.0 to 0 by 0.2.